

Minerogenic Peat Deposits of the Sacramento–San Joaquin Delta, California: A Useful Archive for Anthropogenic Contamination of Mercury and Lead

Charles N. Alpers¹, Judith Z. Drexler¹, Leonid A. Neymark², James B. Paces², and Howard E. Taylor³

¹ U.S. Geological Survey, California Water Science Center, 6000 J Street, Placer Hall, Sacramento, CA 95819-6129

² U.S. Geological Survey, Denver Federal Center, Denver, CO 80225

³ U.S. Geological Survey, 3215 Marine Street, Suite E-127, Boulder, CO 80303

ABSTRACT

At the confluence of the Sacramento and San Joaquin rivers (the Delta), a 1,400 km² marsh region began forming about 7,000 years ago. Within the last 160 years, most of the marsh area was drained and converted to agriculture. A vertical peat profile from two of these islands, Browns Island (BRI), and Franks Wetland (FW) contain higher concentrations of inorganic anthropogenic contaminants including mercury (Hg) and lead (Pb) in the shallow, most-recently deposited peat compared to concentrations in underlying pre-anthropogenic peat. In the top 65 cm of the BRI profile, where peat was deposited since about 1850 A.D. based on ¹³⁷Cs data, Hg concentrations averaged 320 parts per billion (ppb, dry basis), with a standard deviation (s.d.) of 220 ppb. In contrast, the average Hg concentration was 370 ppb (s.d. 13 ppb) in deeper material deposited between about 6,300 and 500 calibrated years before present (cal yr BP), based on radiocarbon dating of plant fossils. In the material of transitional age (500 to 100 cal yr BP) during which time global or regional anthropogenic effects may be present, average Hg concentrations were 106 ppb (s.d. 38 ppb).

Average concentrations of Pb were 42 parts per million (ppm, dry basis)(s.d. 17 ppm) in the top 65 cm of the BRI profile compared with 7 ppm (s.d. 4 ppm) in the lower, older (pre-anthropogenic) material (6,300 to 500 cal yr BP). Normalizing Pb concentrations by Ti to account for variable amounts of inorganic material resulted in a depth profile with near-constant values of Pb/Ti between about 6,300 and 2,300 cal yr BP and an increase in Pb/Ti values with decreasing age beginning about 2,300 cal yr BP. Based on linear least-squares regressions of Pb versus several elements that partition strongly into the inorganic fraction of the peat (Al, Ga, Sc, Ti, and Zr), it appears that the organic fraction of the peat contains between 0.5 and 1.0 ppm Pb. The peat in the interval 2,300 and 500 cal yr BP had relatively low ash content and high organic content. The slight amount of Pb in the organic fraction results in an increase in Pb/Al, Pb/Ga, Pb/Ti, and Pb/Zr (but not Pb/Sc) for this interval. Therefore, caution must be used in normalization procedures for samples with low ash content.

Overall patterns in the Franks Wetland core were similar to those observed at the Browns Island site, however inorganic contents were lower and contaminant (Pb and Hg) concentrations smaller. These results emphasize the highly heterogeneous nature of the Sacramento-San Joaquin Delta and demonstrate the importance of hydrogeomorphic setting in controlling marsh accretion processes.

Lead isotope ratios $^{206}\text{Pb}/^{207}\text{Pb}$ and $^{208}\text{Pb}/^{207}\text{Pb}$ determined from bulk-sediment digestions on samples from cores taken at the BRI site indicate the predominant influence of gasoline lead in the top 65 cm of the peat profile. The observed decline in Pb/Ti values with increasing elevation in the top 10 cm of the profile and the increase in radiogenic Pb isotopic compositions reflect the phasing out of leaded gasoline use by automobiles in the U.S.A. during the late 1970s and 1980s. A systematic shift towards less radiogenic Pb isotope ratios starting at about 450 cal yr BP (approx. 1,500 A.D.) may reflect increased mining and metallurgical activity in Mexico after Spanish colonization.

1. INTRODUCTION

The history of anthropogenic lead and mercury pollution has been investigated worldwide using various geologic materials as archives. Lead pollution has been investigated including ice (*e.g.* Song et al., 1994), lake sediments (*e.g.* Renberg et al., 2001, 2002), marine sediments (*e.g.* Soto-Jimenez et al., 2006), and peat (*e.g.* Shotyk, 1996 and 2002; Shotyk et al., 1997, 1998, and 2001). Global mercury pollution has also been documented using various geologic materials including ice (Schuster et al., 2002), lake sediments (*e.g.* Engstrom et al., 1994; Engstrom and Swain, 1997) and peat bogs (Biester et al., 2006 and references therein).

Peat deposits have received considerable attention in the last several decades as archives of environmental change. In general, ombrotrophic peat deposits are considered optimal for studying trends in atmospheric deposition because of the lack of mineral input from stream sources. However, minerotrophic peats can also be useful archives of historical and recent anthropogenic pollution, especially in areas where ombrotrophic bogs are not available (*e.g.* Shotyk et al., 1996; Espi et al., 1997; Weiss et al., 1999; Shotyk, 2002; Monna et al., 2004).

Mercury is well established as a global pollutant (*e.g.* Hurley et al. 2007). Lead pollution is also global in extent (Patterson, 1992; Hong et al., 1994; Settle and Patterson, 1980), and lead isotopes have been useful in documenting the contributions of regional and local mining and smelting sources (*e.g.* Alfonso et al., 2001; Monna et al., 2004; Baron et al., 2005).

Stable lead isotopes provide a robust way to evaluate the source of anthropogenic lead (*e.g.* Settle and Patterson, 1980; Renberg et al., 2001, 2002). The extensive use of alkyl lead additives during the mid-20th century caused widespread, global lead contamination. Because the isotopic signature of lead used in alkyl lead gasoline additives was different than that of average atmospheric dust, it is possible to trace the contamination. Mining sources of lead are also generally less radiogenic (lower in $^{206}\text{Pb}/^{207}\text{Pb}$ and $^{208}\text{Pb}/^{207}\text{Pb}$) which allows them also to be distinguished from pre-anthropogenic background Pb (*e.g.* Dunlap et al., 2008).

Most of the published studies of historical lead and mercury deposition in peat deposits have been done in Europe. There are relatively few data available for geochemical peat archives showing anthropogenic pollution of heavy metals in North America. Some recent studies (Cooke et al., 2007, 2008) have applied Pb isotopes to deposits in South America that document mining and metallurgy by native cultures prior to European colonization.

Prior to about 1850, there was minimal mining in California. After the discovery of gold by James Marshall at Sutter's Mill in 1848, the California Gold Rush caused major disruption and contamination of Sierra Nevada watersheds. The widespread use of mercury for gold amalgamation led to the loss of approximately 4.5×10^6 kg of mercury to the environment from placer gold mining operations during the latter half of the 19th century, and an additional 1.4 kg from stamp mills at hard-rock mines from the 1870s through the 1930s (Churchill, 2000; Alpers et al. 2005a). In the early 20th century, cyanidation became common practice in the gold mining and extraction industry and the use of mercury amalgamation was phased out, but legacy mercury contamination continues to affect the creeks and rivers of the Sierra Nevada. During and after the California Gold Rush, mercury was transported through the Delta to San Francisco Bay, where elevated Hg concentrations were noted in sediments deposited since 1850 (Hornberger et al., 1999). In addition, the mining of mercury in the Coast Ranges of northern California led to extensive contamination of watersheds such as Cache Creek, a tributary to the Delta through the Yolo Bypass (Domagalski et al. 2003, 2004).

To date there have been no published studies of lead or mercury archived in peat deposits in western North America. Given that ombrotrophic peat deposits are not known to occur in California, the purpose of this study is to evaluate whether the minerogenic deposits of the Sacramento–San Joaquin Delta of northern California (hereinafter referred to as the Delta) are useful archives of anthropogenic heavy metal contamination in the environment.

2. MATERIALS AND METHODS

2.1 Site Description

The Delta is located at the confluence of the Sacramento and San Joaquin Rivers and receives runoff from over 40% of the land area of California (California Department of Water Resources, 1995) (Figure 1). During the last several hundred years, the Delta has been primarily a freshwater tidal system, however current salinity may have been brackish during at least some of its history (Malamud-Roam et al., 2006). Tides are semidiurnal with normal tidal range of approximately one meter, however, during floods river stage can exceed two meters (Shlemon and Begg, 1975; Atwater, 1980). The climate in the Delta is characterized as Mediterranean with cool winters and warm, dry summers (Atwater 1980). Mean annual precipitation is approximately 36 cm, but actual yearly precipitation varies from half to almost four times this amount. More than 80% of precipitation occurs from November through March (Thompson, 1957).

Beginning in the mid-1800s, the Delta was largely drained for agriculture (Thompson, 1957; Atwater, 1980), resulting in its current configuration of more than 100 islands and tracts surrounded by 2250 km of man-made levees and 1130 km of waterways (Prokopovich, 1985). Subsequent to drainage, the farmed islands experienced land-surface subsidence. Recent rates of land-surface subsidence range from approximately 0.5–3.0 cm yr⁻¹ (Rojstaczer and Deverel, 1993, 1995; Deverel and Leighton, 2008).

Study sites chosen for geochemical analysis are from contrasting geomorphic settings and salinity regimes of the Delta. One site (Browns Island) was selected in a high energy environment near the confluence of the Sacramento and San Joaquin Rivers and the other (Franks Wetland) is in a more quiescent environment, associated with a distributary of the San Joaquin River (Fig. 1). The study sites are part of a larger project focused on peat formation and loss in the Delta. In the larger study, a total of eight sites were chosen including four remnant, relatively undisturbed marsh islands and four nearby drained farmed islands (Figure 1). Both of the study sites chosen for geochemical analysis are natural marsh islands. On the farmed islands, much of the peat (in some cases the top 5 meters of the ~7 meter deposit) has been lost to land-surface subsidence processes, namely microbial oxidation (Drexler et al., in press).

Vegetation on the marsh islands is dominated by emergent macrophytes and shrub-scrub wetland species. On Browns Island (BRI), the more brackish of the study sites, vegetation is dominated by *Schoenoplectus americanus* (American bulrush) and *Distichlis spicata* (salt grass). On Franks Wetland (FW) the vegetation is dominated by *Cornus sericea* and *Salix lasiolepis*, with the coring site having a large population of *Athyrium filix-femina* (western lady fern). Several species such as *Schoenoplectus acutus* (hardstem bulrush), *Phragmites australis*, and *Typha* spp. are found at both sites. All botanical nomenclature follows Hickman (1993).

2.2 Coring and sample handling

Cores were collected during 2005 using a Livingstone corer, as described by Drexler et al. (2007 and in press). Individual drives were generally 1 meter in length. Sampling for determination of bulk density and loss on ignition was done at 2-cm intervals (Drexler et al., 2007). A subset of the 2 cm samples was selected for analysis of trace elements, stable lead isotopes, and radiometric dating. Cores, samples, and subsamples were stored chilled at 5 °C or less.

Samples selected for trace-element analysis were excised with a ceramic (ZrO₂) knife to remove material that had been in contact with the core liner. The material was placed in a pre-cleaned glass jar with Teflon-lined lid (I-Chem), frozen on dry ice, and shipped to the USGS laboratory in Boulder, Colorado. After freeze-drying, the samples were milled and a subsample of approximately 100 mg was digested in a Teflon bomb with a mixture of concentrated acids including HCl, HNO₃, and HF, as described by Alpers et al. (2006). Determination of bulk density and loss on ignition were made using standard methods described by Drexler et al. (in press).

2.3 Trace element determinations

At the U.S. Geological Survey Laboratory in Boulder, Colorado, samples were freeze-dried before analysis. Trace-metal concentrations were determined using inductively coupled plasma mass spectrometry (ICP-MS) using a Perkin Elmer Elan Model 6000. Samples were completely dissolved using an HCl-HNO₃-HF acid, microwave, total-digestion procedure (Hayes, 1993). The digested samples were diluted at 1:10 (volume:volume, digest:deionized water) with 18 megaohm-cm deionized water and were preserved with distilled nitric acid. Aerosols of

acidified aqueous samples were introduced into the spectrometer with a cone-spray pneumatic nebulizer. Multiple internal standards (indium, iridium, and rhodium), which covered the mass range, were used to normalize the system for drift. Additional details regarding the specific analysis techniques, procedures, and instrumental settings for ICP-MS analyses can be found in Garbarino and Taylor (1996) and Taylor (2001). Mercury was determined by atomic fluorescence spectrometry on the digested samples.

2.4 Stable Pb isotopes

Isotopic compositions of Pb in peat samples were determined at the USGS Yucca Mountain Project Branch laboratory in Denver, Colorado, on splits of samples digested for the ICP-MS analyses. Aliquots were spiked with ^{205}Pb -enriched isotope tracer (Neymark and Amelin, 2008) followed by anion-exchange columns and loading on outgassed Re filaments along with silica gel for Pb-isotope analyses. The Pb isotopic analyses were conducted using multi-collector ThermoFinnigan TritonTM thermal ionization mass spectrometer (TIMS) in a static mode. Use of high-efficiency silica gel (Gerstenberger and Haase, 1997) allowed measurements of all Pb isotope ratios ($^{206}\text{Pb}/^{204}\text{Pb}$, $^{207}\text{Pb}/^{204}\text{Pb}$, and $^{208}\text{Pb}/^{204}\text{Pb}$) on Faraday cups. Raw Pb-isotope ratios were corrected for spike and blank contributions, and for mass fractionation of 0.0010 ± 0.0003 per mass unit using data for Pb-isotope standards SRM-981 and SRM-982 from the National Institute of Standards (NIST) measured under the same run conditions. A weighted average Pb blank of 0.02 ± 0.01 nanogram per milliliter was measured by isotope dilution (ID) TIMS on eight splits used for ICP-MS blanks. Lead concentrations in peat samples determined by ICP-MS and ID TIMS are in excellent agreement (Spearman rank correlation coefficient 0.995). Pb isotopes were determined for 40 samples in the BRI profile representing the full depth range of the cores.

2.5 Dating by ^{14}C and ^{137}Cs

Radiocarbon (^{14}C) analyses were done at the Lawrence Livermore National Laboratory in Livermore, California, using accelerator mass spectrometry (AMS) methods. Achenes (fruiting bodies of *Scirpus* spp.) and charcoal recovered from the peat cores were considered to be the most reliable materials available (Drexler et al., in press)

Activity of ^{137}Cs in the core sections was counted using a gamma detector (sodium iodide crystal, low background germanium detector) and a multi-channel analyzer. Analyses were done at the USGS laboratory in Denver, Colorado. Samples were analyzed for 24 to 48 hours to achieve desired sensitivity. The sediment surface from 1963, the time of peak atmospheric fallout from nuclear testing, was identified based on the maximum activity of ^{137}Cs .

3. RESULTS

3.1 Development of age-depth models

Analyses of radiometric ^{14}C age in achenes (*Scirpus* spp.) and charcoal recovered from peat cores were used by Drexler et al. (in press) to develop age-depth models for peat deposits at the cored locations (Fig. 2). The age-depth models based on ^{14}C are considered reliable for deposits at least 300 cal yr BP (A.D. 1650) based on uncertainty analysis (Drexler et al. in press).

Analyses of ^{137}Cs provided additional constraints on age-depth relationships in the shallower, more recent peat deposits. Both the FW and BRI profiles had peaks in unsupported ^{137}Cs in depth range of 18-20 cm (Fig. 3). The peaks were assigned to the year 1963 and dates were assigned assuming a constant rate of peat accretion (Ritchie and McHenry 1990). Because compression and compaction of peat is minimal in the top meter of the vertical profiles (Drexler et al., in press), the accretion rate for 1963–present was applied to material deposited prior to 1863 to provide an estimate of the depth of the 1850 surface.

3.2 Variation of inorganic and organic components with depth

Several elements have been used in studies of organic rich soils to provide a quantitative estimate of the amount of inorganic material present. The qualities of a suitable inorganic-proxy element are that it should not phytoaccumulate and that it should occur uniformly over a range of grain sizes so that variations in grain size will not lead to variations in the proxy element. For this study we explored the use of Al, Ga, Sc, Ti, and Zr as inorganic proxies.

At the BRI site, large variations with depth were observed in the inorganic content of the peat. Ash content and concentrations of the inorganic-proxy elements Al, Ga, Sc, Ti, and Zr were relatively abundant in the lower part of the vertical profile and were relatively low (reflecting high organic content) in the depths interval 2.1 to 0.5 meters below mean sea level (MSL), which corresponds to the period 2,300 to 500 cal yrs BP (Fig. S-1A). At the FWI site, the inorganic content was much more uniform through depth (Fig. S-1B), indicating a more stable and quiescent hydrogeomorphic setting.

Each of the five potential inorganic-proxy elements (Al, Ga, Sc, Ti, and Zr) correlated well with ash content. Spearman rank coefficients for ash content with respect to individual elements range from 0.86 to 0.91 at the BRI site (Figure S-2A, $n=119$) and from 0.79 to 0.94 at the FW site (Fig. S-2B, $n=25$).

3.3 Variation of Pb and Hg with depth

At both study sites, concentrations of Pb were relatively high ($> 15 \mu\text{g/g}$) in the more recent peat deposits (post-1850 A.D.) near the top of the vertical section, and lower ($< 15 \mu\text{g/g}$) in the older

deposits (pre-1850 A.D.) at depths greater than 0.2 meters below MSL (Fig. 4). Clay-rich material at the base of the BRI profile had a Pb concentration of about 10 $\mu\text{g/g}$, similar to Pb in the peat in the lower half of the profile. Moving upward in the vertical BRI profile, Pb concentrations declined to values consistently less than 10 $\mu\text{g/g}$ starting at a depth of about 3 m below MSL. The depth interval with Pb < 10 $\mu\text{g/g}$ (about 3 m to 0.5 m below MSL) corresponds to a zone with lower concentrations of inorganic proxy elements (Fig. S1A). Pb concentrations in the FW profile had a similar overall pattern to those in the BRI profile, with values between 10 to 15 $\mu\text{g/g}$ at depth, values < 10 $\mu\text{g/g}$ in the middle portion, and values > 15 $\mu\text{g/g}$ in the upper portion.

Comparing the variations of Pb to the age of peat determined by ^{14}C and ^{137}Cs methods, there are two time horizons when Pb increased sharply — one at about 500 cal yr BP (~1450 A.D.) and another at about 100 cal yr BP (~1850 A.D.) (Fig. 4). The period 1940 to 1980 had consistently high Pb concentrations, and there was a systematic decline in the Pb content of peat younger than 1980.

The vertical distribution of Hg at the two study sites was similar to that of Pb, in that the highest concentrations were found in a zone just beneath the shallowest, most recent deposits. At depths greater than about 0.5 m below MSL, Hg concentrations were consistently < 40 ng/g at the FW site and < 75 ng/g at the BRI site (Fig. 5). In contrast, nearly all samples from the top meter of both profiles had Hg concentrations > 100 ng/g.

As with Pb, there were sharp increases in Hg concentration with decreasing depth at approximately 500 and 100 cal yr BP. In the BRI core, which had the higher density of samples, the highest Hg concentrations were in peat samples from 0.28 to 0.40 m above MSL, corresponding to ^{137}Cs ages of about 1940 to 1970 A.D. During this period, Hg concentrations consistently were greater than 400 ng/g. At the very top of the BRI profile, between 0.4 m above MSL and the surface (0.56 m above MSL), Hg concentrations in peat ranged from 190 to 310 ng/g.

3.4 Variation of Pb isotopes with depth

A plot of $^{206}\text{Pb}/^{207}\text{Pb}$ vs. depth for the BRI site (Fig. 6) shows that most of the samples in the age range 2,300 to 500 cal yr BP have $^{206}\text{Pb}/^{207}\text{Pb}$ values in the same range as pre-anthropogenic background (1.216 to 1.224). The oldest sample that is clearly different isotopically from the pre-anthropogenic samples is the sample corresponding to 527 cal yr BP in the ^{14}C age-depth model. The sample just below it, from a depth corresponding to an age of 840 cal yr BP, has a slight variation in $^{206}\text{Pb}/^{207}\text{Pb}$ but does not show a significant difference in $^{208}\text{Pb}/^{207}\text{Pb}$ (Fig. S3) and therefore does not demonstrate clear evidence of anthropogenic contamination.

4. DISCUSSION

4.1 Distinguishing between natural and anthropogenic Pb using Ti

A variety of methods have been used to distinguish between natural and anthropogenic Pb in peat deposits. Assuming that all Pb occurs in the inorganic fraction of the peat, the concentration of an inorganic proxy element (such as Al, Ga, Sc, Ti, or Zr) and the assumption of a constant ratio of Pb concentration to the concentration of the proxy element (*e.g.* Pb/Ti) can be used to calculate the lithogenic (natural) Pb contribution. The lithogenic Pb can then be subtracted from the total Pb concentration to yield the anthropogenic Pb contribution. For example, Shotyk et al. (2002b) used Pb/Sc in this manner to compute anthropogenic Pb in peat cores from Switzerland.

In this study, we evaluated the possible use of Al, Ga, Sc, Ti, and Zr as inorganic proxies for improving the understanding of Pb sources and temporal trends. As shown in Figures S-1 and S-2, each of these elements correlates well with ash content, and has similar concentration-depth profiles in both the FW and BRI cores. Ti was chosen as the proxy of choice for this report because its behavior was most consistent.

In the FW core, Pb/Ti ranged from 0.003 to about 0.006 in samples older than 500 cal yr BP, increased sharply to values above 0.01 in samples younger than 100 cal yr BP, then declined in the most recent samples, younger than 1963 A.D. (Fig. 7A). In the BRI core, Pb/Ti was near-constant at values between 0.002 and 0.003 in the age range 6300 to 2300 cal yr BP (Fig. 7B). In the age range 2300 to 500 cal yr BP, there was an increase in Pb/Ti to values between 0.003 and 0.006. This comes at an intriguing time in history, when Roman mining activity was active at several sites in Europe, and anthropogenic Pb is well documented in cores of ice (Song et al., 1974) and peat (Shotyk et al., 2001) starting around 2000 cal yr BP. In samples younger than 500 cal yr BP in the BRI core, there was a further increase in Pb/Ti, to values greater than 0.006. The most extreme values of Pb/Ti (> 0.02) were from the period younger than 100 cal yr BP (1850 A.D., around the start of the California Gold Rush), including the mid-1900's when leaded gasoline was in widespread use.

Correlation plots of Ti vs. Pb (Fig. 8) reveal a more complex story, including a cautionary tale regarding the use of inorganic proxies. Looking at the entire BRI data set, there is a clear distinction between samples older than 500 cal yr BP, which have Pb/Ti < 0.006 , and those younger than 500 cal yr BP, which have Pb/Ti > 0.006 . Samples in the time range 2,300 to 500 cal yr BP had much lower inorganic content than others in the BRI profile, so they plot closer to the origin in Fig. 8. Subsets of the BRI data from 3,550 to 2,300 cal yr BP and from 2,300 to 500 cal yr BP are normally distributed with regard to Pb, Ti, and the other inorganic proxy elements considered, so linear least-squares regressions could be computed. Assuming that the Ti concentration in the organic fraction of the peat is zero, the intercept on the Pb axis represents an estimate of the Pb content of the organic fraction of the peat. The regressions for Pb vs. Ti for the BRI site (Fig. 8B) indicate an intercept on the Pb axis of approximately 0.5 to 0.9 $\mu\text{g/g}$. Plots of Ti vs. Pb for the FW site indicate similar values of the Pb intercept, between 0.5 and 0.7 $\mu\text{g/g}$. (Fig. S4). Similar plots for Pb versus the other inorganic proxy elements (Al, Ga, Sc, and Zr) in the FW and BRI cores (Figs. S5-S8) show similar results to those for Ti (Figs. 8 and S4). A summary of regression coefficients for 6 inorganic proxies (Al, Ga, Sc, Ti, Zr, and ash content)

is given in Table 1. Using the top five inorganic proxies (based on the regression coefficient, R^2), the average Pb estimated content of the organic fraction in pre-anthropogenic peat at Browns Island was 0.7 to 0.8 $\mu\text{g/g}$ and at Franks Wetland was 0.3 to 0.5 $\mu\text{g/g}$.

The similarity of estimated Pb concentrations from the intercepts of the various regressions indicate a high probability that the increase in Pb/Ti in the points between 2,300 and 500 cal yr BP at Browns Island (Fig. 7B) is a consequence of the Pb content of the organic fraction, and does not represent anthropogenic (i.e. Roman) lead. Lead isotopes (as presented above and discussed below) provide independent confirmation of that conclusion.

4.2 Determining the predominant sources of Pb using Pb Isotopes

Other recent studies have documented the Pb isotope composition of sediments in the Sacramento River, the major tributary to the Delta, as well as cores in San Francisco Bay, downstream of the Delta (Dunlap et al., 2008 and references therein). On a plot of $^{208}\text{Pb}/^{207}\text{Pb}$ vs. $^{206}\text{Pb}/^{207}\text{Pb}$, the deep samples from the BRI profile (6,300 to 2,300 cal yr BP) plot exactly in coincidence with the deep cores from San Francisco Bay (Fig. 9). A shift to less radiogenic lead begins with the sample mentioned above corresponding to an age of 527 cal yr BP, and continues for the samples in the age range 500 to 100 cal yr BP. The most radiogenic of these samples, from a depth corresponding to an age of 447 cal yr BP, is demonstrably older than the California Gold Rush with 95% confidence, based on the error analysis associated with the ^{14}C age curve (Fig. 2B; Drexler et al., in press). As there was no obvious geologic or mining source in California at that time (approximately 1500 A.D.), it is worth considering the possibility that the associated anthropogenic lead came from mining in another area such as China or Mexico, and the lead was transported to California as atmospheric dust.

The most extremely non-radiogenic Pb in peat samples in the BRI profile have Pb isotope data that plot in the field for leaded gasoline used in U.S.A during 1964–1979. These peat samples are from depths corresponding to ages of ~1900 to 1970 based on ^{137}Cs dating. Because lead wasn't added to gasoline until the 1930's it is necessary to explain the occurrence of lead contamination isotopically tied to gasoline in peat that is apparently older than 1930. It is possible that Pb was transferred to lower elevations by a physical or chemical process that did not transfer Cs. The three most recent peat samples for which there are Pb isotope data plot in the field for leaded gasoline from the 1980s (Fig. 9). Based on our interpretation of the ^{137}Cs data, these peat samples are from depths with ages approximately 1980 to 1995 A.D. (Fig. 3).

Our data contain evidence that anthropogenic Pb partitions into the organic fraction of the peat more readily than non-anthropogenic Pb. Four pairs of samples from within the top meter of the BRI profile represent organic-rich and clay-rich subsamples from the same 2-cm vertical interval (triangles and squares, respectively, as indicated on several figures). The Pb concentration of the organic-rich subsamples was greater than or equal to that of the co-located clay-rich subsamples (Fig. 4). Pb isotopes of the organic-rich subsamples were less radiogenic than the clay-rich counterparts (Figs. 6 and 9). This is consistent with the fact that alkyl lead gasoline additives are

an organic form of lead that partitions preferentially into the organic fraction (Shotyk et al. 2002b).

4.3 Mercury from the California Gold Rush and other mining sources

Anthropogenic mercury in the Delta peat deposits likely includes local mining-related sources as well as regional and global industrial sources. Local mining-related sources increased dramatically around 1850, at the start of the California Gold Rush. Schuster et al. (2002) documented Hg contamination in an ice core from a glacier in the Wind River Range, Wyoming, in which the California Gold Rush is clearly represented by a significant increase in Hg, as are other industrial events such as the World War II era (early 1940s) during which munitions plants with Hg emissions were active in the San Francisco Bay Area. Global production and U.S. consumption of mercury were at a maximum during the period 1940–1970 (Engstrom and Swain, 1997), which corresponds well to the age of the peat with the highest Hg content at Browns Island (Fig. 5).

Given the history of mining and industrial activity in northern California, the observed increase in Hg of the FW and BRI peat deposits starting about 1850 is understandable. However the cause of the increase observed about 500 cal yr BP is less certain, as there was no large-scale mining activity in California at that time. In the BRI profile, the interval of 2300 to 500 cal yr BP had Hg concentrations between about 70 to 200 ng/g, a range that is significantly elevated over pre-anthropogenic baseline conditions. As there are no obvious local sources in California for this contamination, the most likely possibilities are: (1) global sources (Europe), (2) Asian sources (China), and (3) other North American sources (Mexico). Because lead isotopes indicate sources of non-radiogenic lead contamination during this period, a source related to mining and smelting activity is most likely.

Spanish colonization of southern North America (now Mexico) and western South America (now Peru, Bolivia, and Ecuador) started during the early 16th century, approximately 450 cal yr BP (1500 A.D.). Mining activity in Mexico produced lead and mercury along with gold and silver (Nriagu, 1998). The timing of the anomalous Pb in the BRI core is consistent with a source related to Spanish mining and smelting activity in Mexico, but there remains the question of atmospheric circulation. Given global wind patterns, is it reasonable for a sufficient quantity of atmospheric dust to be transported from south to north? There is the additional uncertainty regarding global wind patterns 500 years ago compared to present-day patterns. There are various global circulation models aimed at understanding climate change that may be informative on this aspect, but this possibility has not yet been explored.

4.4 Comparison of Lead and Mercury Trends

Both lead and mercury remained at pre-anthropogenic concentrations in Browns Island and Franks Wetland peat cores until about 500 cal yr BP (1450 A.D.). During the period 500 cal yr BP to 100 cal yr BP (1450 to 1850 A.D.), both Pb and Hg were elevated above the pre-anthropogenic baseline. As there was no large-scale mining in California during that time, the sources of the Pb and Hg were likely outside California. Variations in the ratio Pb/Hg (Figs. S9, S10A, and S10B) shed some light on the timing of increases in both constituents and the degree

to which they may share a common source. With the exception of a few outliers, most samples from both cores had Pb/Hg in the range of 50 to 500. In the BRI core, most material in the age range 6300 to 2,300 cal yr BP had Pb/Hg values around 200. The material of age 2,300 to 500 cal yr BP had values of Pb/Hg in the range of 50 to 200, lower than those in the underlying material. This change was caused by significantly lower Pb in this interval associated with the lower inorganic content (Figs. 4, S1B). Although Hg concentrations were somewhat lower in this interval compared with the deeper section, Hg partitions into the organic fraction to a greater degree than Pb. Thus, the variations in Pb/Hg are consistent with non-anthropogenic sources prior to 500 cal yr BP.

In peat of age 500 to 100 cal yr BP, both Pb and Hg concentrations were greater than in the material older than 500 cal yr BP, and the Pb/Hg ratio for most samples was in the range 70 to 100 (Fig. S9). A plot of Ti vs. Pb/Hg (Fig. S10C) is consistent with the interpretation that Pb partitions more strongly than Hg into the inorganic fraction. Much of the variation in Pb/Hg appears to be controlled by variations in the inorganic / organic content. An exception is the most recent peat (post-1963) which had lower Pb/Hg for a given Ti concentration compared with the overall trend (Fig S10C). Thus, despite a high level of global and regional Pb contamination from leaded gasoline during about 1940 to 1980, global mercury emissions appear to have had proportionately more influence on Delta peat chemistry during the mid-1900s.

Concentrations of both Pb and Hg increased sharply during the California Gold Rush and stayed elevated during the first several decades of the 20th century. Lead concentrations increased greatly because of gasoline additives, peaking in the early 1960s, then declined as leaded gasoline was phased out in late 1970s and early 1980s. Mercury reached a maximum globally and regionally during 1950 – 1970, then declined as Hg use declined. The peat deposits of the Sacramento–San Joaquin Delta appear to track expected environmental changes in Pb and Hg emissions and deposition on a decadal scale. This would be expected for ombrotrophic peat that gets atmospheric deposition directly, however minerogenic peats may experience a lag time associated with erosion and river transport. The close correspondence of Pb and Hg variations to expected fluxes indicates that the lag time for the Delta system, if any, is apparently less than about 10 years.

5. CONCLUSIONS

1. The peat deposits of the Sacramento–San Joaquin Delta contain an archive of pre-anthropogenic, natural conditions in the region. Consistent results were obtained on cores from two unfarmed marsh locations in the Delta, Browns Island and Franks Wetland.
2. Based on uniform concentrations of Pb/Ti (normalized to account for variable inorganic content) and Pb-isotope composition (a sensitive indicator of anthropogenic lead), the peat deposits older than 2,300 cal yr BP (350 B.C) in these undisturbed marshes were clearly unaffected by anthropogenic activity.

3. Peat deposited during the period 2,300 to 500 cal yr BP (350 B.C. to 1450 A.D.) at Browns Island, based on ^{14}C dating, had elevated values of the Pb/Ti ratio relative to the material at depth, but this Pb is likely non-anthropogenic. The peat had relatively low inorganic content and the ratio Pb/Ti was influenced by finite Pb concentrations (~0.5 to 0.9 ppm) in organic material. The Pb-isotope data indicate non-anthropogenic sources of Pb during this period.
4. In the material younger than 500 cal yr BP (350 B.C.), there are two clear non-radiogenic peaks in Pb-isotopes indicating anthropogenic Pb: the older peak at ~450 cal yr BP (~1500 A.D.) is likely related to mining and/or smelting activity. As there was no major mining activity in California at that time, the likely source(s) were (1) Mexico and/or (2) China. The younger peak (20th century) is likely related to alkyl lead gasoline additives.
5. In the 20th century peat samples, a more pronounced Pb-isotope signature relating the samples to alkyl lead gasoline additives was found in organic-rich samples vs. inorganic-rich samples from the same depths. This is consistent with the organic nature of the lead added to gasoline.
6. Maximum concentrations of Hg (> 400 ng/g or ppb) in Browns Island peat were found in deposits from ~1940–1970 based on ^{137}Cs dating. This period had the highest global production and highest U.S. consumption of mercury, and was a period of relatively low mining activity in California, suggesting that atmospheric sources dominated over local mining sources during this period.
7. Minerogenic peats such as those found in the Sacramento–San Joaquin Delta can be useful archives of environmental change at decadal to millennial time scales.

Acknowledgments -- This study was funded by the CALFED Science Program of the State of California Resources Agency, Agreement #F-O3-RE-029. We thank Jacob Fleck and Kim Taylor (USGS) for their help in developing the project. Jim Orlando, Jacob Fleck, Matt Kerlin, and Curt Battenfeld (USGS) provided field support. Laboratory facilities were generously provided by Greg Pasternack at the University of California, Davis. We extend a special thanks to Stephanie Wong, Patricia Orlando, Christian de Fontaine, Nicole Lunning, Terry Plowman, Dale Peart, David Roth, Ronald Antweiler, and Loretta Kwak (USGS) for their assistance in the laboratory. Michelle Sneed and Gerald Bawden (USGS) and Marti Ikehara (Coast and Geodetic Survey) assisted with the elevation survey. Thomas Brown (Center for Accelerator Mass Spectrometry, Lawrence Livermore National Laboratory) provided radiocarbon analysis and support. Cesium isotope data were provided by Jim Budahn (USGS).

REFERENCES

- Alfonso, S., Grousset, F., Massé, L., and Tastet, J. -P. (2001) A European lead isotope signal recorded from 6000 to 300 years BP in coastal marshes (SW France). *Atmosphere and Environment* **35**, 3595–3605.
- Alpers, C. N., Hunerlach, M. P., May, J. T., and Hothem, R. L. (2005) Mercury contamination from historical gold mining in California: U.S. Geological Survey Fact Sheet 2005-3014, 6 p. <http://pubs.water.usgs.gov/fs2005-3014>
- Alpers, C. N., Hunerlach, M. P., Marvin-DiPasquale, M. C., Antweiler, R. C., Lasorsa, B. K., De Wild, J. F., and Snyder, N. P. (2006) Geochemical data for mercury, methylmercury, and other constituents in sediments from Englebright Lake, California, 2002. U.S. Geological Survey Data Series **151**, 95 p. <http://pubs.water.usgs.gov/ds151/>
- Atwater, B. F. (1980) Attempts to correlate late Quaternary climatic records between San Francisco Bay, the Sacramento-San Joaquin Delta, and the Mokelumne River, California. Ph.D. Dissertation. University of Delaware, Newark, DE, USA.
- Baron, S., Lavoie, M., Ploquin, A., Carignan, J., Pulido, M. and deBeaulieu, J. L. (2005) Record of metal workshops in peat deposits: History and environmental impact on the Mont Lozère Massif, France. *Environmental Science and Technology* **39**, 5131–40.
- Barron, J. A., Heusser, L., Herbert, T., and Lyle, M. (2003) High-resolution climatic evolution of coastal northern California during the past 16,000 years. *Paleoceanography* **18**, 1020.
- Biester, H., Bindler, R., Martínez-Cortizas, A., and Engstrom, D. R (2007) Modeling the past atmospheric deposition of mercury using natural archives. *Environmental Science & Technology* **41**, 4851–4860.
- Bindler, R. (2006) Mired in the past — looking to the future: Geochemistry of peat and the analysis of past environmental changes. *Global and Planetary Change* **53**, 209–221.
- Bollhöfer, A. and Rosman, K. J. R. (2001) Isotopic source signatures for atmospheric lead: the Northern Hemisphere. *Geochimica et Cosmochimica Acta* **65**, 1727–1740.
- California Department of Water Resources (1995) Sacramento-San Joaquin Delta Atlas. Central District, Sacramento, CA, USA, <http://baydeltaoffice.water.ca.gov/DeltaAtlas/index.cfm>.
- Choi, M.-S., Yi, H.-I., Yang, S. Y., Lee, C.-B., and Cha, H.-J. (2007) Identification of Pb sources in Yellow Sea sediments using stable Pb isotope ratios. *Marine Chemistry* **107**, 255-274.
- Churchill, R. K. (2000) Contributions of mercury to California's environment from mercury and gold mining activities; Insights from the historical record, in Extended abstracts for the U.S. Environmental Protection Agency sponsored meeting, Assessing and Managing Mercury from

Historic and Current Mining Activities: November 28–30, 2000, San Francisco, Calif., p. 33–36 and S35–S48.

Cooke, C. A., Abbott, M. B., Wolfe, A. P. and Kittleson, J. L. (2007) A millennium of metallurgy recorded by lake sediments from Morococha, Peruvian Andes. *Environmental Science and Technology* **41**, 3469–3474.

Cooke, C. A., Abbott, M. B., and Wolfe, A. P. (2008) Late-Holocene atmospheric lead deposition in the Peruvian and Bolivian Andes. *The Holocene* **18**, 353

Deverel, S. J., and Leighton, D. A. (2008) Subsidence causes and rates in the Sacramento-San Joaquin Delta and Suisun Marsh. *San Francisco Estuary and Water Science*, in press.

Domagalski, J. L., Slotton, D. G., Alpers, C. N., Suchanek, T. H., Churchill, R., Bloom, N., Ayers, S. M., and Clinkenbeard, J. (2003) Summary and Synthesis of Mercury Studies in the Cache Creek Watershed, California, 2000-2001. U.S. Geological Survey Water –Resources Investigations Report 03-4355, 30 p. <http://water.usgs.gov/pubs/wri/wri034335/>

Domagalski, J. L., Alpers, C. N., Slotton, D. G., Suchanek, T. H., Ayers, S. M. (2004) Mercury and methylmercury concentrations and loads in the Cache Creek Watershed, California. *Science of the Total Environment* **327**, 215-237.

Drexler, J. Z., de Fontaine, C. S., and Knifong, D. L. (2007) Age determination of the remaining peat in the Sacramento-San Joaquin Delta, California, USA. U.S. Geological Survey Open File Report **2007-1303**. 2 p.

Drexler, J. Z., de Fontaine, C. S., and Deverel, S. J. (in press) The legacy of wetland drainage on peat resources in the Sacramento – San Joaquin Delta, California, USA. *Wetlands*.

Dunlap, C. E., Alpers, C. N., Taylor, H. E., Unruh, D. M., Flegal, A. R. (2008) The persistence of lead from past gasoline emissions and mining drainage in a large riparian system: Evidence from lead isotopes in the Sacramento River, California. *Geochimica et Cosmochimica Acta* **72**, 5935–5948.

Engstrom, D. R., and Swain, E. B. (1997) Recent declines in atmospheric mercury deposition in the upper Midwest. *Environmental Science & Technology* **31**, 60–67.

Engstrom, D. R., Swain, E. B., Henning, T. A., Brigham, M. E. and Brezonik, P. L. (1994) Atmospheric mercury deposition to lakes and watersheds – a quantitative reconstruction from multiple sediment cores. In Baker, L.A., editor, *Environmental chemistry of lakes and reservoirs*. American Chemical Society, 33–66.

Espi, E., Boutron, C. F., Hong, S., Pourchet, M., Ferrari, C., Shotyk, W., and Charlet, L. (1997) Changing concentrations of Cu, Zn, Cd, and Pb in a high altitude peat bog from Bolivia during the past three century. *Water Air and Soil Pollution* **100**, 289–296.

- Garbarino, J. R., and Taylor, H. E. (1996) Inductively coupled plasma-mass spectrometric method for the determination of dissolved trace elements in natural water: U.S. Geological Survey Open-File Report No. 94-358, 88 p.
- Gerstenberger, H., and Haase, G. (1997) A highly effective emitter substance for mass spectrometric Pb isotope ratio determinations. *Chemical Geology* **136**, 309–312.
- Glooschenko, W. A., Holloway, L., and Arafat, N. (1986) The use of mires in monitoring the atmospheric deposition of heavy metals. *Aquatic Botany* **25**, 179–190.
- Hayes, H.C. (1993) Metal associations in suspended sediments and bed sediments from the Mississippi River: Golden, Colo., Colorado School of Mines, M.S. thesis, 131 p.
- Hickman, J. C. (ed.) (1993) The Jepson Manual. Berkeley, CA: University of California Press.
- Hong, S., Candelone, J. -P., Patterson, C. C., Boutron, C. F. (1994) Greenland ice evidence of hemispheric lead pollution two millennia ago by Greek and Roman civilizations. *Science* **265**, 1841–1843.
- Hong, S., Candelone, J.-P., Patterson, C. C., and Boutron, C. F. (1996) History of ancient copper smelting pollution during Roman and Medieval times recorded in Greenland ice. *Science* **272**, 246–249.
- Hornberger, M. I., Luoma, S. N., van Geen, A., Fuller, C., and Anima, R. (1999) Historical trends of metals in the sediments of San Francisco Bay, California. *Marine Geology* **64**, 39–55.
- Hurley, M. P. Krabbenhoft, D. P., Weiner, J. G., and Babiarz, C. L. (2007) Preface to the Madison Declaration and Critical Synthesis Papers on Mercury Pollution, Eighth International Conference on Mercury as a Global Pollutant, Madison, Wisconsin, USA, 6–11 August 2006. *Ambio* **36**, 1–2.
- Malamud-Roam, F. P., Ingram, B. L., Hughes, M., and Florsheim, J. L. (2006) Holocene paleoclimate records from a large California estuarine system and its watershed region: linking watershed climate and bay conditions. *Quaternary Science Reviews* **25**, 1570–1598.
- Martínez-Cortizas A., Pontevedra Pombal X., García-Rodeja E., Nóvoa Munõz, J. C., and Shotyk W. (1999) Mercury in a Spanish peat bog: archive of climate change and atmospheric metal deposition. *Science* **284**, 939–942.
- Monna, F., Galop, D., Carozza, L., Tual, M., Beyrie, A., Marembert, F., Chateau, C., Dominik, J., and Grousset, F. E. (2004) Environmental impact of early Basque mining and smelting recorded in a high ash minerogenic peat deposit. *Science of the Total Environment* **327**, 197–214.
- Neymark, L. A., and Amelin, Y. (2008) Natural radionuclide mobility and its influence on the U-Th-Pb dating of secondary minerals from the unsaturated zone, Yucca Mountain, Nevada. *Geochimica et Cosmochimica Acta* **72**, 2067–2089.

Nriagu, J. O. (1998) Tales told in lead. *Science* **281**, 1622–1623.

Prokopovich, N. P. (1985) Subsidence of peat in California and Florida. *Bulletin of the Association of Engineering Geologists* **22**, 395–420.

Renberg, I., Bindler, R., and Brännvall, M. –L. (2001) Using the historical atmospheric lead-deposition record as a chronological marker in sediment deposits in Europe. *The Holocene* **11**, 511–516.

Renberg, I., Brännvall, M. L., Bindler, R., and Emteryd, O. (2002) Stable lead isotopes and lake sediments – a useful combination for the study of atmospheric lead pollution history. *Science of the Total Environment* **292**, 45–54.

Renberg, I., Pearson, M. W., and Emteryd, O. (1994) Pre-industrial atmospheric lead contamination detected in Swedish lake sediments. *Nature* **368**, 323–326.

Ritchie, J. C., and McHenry, J. R. (1990) Application of radioactive fallout Cesium-137 for measuring soil erosion and sediment accumulation rates and patterns: A review. *Journal of Environmental Quality* **19**: 214-233.

Rojstaczer, S., and Deverel, S. J. (1993) Time dependence in atmospheric carbon inputs from drainage of organic soils. *Geophysical Research Letters* **20**:1383–1386.

Rojstaczer, S., and Deverel, S. J. (1995) Land subsidence in drained histosols and highly organic mineral soils of California. *Soil Science Society of America Journal* **59**:1162–1167.

Schuster, P. F., Krabbenhoft, D. P., Naftz, D. L., Cecil, L. D., Olson, M. L., Dewild, J. F., Susong, D. D., Green, J. R., and Abbott, M. L. (2002) Atmospheric mercury deposition during the last 270 years, a glacial ice core record of natural and anthropogenic sources. *Environmental Science & Technology* **36**, 2303–2310.

Settle, D. M., and Patterson, C. C. (1980) Lead in albacore: Guide to lead pollution in Americans. *Science* **207**, 1167–1176.

Shlemon, R. J. and Begg, E. L. (1975) Late Quaternary evolution of the Sacramento-San Joaquin Delta, California. pp. 259-266 In R.P. Suggate and M.M. Creswell (eds.) Quaternary Studies. The Royal Society of New Zealand, Wellington, New Zealand.

Shotyk, W. (1996) Natural and anthropogenic enrichments of As, Cu, Pb, Sb, and Zn in ombrotrophic vs. minerotrophic peat bog profiles, Jura Mountains, Switzerland. *Water Air and Soil Pollution* **90**, 375–405.

Shotyk, W. (2002) The chronology of anthropogenic, atmospheric Pb deposition recorded by peat cores in three minerogenic peat deposits from Switzerland. *Science of the Total Environment* **292**, 19–31.

Shotyk, W., Weiss, D., Appleby, P., Cherbukin, A., Frei, R., Gloor, M., Kramer, J., Reese, S., Van der Knaap, W. (1998) History of atmospheric lead deposition since 12,370 ^{14}C yr BP from a peat bog, Jura Mountains, Switzerland. *Science* **281**, 1635–1640.

Shotyk W., Weiss D., Kramers J. D., Frei R., Cheburkin A. K., Gloor M., and Reese S. (2001) Geochemistry of the peat bog at Etang de la Gruère, Jura Mountains, Switzerland and its record of atmospheric Pb and lithogenic trace elements (Sc, Ti, Y, Zr, Hf and REE) since 12,370 ^{14}C yr BP. *Geochimica et Cosmochimica Acta* **65**, 2337–2360.

Shotyk, W., Krachler, M., Martínez-Cortizas, A., Cheburkin, A.K., and Emons, H. (2002a) A peat bog record of natural, pre-anthropogenic enrichments of trace elements in atmospheric aerosols since 12,370 ^{14}C yr BP, and their variation with Holocene climate change. *Earth and Planetary Science Letters* **199**, 21–37.

Shotyk, W., Weiss, D., Heisterkamp, M., Cheburkin, A. K., Appleby, P. G., and Adams, F. C. (2002b) New peat bog record of atmospheric lead pollution in Switzerland: Pb concentrations, enrichment factors, isotopic composition, and organolead species. *Environmental Science & Technology* **36**, 3893–3900.

Soto-Jiménez, M. F., Hibdon, S. A., Rankin, C. W., Aggarawl, J., Ruiz-Fernandez, A. C. Páez-Osuna, F., and Flegal, A. R. (2006) Chronicling a century of lead pollution in Mexico: Stable lead isotopic composition analyses of dated sediment cores. *Environmental Science & Technology* **40**, 764–770.

Soto-Jiménez, M. F., Páez-Osuna, F., Scelfo, G., Hibdon, S., Franks, R., Aggarawl, J., and Flegal, A. R. (2008) Lead pollution in subtropical ecosystems on the SE Gulf of California Coast: A study of concentrations and isotopic composition. *Marine Environmental Research* **66**: 451–458.

Taylor, H. E. (2001) Inductively coupled plasma-mass spectrometry—practices and techniques: San Diego, Calif., Academic Press, 294 p.

Thompson, J. (1957) The settlement geography of the Sacramento-San Joaquin Delta, California. Ph.D. Dissertation. Stanford University, Stanford, CA, USA.

Weiss, D., Shotyk, W., Appleby, P. G., Kramers, J. D., Cheburkin, A. K. (1999) Atmospheric Pb deposition since the Industrial Revolution recorded by five Swiss peat profiles: enrichment factors, fluxes, isotopic composition, and sources. *Environmental Science & Technology* **33**, 1340–1352.

Tables

Table 1. Results of linear least-squares regressions of lead vs. various inorganic proxies in the Browns Island and Franks Wetland cores.

Table 1. Results of linear least-squares regressions of lead vs. various inorganic proxies

Regressions of the form: $(Pb) = b(1)[x] + b(0)$, where (x) = independent variable and (Pb) is lead concentration
 R^2 , correlation coefficient; n, number of data points; cal yr BP, calibrated years before present (1950) based on ^{14}C age model
 $b(0)$ intercept represents estimate of Pb concentration of organic component, assuming Ti concentration is zero.

A. Browns Island

Independent variable	Model age (cal yr BP)	b(1)	b(0)	R^2	n	Model age (cal yr BP)	b(1)	b(0)	R^2	n
Ti (%)	2300-3550	23.5	0.49	0.96	27	500-2300	24.3	0.85	0.85	18
Zr (ppm)	2300-3550	0.092	0.49	0.95	27	500-2300	0.097	0.69	0.85	18
Al (%)	2300-3550	1.26	0.23	0.98	27	500-2300	1.2	0.74	0.81	18
Sc (ppm)	2300-3550	0.31	1.56	0.57	27	500-2300	0.38	0.42	0.78	18
Ga (ppm)	2300-3550	0.47	1.01	0.98	27	500-2300	0.51	0.77	0.77	18
ash (%)	2300-3550	0.065	0.17	0.24	27	500-2300	0.11	-0.15	0.64	18
average (top 3)			0.40					0.76		
average (top 5)			0.76					0.69		

B. Franks Wetland

Independent variable	Model age (cal yr BP)	b(1)	b(0)	R^2	n	Model age (cal yr BP)	b(1)	b(0)	R^2	n
Ti (%)	2300-5550+	39.6	0.49	0.76	9	500-2300	33.6	0.65	0.94	9
Zr (ppm)	2300-5550+	0.13	1.01	0.66	9	500-2300	0.15	0.40	0.85	9
Al (%)	2300-5550+	1.91	-0.26	0.81	9	500-2300	1.48	0.22	0.87	9
Sc (ppm)	2300-5550+	0.38	2.1	0.39	9	500-2300	0.47	0.42	0.47	9
Ga (ppm)	2300-5550+	0.74	0.04	0.92	9	500-2300	0.76	0.27	0.94	9
ash (%)	2300-5550+	0.15	0.2	0.90	9	500-2300	0.08	0.95	0.91	9
average (top 3)			-0.01					0.62		
average (top 5)			0.30					0.50		

Figure Captions

Figure 1. Map showing coring locations for the REPEAT project in the Sacramento–San Joaquin Delta, California. Adapted from Drexler et al. (in press).

Figure 2. Age-depth models based on ^{14}C data showing uncertainty envelope. (A) Franks Wetland (FWI) (B) Browns Island (BRI). Adapted from Drexler et al. (in review).

Figure 3. Plots of ^{137}Cs with depth: (A) FW site, (B) BRI site. Purple symbols indicate age of 1963 A.D. or younger based on ^{137}Cs . Light blue symbols indicate age older than 1963 A.D. but younger than 1850 A.D.

Figure 4. Plots of Pb concentration versus depth: (A) FW site (B) BRI site: full profile, upper 3 meters and upper meter. Symbol colors: Purple, 1963 A.D. to present; light blue, 1850 A.D. to 1963 A.D.; green, 1450 A.D. (500 cal yr BP) to 1850 A.D. (100 cal yr BP); red, 350 B.C. (2300 cal yr BP) to 1450 A.D. (500 cal yr BP); black, 4350 A.D. (6300 cal yr BP) to 350 B.C. (2300 cal yr BP); gray, older than 4350 B.C. (6300 cal yr BP).

Figure 5. Plots of Hg concentration versus depth: (A) FW site, (B) BRI site: full profile, upper 3 meters and upper meter. Symbol colors: Purple, 1963 A.D. to present; light blue, 1850 A.D. to 1963 A.D.; green, 1450 A.D. (500 cal yr BP) to 1850 A.D. (100 cal yr BP); red, 350 B.C. (2300 cal yr BP) to 1450 A.D. (500 cal yr BP); black, 4350 A.D. (6300 cal yr BP) to 350 B.C. (2300 cal yr BP); gray, older than 4350 B.C. (6300 cal yr BP).

Figure 6. Plots of $^{206}\text{Pb}/^{207}\text{Pb}$ ratios vs. depth in BRI core: full profile and top 3 meters. Error bars represent 2-sigma analytical uncertainty. Numbers represent model ages for individual depth intervals. Symbol colors: Purple, 1963 A.D. to present; light blue, 1850 A.D. to 1963 A.D.; green, 1450 A.D. (500 cal yr BP) to 1850 A.D. (100 cal yr BP); red, 350 B.C. (2300 cal yr BP) to 1450 A.D. (500 cal yr BP); black, 4350 A.D. (6300 cal yr BP) to 350 B.C. (2300 cal yr BP); gray, older than 4350 B.C. (6300 cal yr BP).

Figure 7. Plots of Pb/Ti versus depth: (A) FW site, (B) BRI site. Symbol colors: Purple, 1963 A.D. to present; light blue, 1850 A.D. to 1963 A.D.; green, 1450 A.D. (500 cal yr BP) to 1850 A.D. (100 cal yr BP); red, 350 B.C. (2300 cal yr BP) to 1450 A.D. (500 cal yr BP); black, 4350 A.D. (6300 cal yr BP) to 350 B.C. (2300 cal yr BP); gray, older than 4350 B.C. (6300 cal yr BP).

Figure 8. Plots of Ti versus Pb in peat in BRI core: (A) full profile. Symbol colors: Purple, 1963 A.D. to present; light blue, 1850 A.D. to 1963 A.D.; green, 1450 A.D. (500 cal yr BP) to 1850 A.D. (100 cal yr BP); red, 350 B.C. (2300 cal yr BP) to 1450 A.D. (500 cal yr BP); black, 4350 A.D. (6300 cal yr BP) to 350 B.C. (2300 cal yr BP); gray, older than 4350 B.C. (6300 cal yr BP); (B) lower profile showing linear-least squares regressions for samples in two age ranges: red: 2300 to 500 cal yr BP; blue: 3500 to 2300 cal yr BP. Ti and Pb are normally distributed within the red and blue age-depth intervals. Black symbols indicate samples in age range 6300 to 3500 cal yr BP (not included in regressions). Colored dashed lines represent linear least-squares regressions; dotted lines represent 95% confidence intervals. Grey lines show constant values of

Pb/Ti, passing through the origin. The intercepts on the vertical axis represent estimates of the Pb content of the organic fraction of the peat.

Figure 9. Plots of $^{208}\text{Pb}/^{207}\text{Pb}$ vs. $^{206}\text{Pb}/^{207}\text{Pb}$: (A) BRI cores. Symbol colors: Purple, 1963 A.D. to present; light blue, 1850 A.D. to 1963 A.D.; green, 1450 A.D. (500 cal yr BP) to 1850 A.D. (100 cal yr BP); red, 350 B.C. (2300 cal yr BP) to 1450 A.D. (500 cal yr BP); black, 4350 A.D. (6300 cal yr BP) to 350 B.C. (2300 cal yr BP); gray, older than 4350 B.C. (6300 cal yr BP). (B) Sacramento River and San Francisco Bay sediments (from Dunlap et al. 2008). Fields for leaded gasoline used in U.S.A from Dunlap et al. (2008) and sources within.

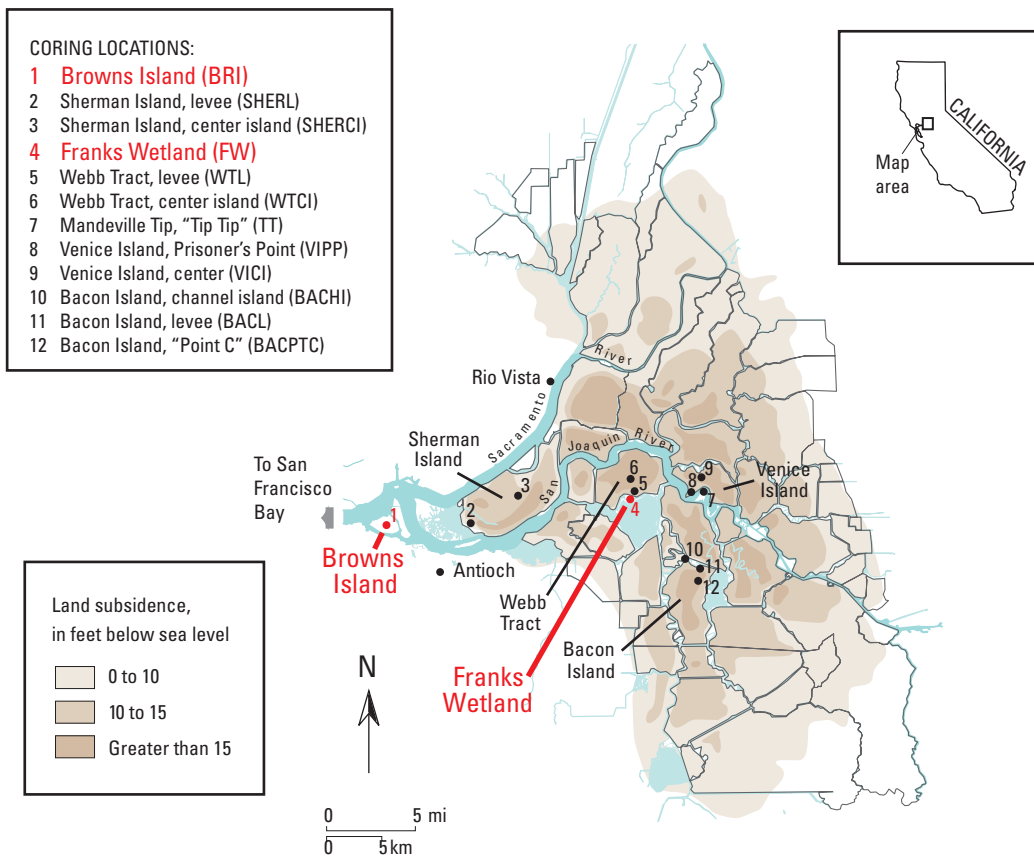
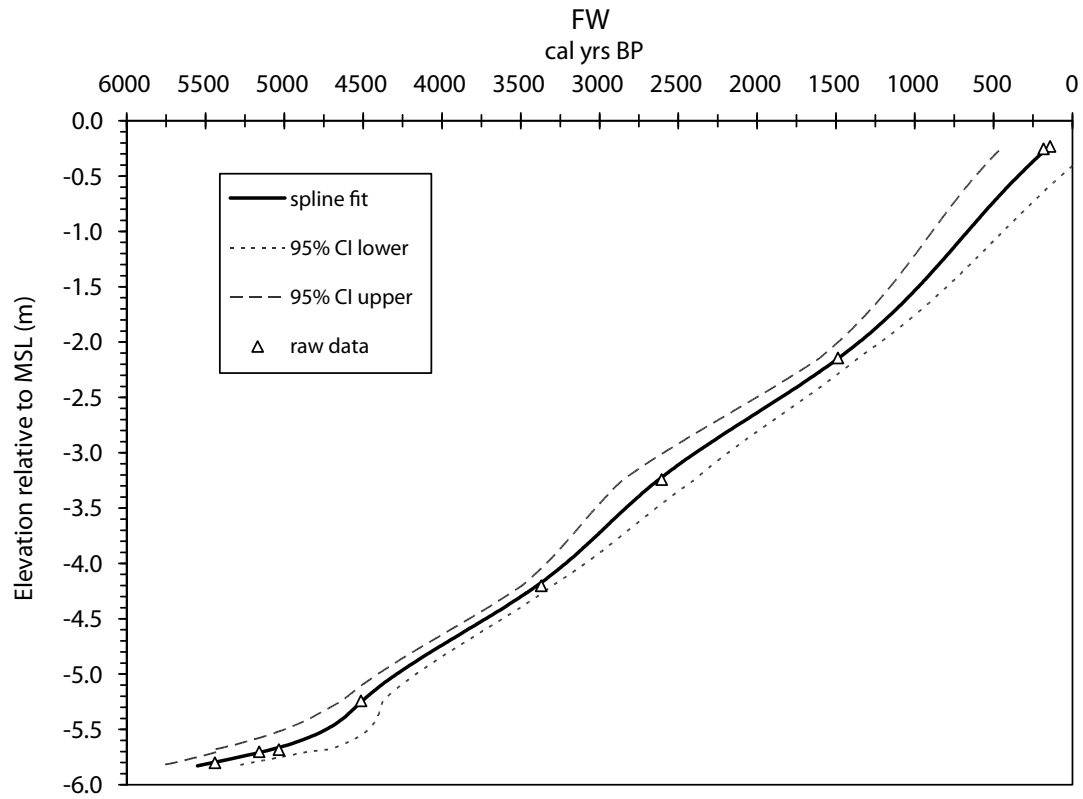


Fig. 1

A



B

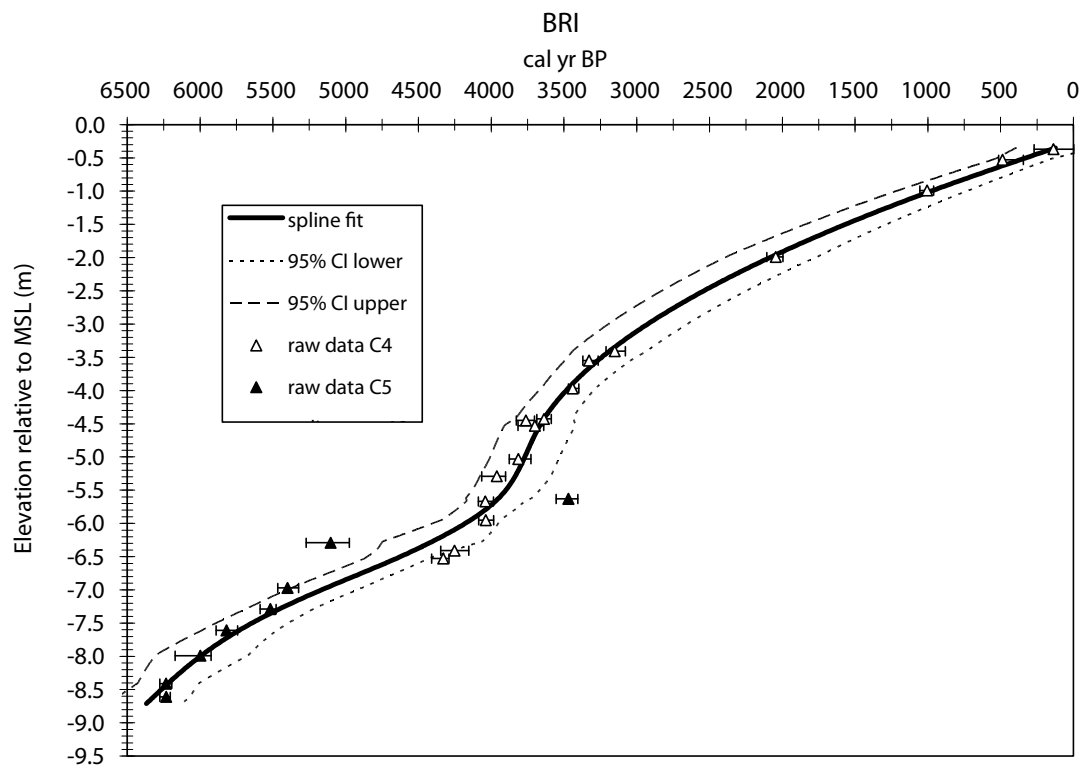
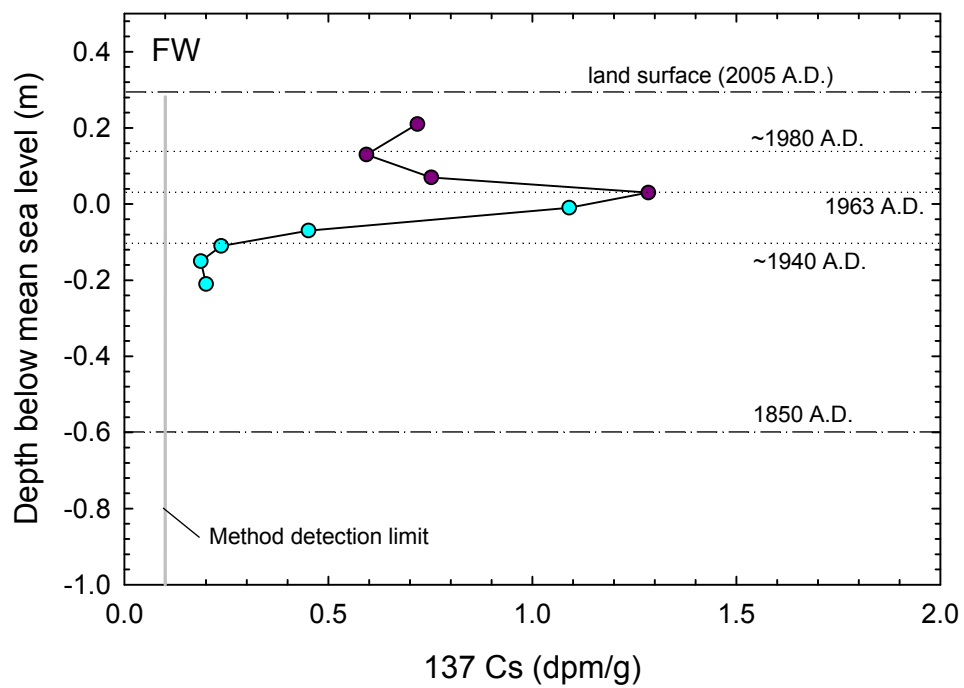


Fig. 2

A



B

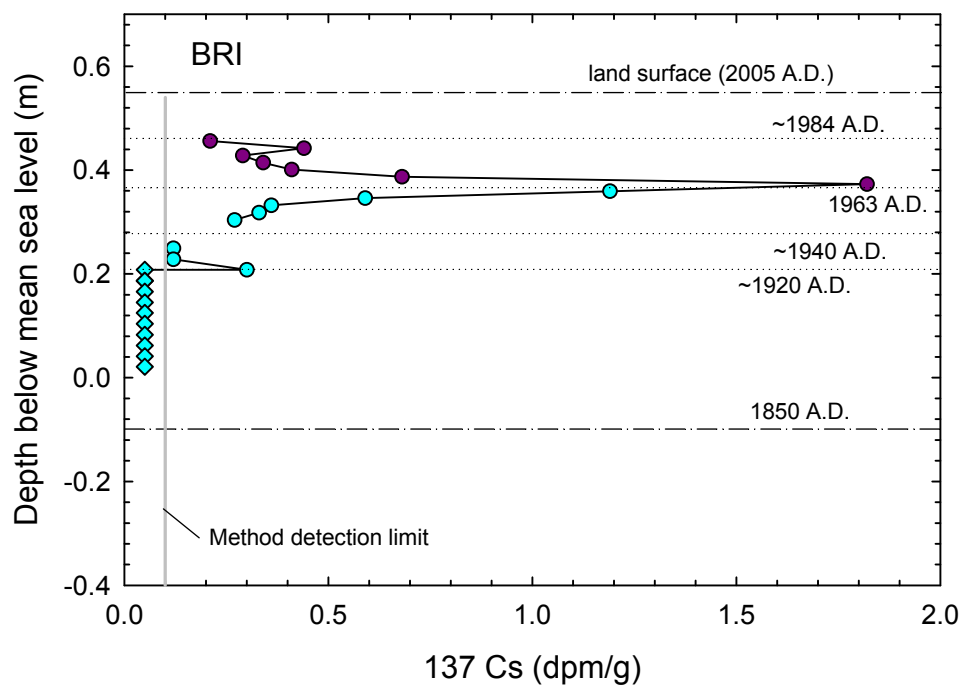
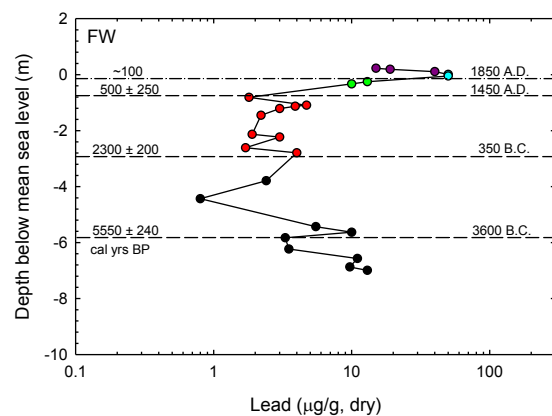


Fig. 3

A



B

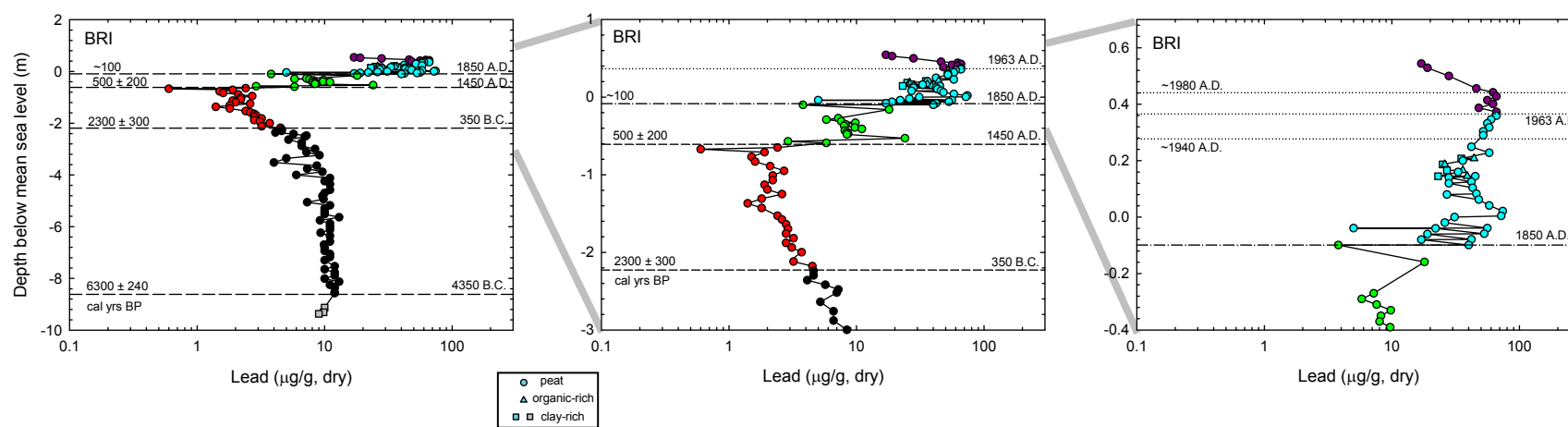
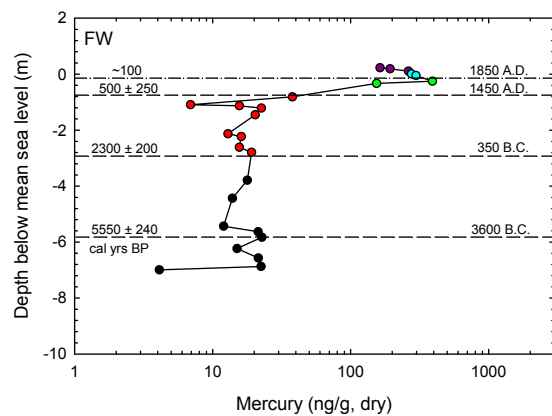


Fig. 4

A



B

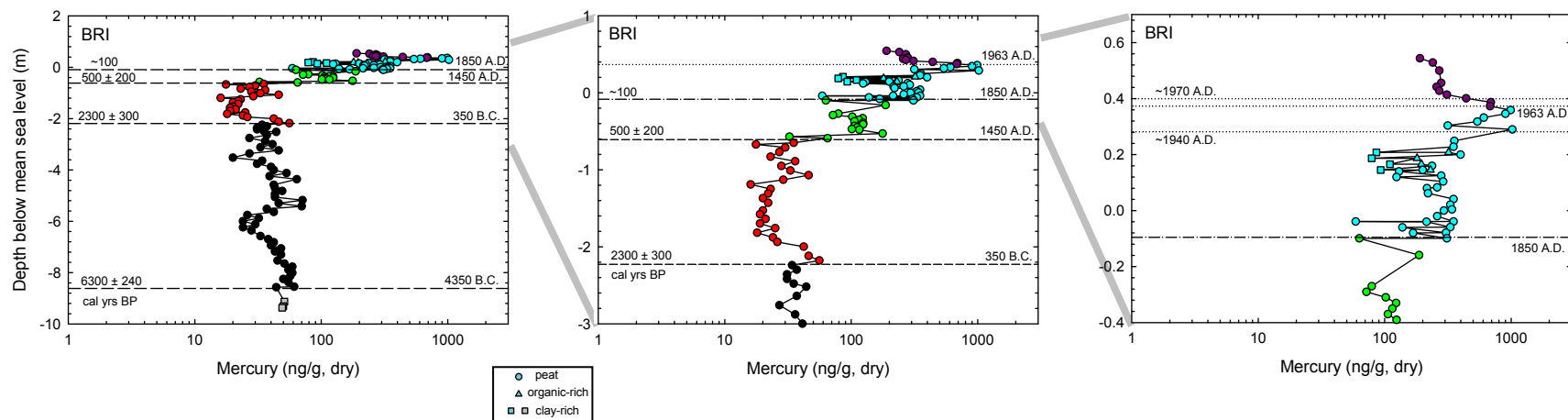


Fig. 5

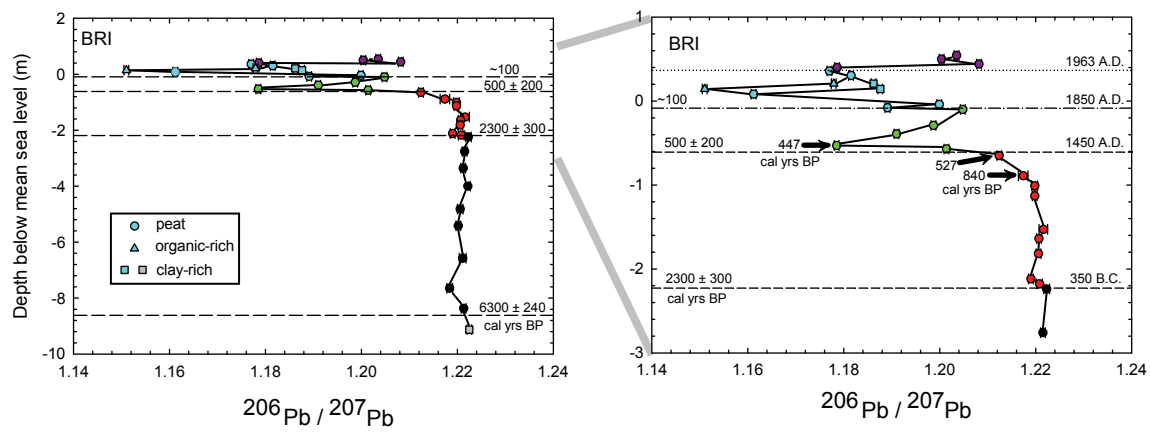
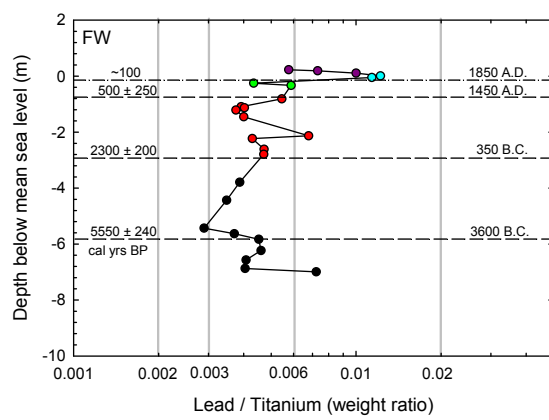


Fig. 6

A



B

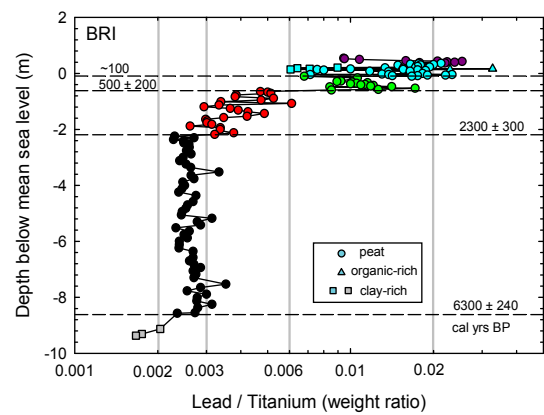


Fig. 7

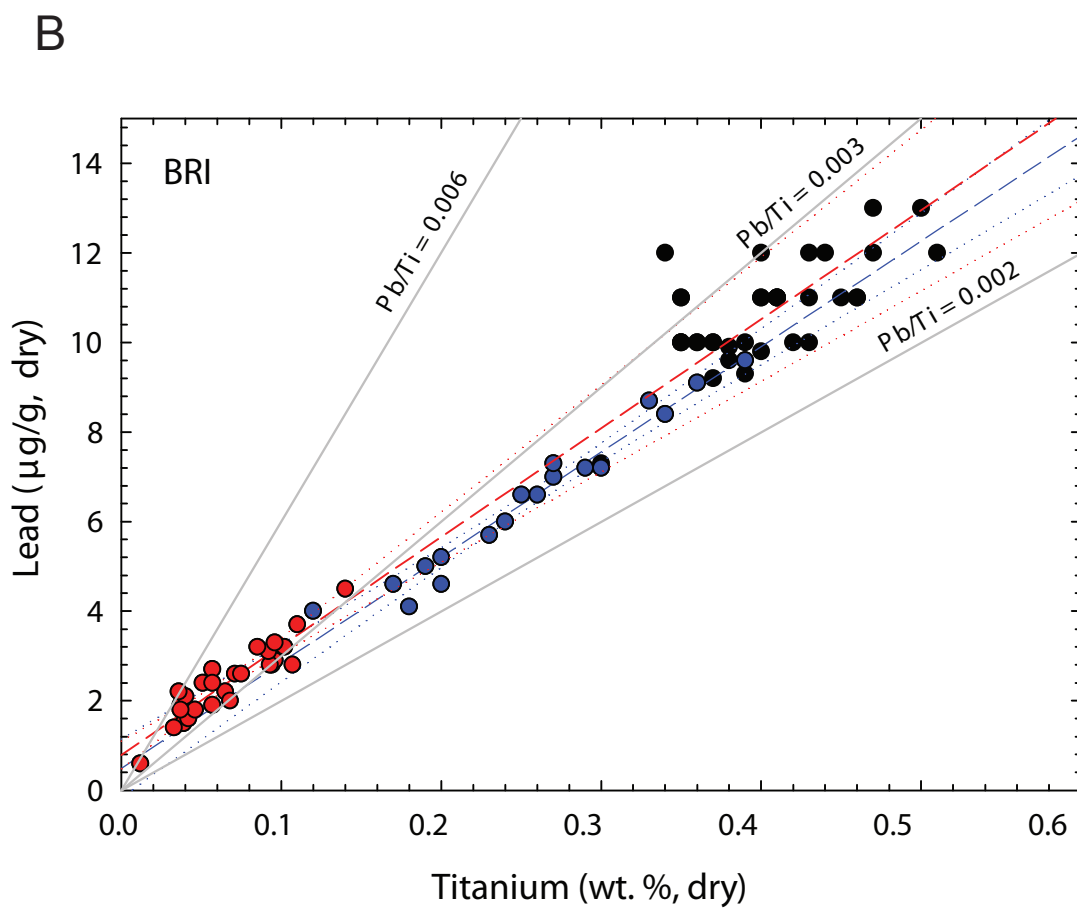
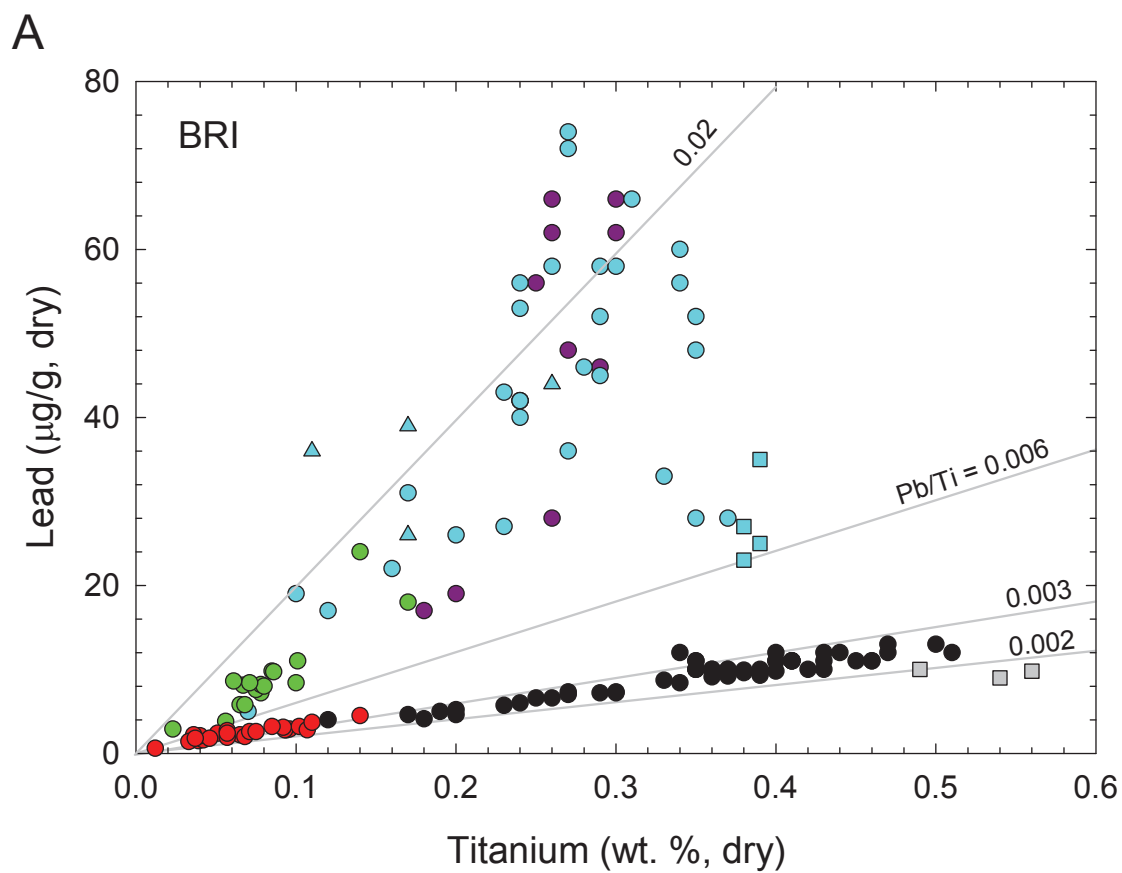


Fig. 8

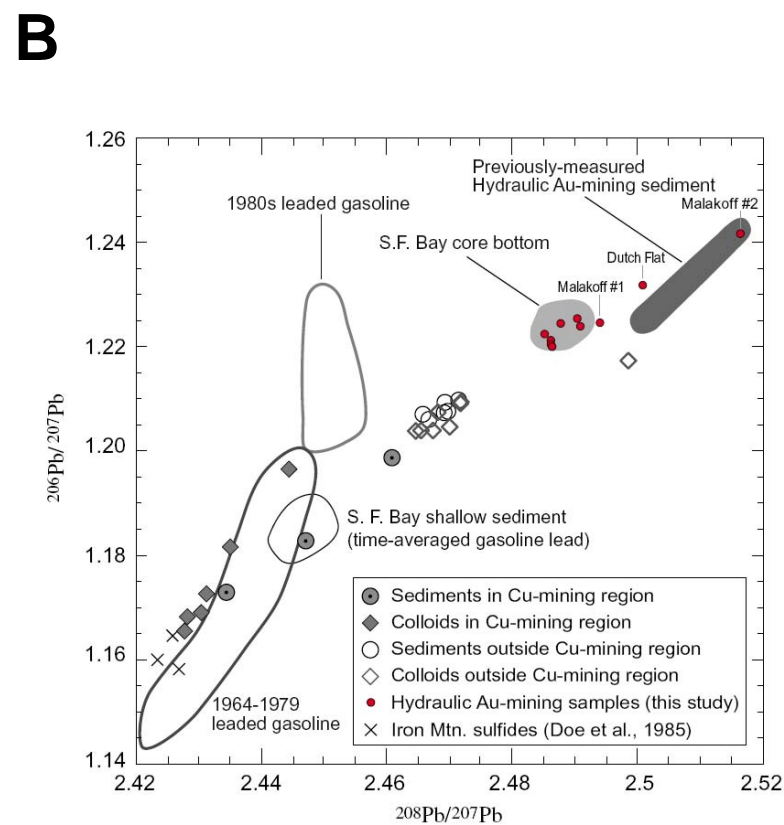
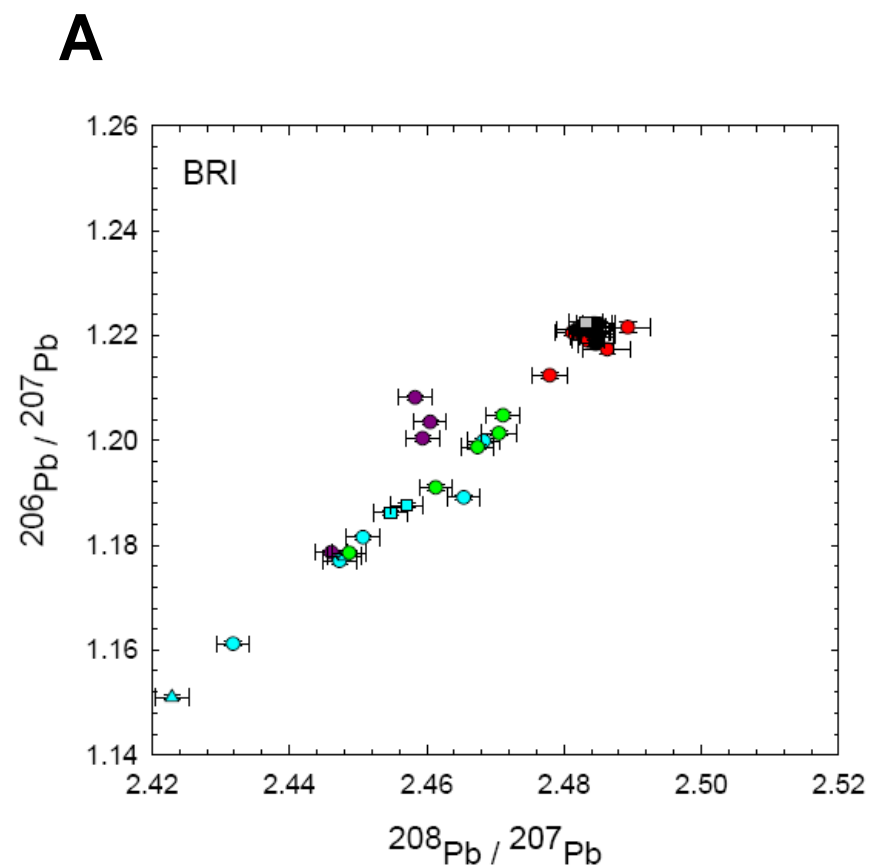


Fig. 9

Supplemental Figures

Figure S1. Vertical profiles of ash content and, concentrations of inorganic-proxy elements Al, Ga, Sc, Ti, and Zr: (A) FW site, (B) BRI site. Symbol colors: Purple, 1963 A.D. to present; light blue, 1850 A.D. to 1963 A.D.; green, 1450 A.D. (500 cal yr BP) to 1850 A.D. (100 cal yr BP); red, 350 B.C. (2300 cal yr BP) to 1450 A.D. (500 cal yr BP); black, 4350 A.D. (6300 cal yr BP) to 350 B.C. (2300 cal yr BP); gray, older than 4350 B.C. (6300 cal yr BP).

Figure S2. Plots of ash content versus concentration of various elements (Al, Ga, Sc, Ti, and Zr) indicative of the inorganic component of peat: (A) FW cores, (B) BRI cores.

Figure S3. Plots of $^{208}\text{Pb}/^{207}\text{Pb}$ vs. depth in BRI core: (A) full profile, (B) top 3 meters. Symbol colors: Purple, 1963 A.D. to present; light blue, 1850 A.D. to 1963 A.D.; green, 1450 A.D. (500 cal yr BP) to 1850 A.D. (100 cal yr BP); red, 350 B.C. (2300 cal yr BP) to 1450 A.D. (500 cal yr BP); black, 4350 A.D. (6300 cal yr BP) to 350 B.C. (2300 cal yr BP); gray, older than 4350 B.C. (6300 cal yr BP).

Figure S4. Plots of Ti versus Pb in peat in FW core: (A) full profile, (B) lower profile. Symbol colors: Purple, 1963 A.D. to present; light blue, 1850 A.D. to 1963 A.D.; green, 1450 A.D. (500 cal yr BP) to 1850 A.D. (100 cal yr BP); red, 350 B.C. (2300 cal yr BP) to 1450 A.D. (500 cal yr BP); black, 4350 A.D. (6300 cal yr BP) to 350 B.C. (2300 cal yr BP); gray, older than 4350 B.C. (6300 cal yr BP).

Figure S5. Plots of Al versus Pb in peat: (A) FW site, full profile, (B) FW site, lower profile, (C) BRI site, full profile, (D) BRI site, lower profile. Symbol colors for (A), (B), and (C): Purple, 1963 A.D. to present; light blue, 1850 A.D. to 1963 A.D.; green, 1450 A.D. (500 cal yr BP) to 1850 A.D. (100 cal yr BP); red, 350 B.C. (2300 cal yr BP) to 1450 A.D. (500 cal yr BP); black, 4350 A.D. (6300 cal yr BP) to 350 B.C. (2300 cal yr BP); gray, older than 4350 B.C. (6300 cal yr BP); Symbol colors for (D): red: 2300 to 500 cal yr BP; blue: 3500 to 2300 cal yr BP; black: 6300 to 3500 cal yr BP. Al and Pb are normally distributed within the red and blue age-depth intervals. Colored dashed lines in (B) and (D) represent linear least-squares regressions.

Figure S6. Plots of Ga versus Pb in peat: (A) FW site, full profile, (B) FW site, lower profile, (C) BRI site, full profile, (D) BRI site, lower profile. Symbol colors for (A), (B), and (C): Purple, 1963 A.D. to present; light blue, 1850 A.D. to 1963 A.D.; green, 1450 A.D. (500 cal yr BP) to 1850 A.D. (100 cal yr BP); red, 350 B.C. (2300 cal yr BP) to 1450 A.D. (500 cal yr BP); black, 4350 A.D. (6300 cal yr BP) to 350 B.C. (2300 cal yr BP); gray, older than 4350 B.C. (6300 cal yr BP); Symbol colors for (D): red: 2300 to 500 cal yr BP; blue: 3500 to 2300 cal yr BP; black: 6300 to 3500 cal yr BP. Ga and Pb are normally distributed within the red and blue age-depth intervals. Colored dashed lines in (B) and (D) represent linear least-squares regressions.

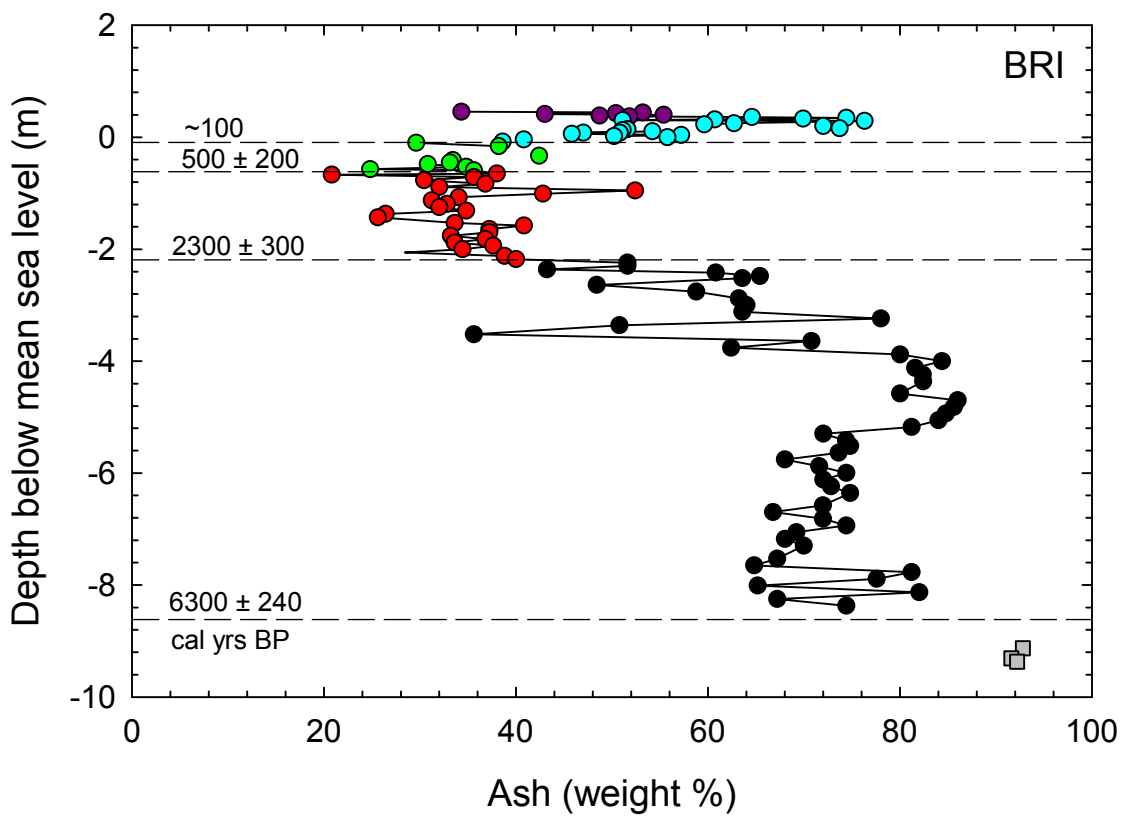
Figure S7. Plots of Sc versus Pb in peat: (A) FW site, full profile, (B) FW site, lower profile, (C) BRI site, full profile, (D) BRI site, lower profile. Symbol colors for (A), (B), and (C): Purple, 1963 A.D. to present; light blue, 1850 A.D. to 1963 A.D.; green, 1450 A.D. (500 cal yr BP) to 1850 A.D. (100 cal yr BP); red, 350 B.C. (2300 cal yr BP) to 1450 A.D. (500 cal yr BP); black, 4350 A.D. (6300 cal yr BP) to 350 B.C. (2300 cal yr BP); gray, older than 4350 B.C. (6300 cal yr BP); Symbol colors for (D): red: 2300 to 500 cal yr BP; blue: 3500 to 2300 cal yr BP; black:

6300 to 3500 cal yr BP. Sc and Pb are normally distributed within the red and blue age-depth intervals. Colored dashed lines in (B) and (D) represent linear least-squares regressions.

Figure S8. Plots of Zr versus Pb in peat: (A) FW site, full profile, (B) FW site, lower profile, (C) BRI site, full profile, (D) BRI site, lower profile. Symbol colors for (A), (B), and (C): Purple, 1963 A.D. to present; light blue, 1850 A.D. to 1963 A.D.; green, 1450 A.D. (500 cal yr BP) to 1850 A.D. (100 cal yr BP); red, 350 B.C. (2300 cal yr BP) to 1450 A.D. (500 cal yr BP); black, 4350 A.D. (6300 cal yr BP) to 350 B.C. (2300 cal yr BP); gray, older than 4350 B.C. (6300 cal yr BP); Symbol colors for (D): red: 2300 to 500 cal yr BP; blue: 3500 to 2300 cal yr BP; black: 6300 to 3500 cal yr BP. Zr and Pb are normally distributed within the red and blue age-depth intervals. Colored dashed lines in (B) and (D) represent linear least-squares regressions.

Figure S9. Plots of Pb/Hg ratio versus depth: (A) FW site, (B) BRI site, full profile, top 3 meters, and top meter. Symbol colors: Purple, 1963 A.D. to present; light blue, 1850 A.D. to 1963 A.D.; green, 1450 A.D. (500 cal yr BP) to 1850 A.D. (100 cal yr BP); red, 350 B.C. (2300 cal yr BP) to 1450 A.D. (500 cal yr BP); black, 4350 A.D. (6300 cal yr BP) to 350 B.C. (2300 cal yr BP); gray, older than 4350 B.C. (6300 cal yr BP).

Figure S10. Plots relating Pb, Hg and Ti for the BRI site: (A) $\log(\text{Pb})$ vs. $\log(\text{Hg})$, (B) $\log(\text{Pb}/\text{Ti})$ vs. $\log(\text{Hg}/\text{Ti})$, (C) Ti vs. $\log(\text{Pb}/\text{Hg})$. Symbol colors: Purple, 1963 A.D. to present; light blue, 1850 A.D. to 1963 A.D.; green, 1450 A.D. (500 cal yr BP) to 1850 A.D. (100 cal yr BP); red, 350 B.C. (2300 cal yr BP) to 1450 A.D. (500 cal yr BP); black, 4350 A.D. (6300 cal yr BP) to 350 B.C. (2300 cal yr BP); gray, older than 4350 B.C. (6300 cal yr BP).



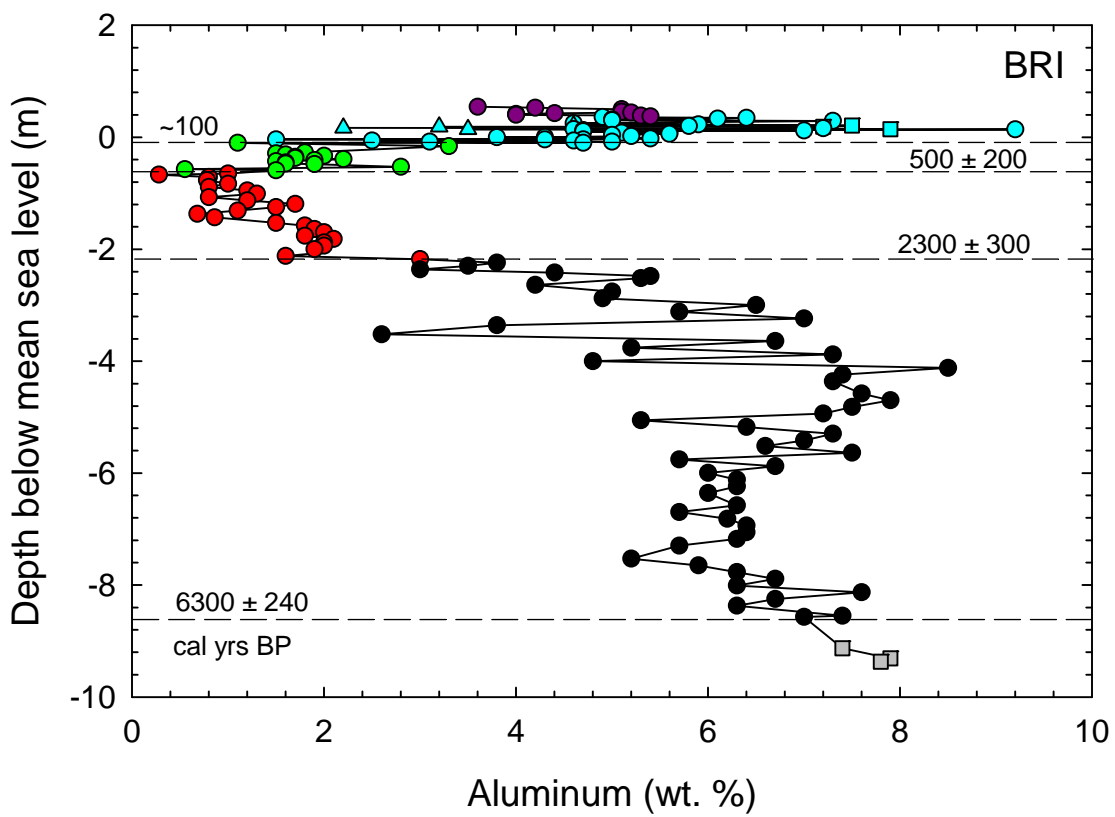


Fig. S-1A-2

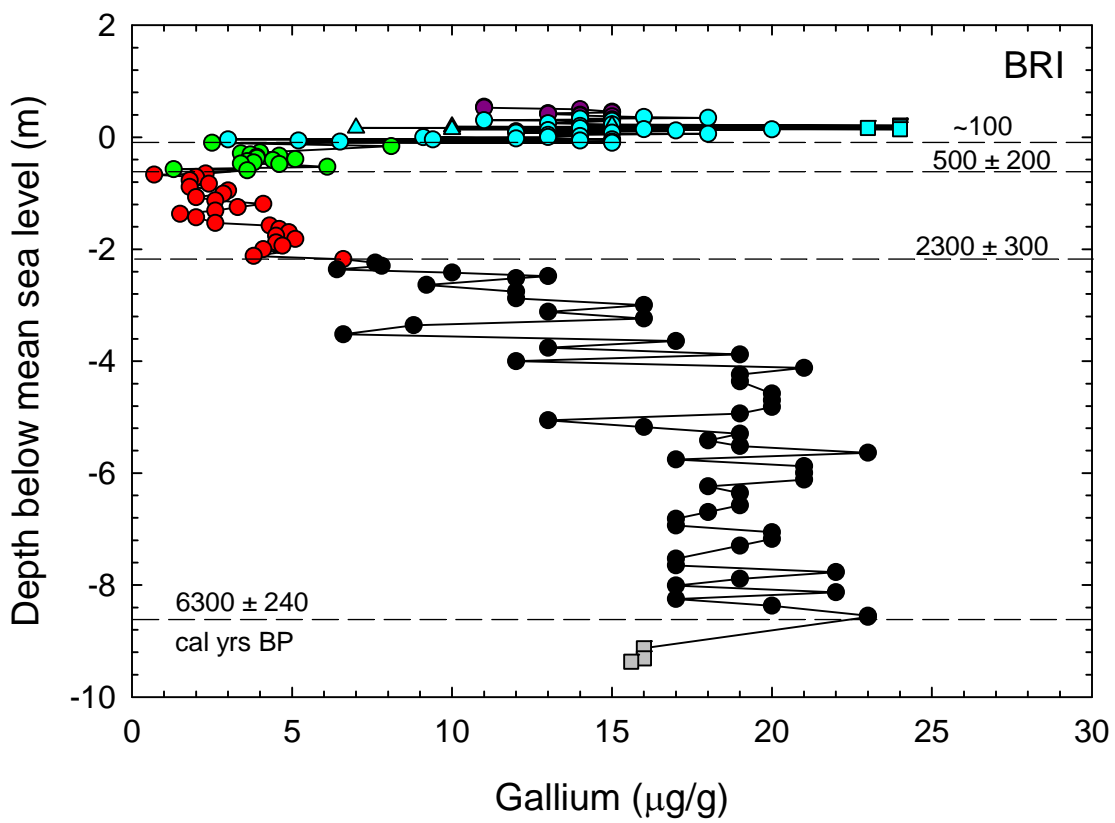


Fig. S-1A-3

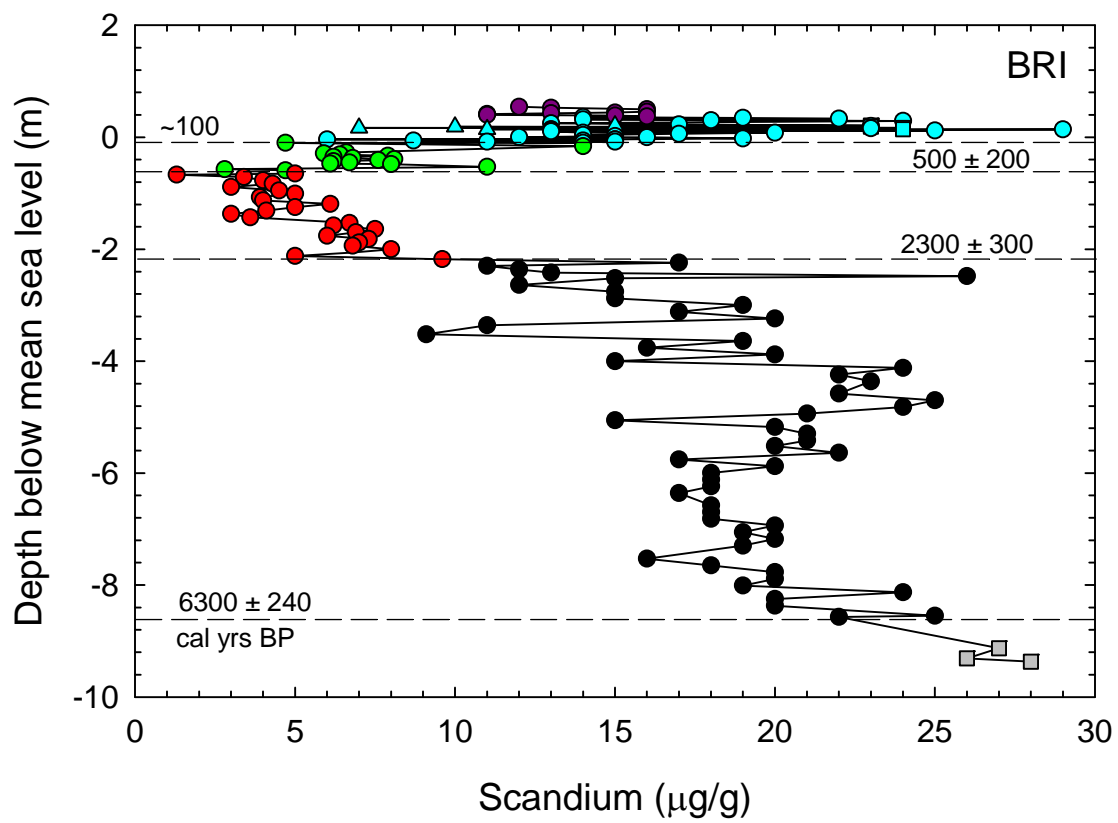


Fig. S-1A-4

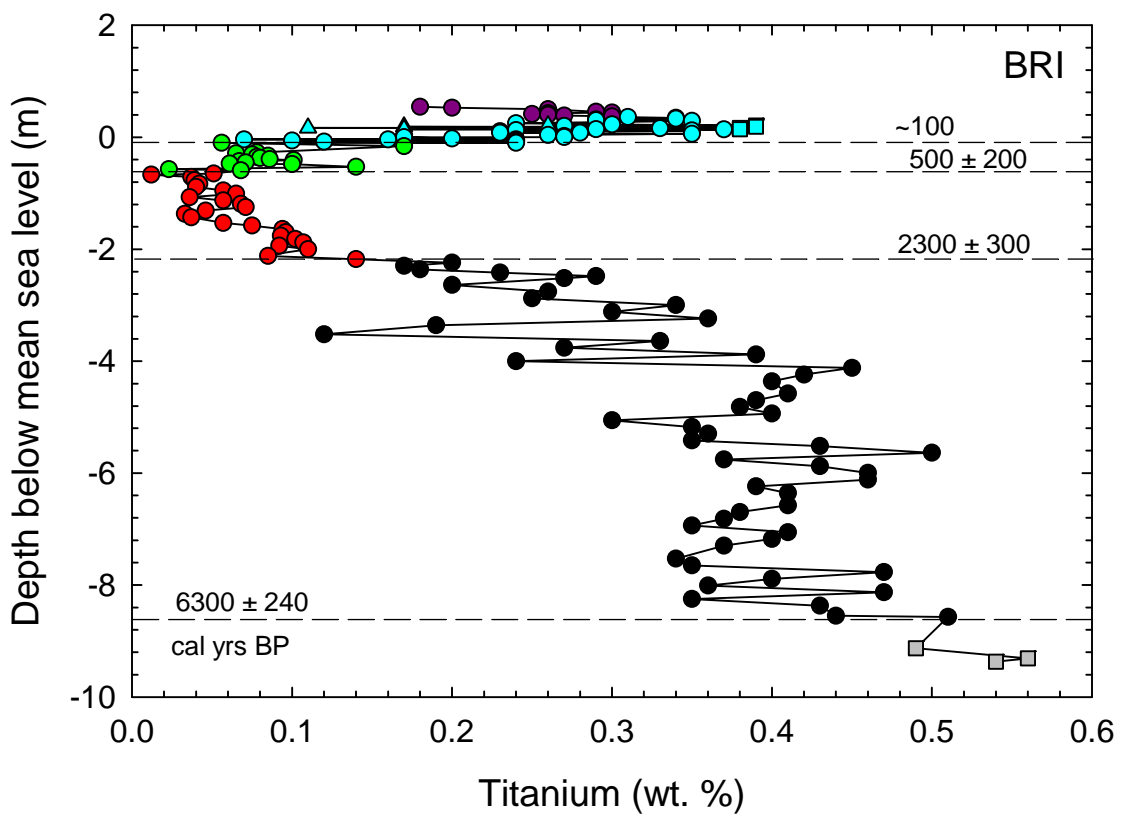


Fig. S-1A-5

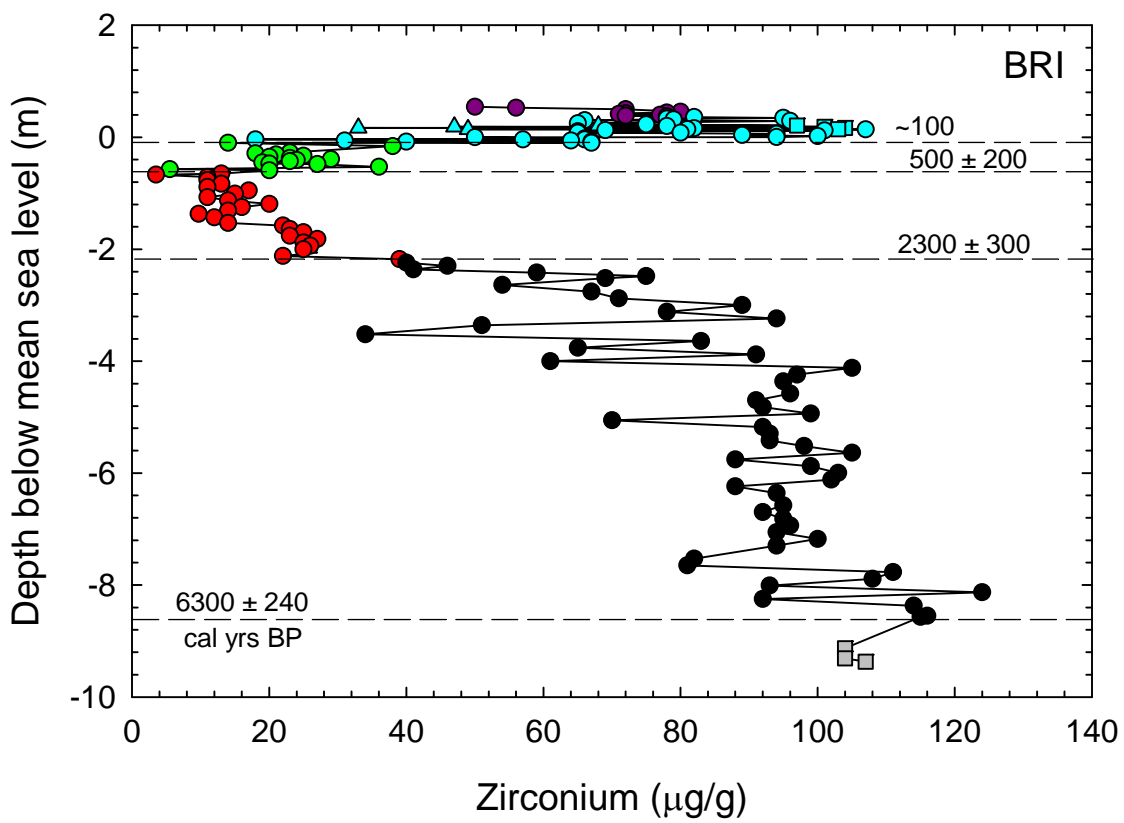


Fig. S-1A-6

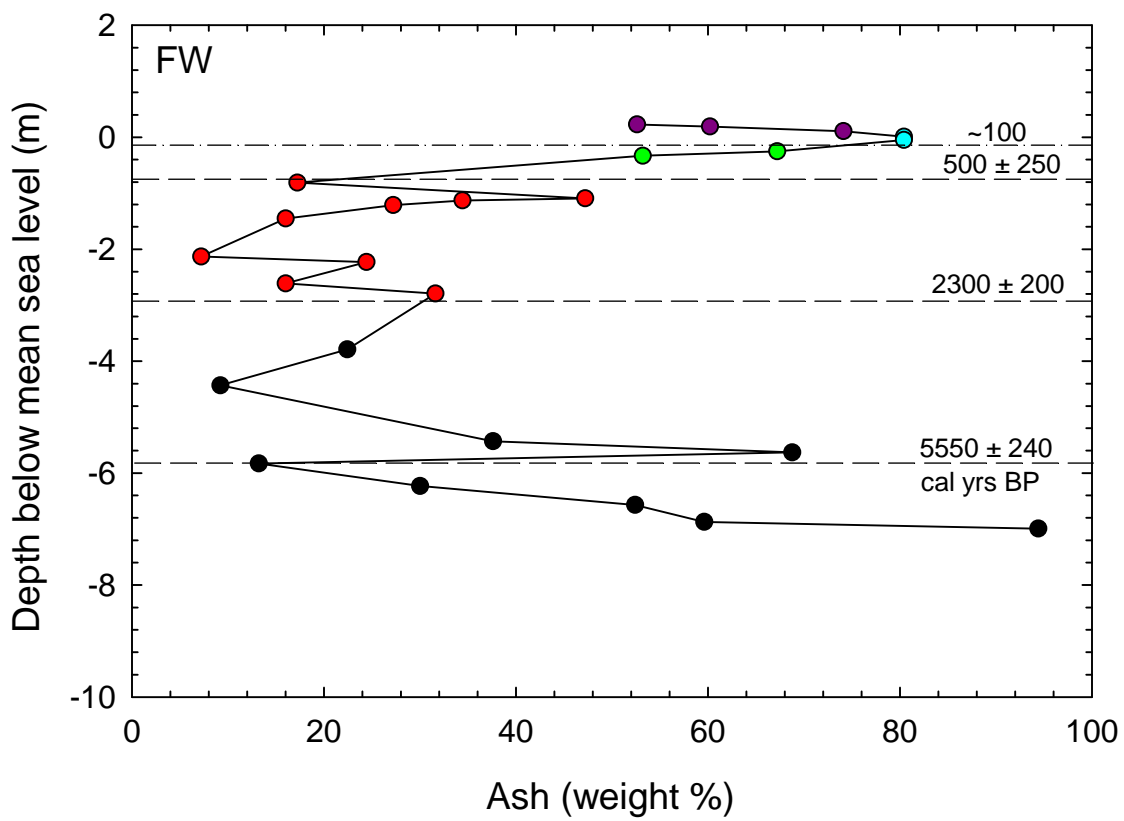


Fig. S-1B-1

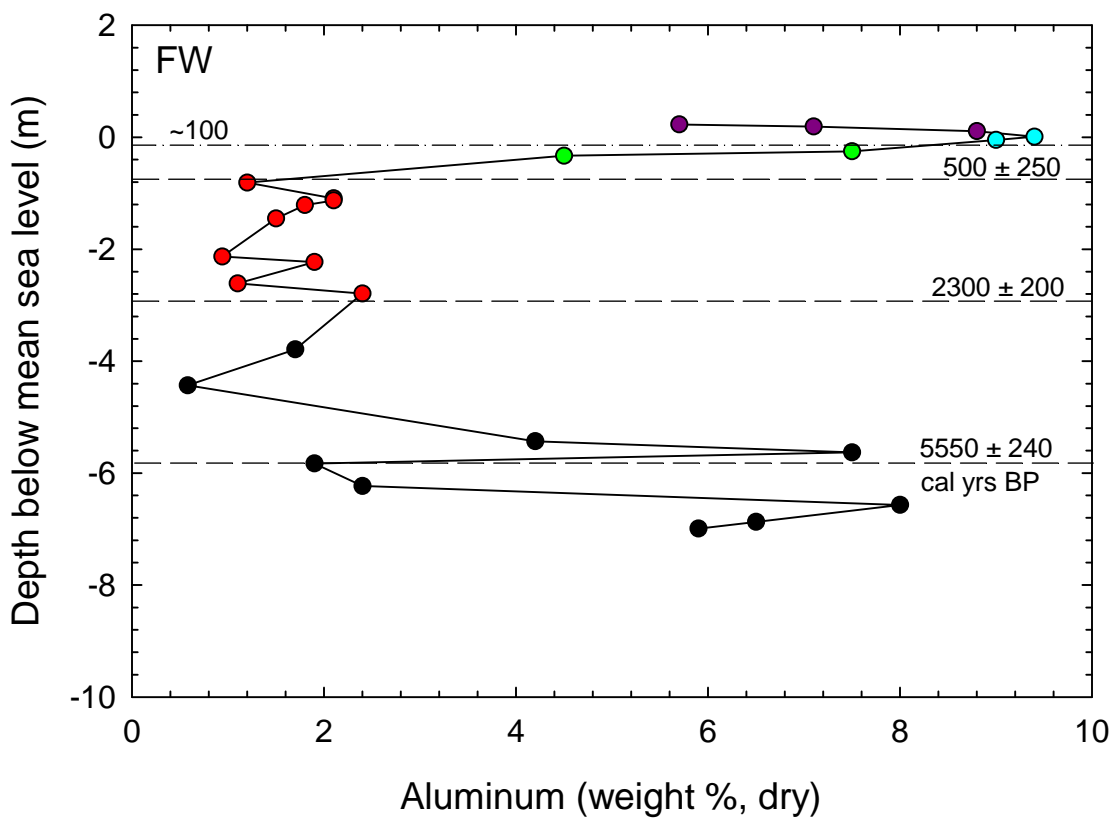
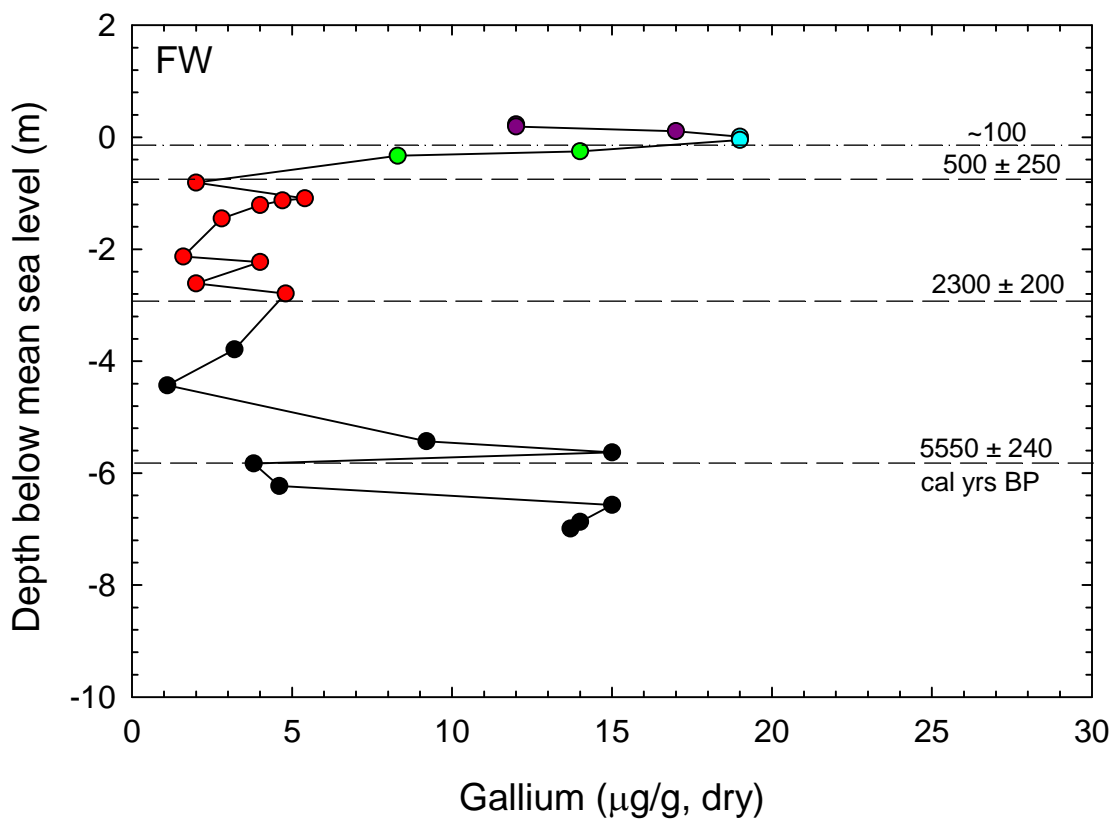


Fig. S-1B-2



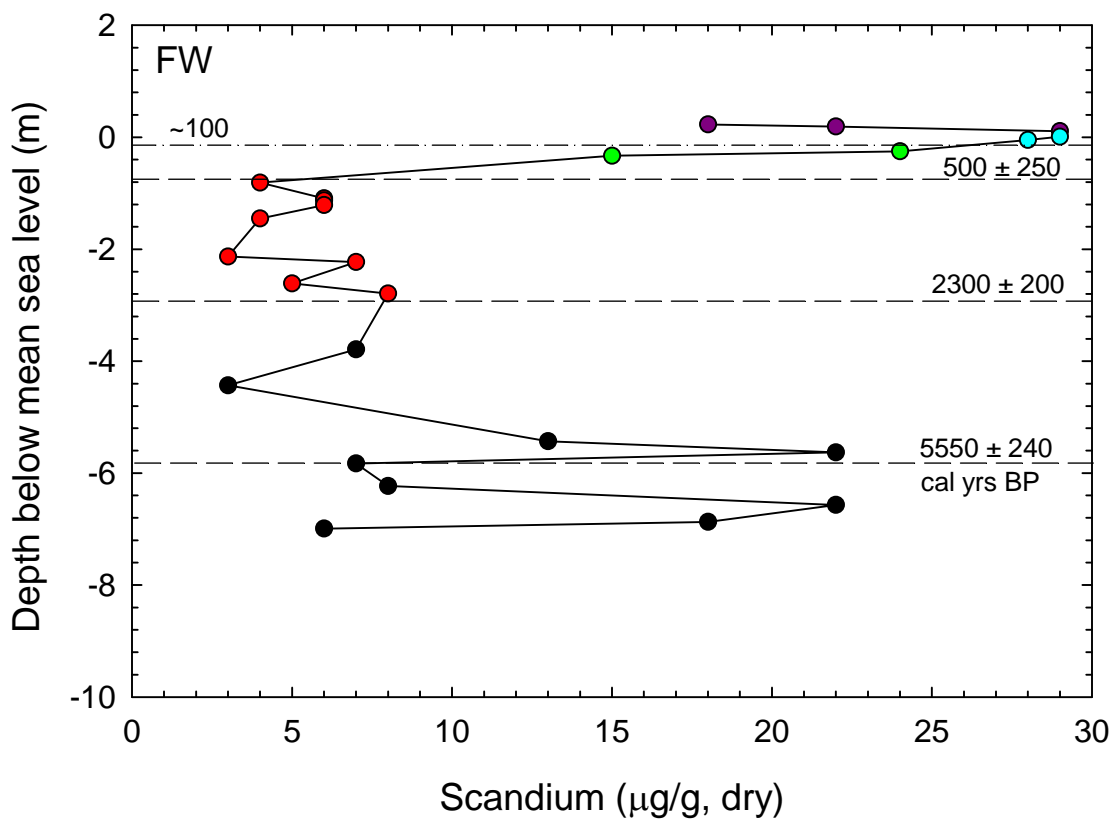


Fig. S-1B-4

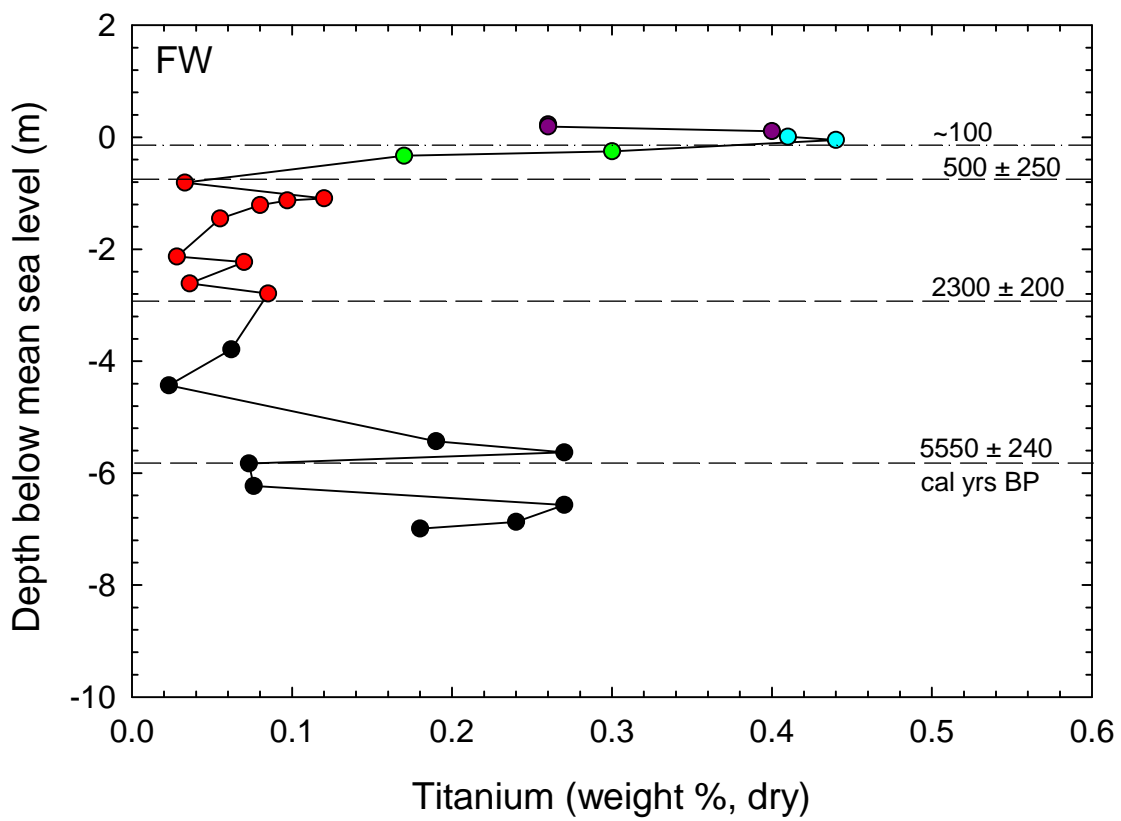


Fig. S-1B-5

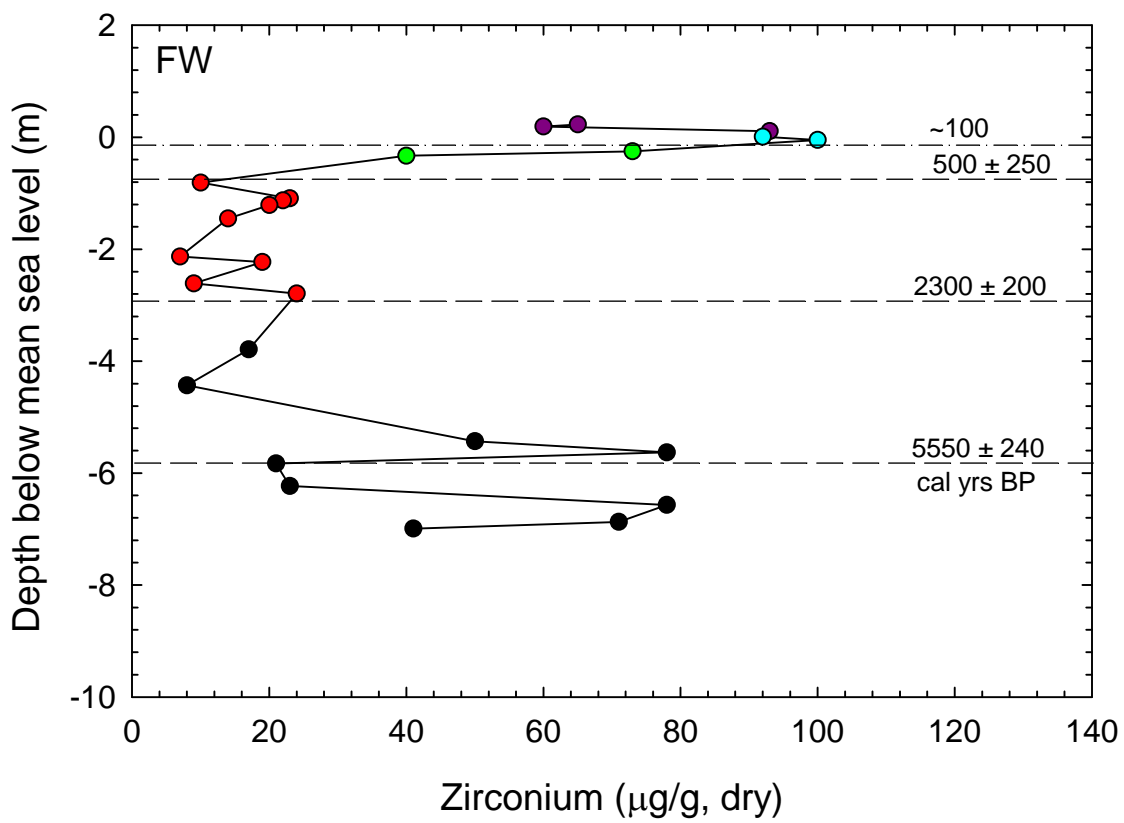


Fig. S-1B-6

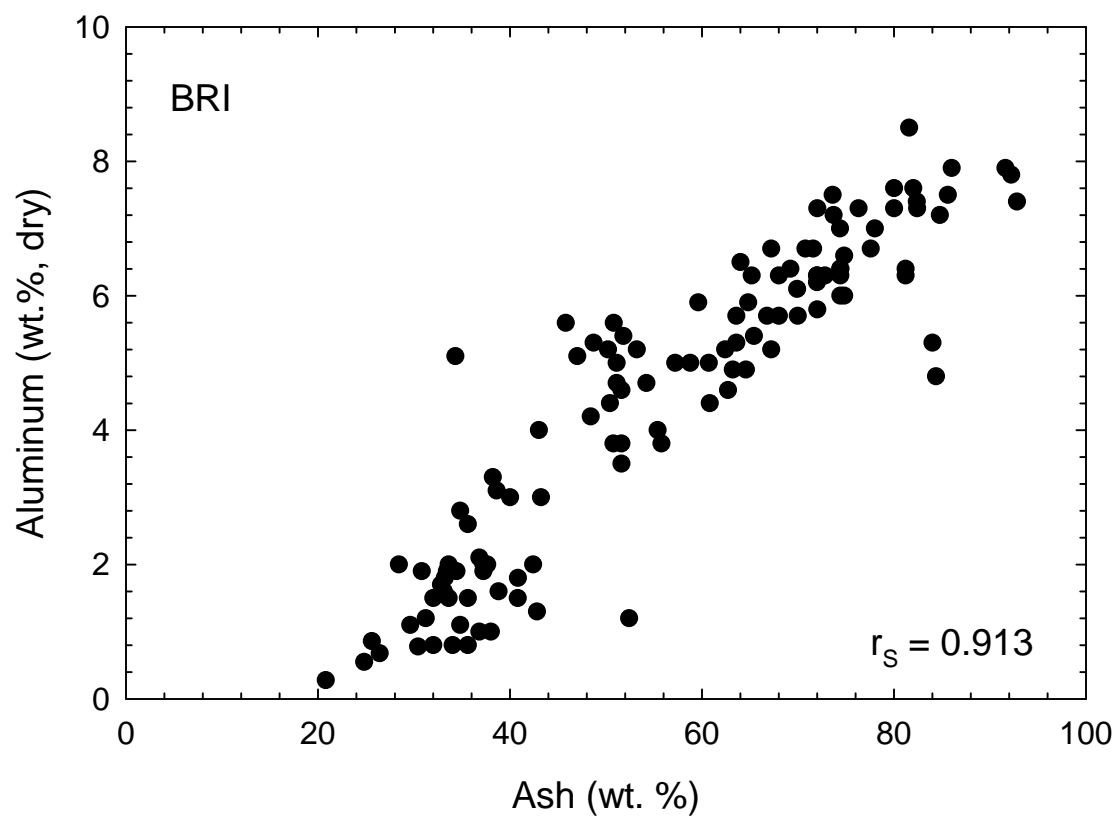


Fig. S-2A-1

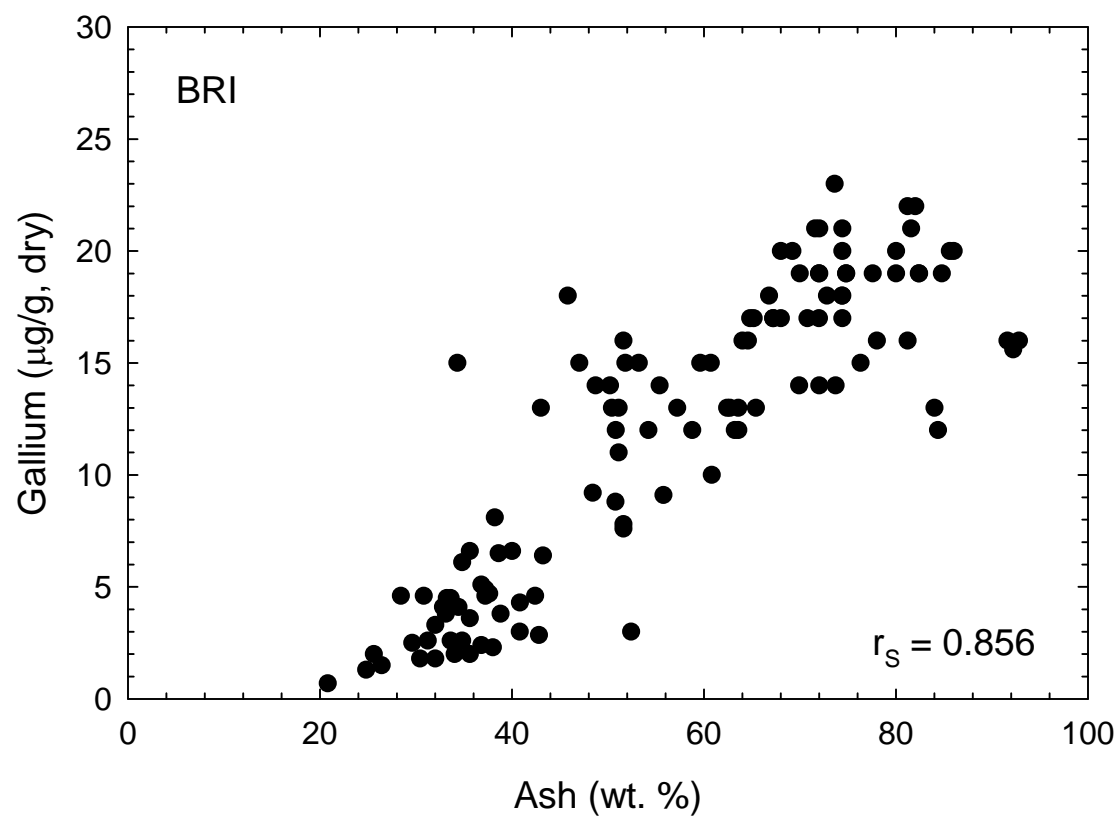


Fig. S-2A-2

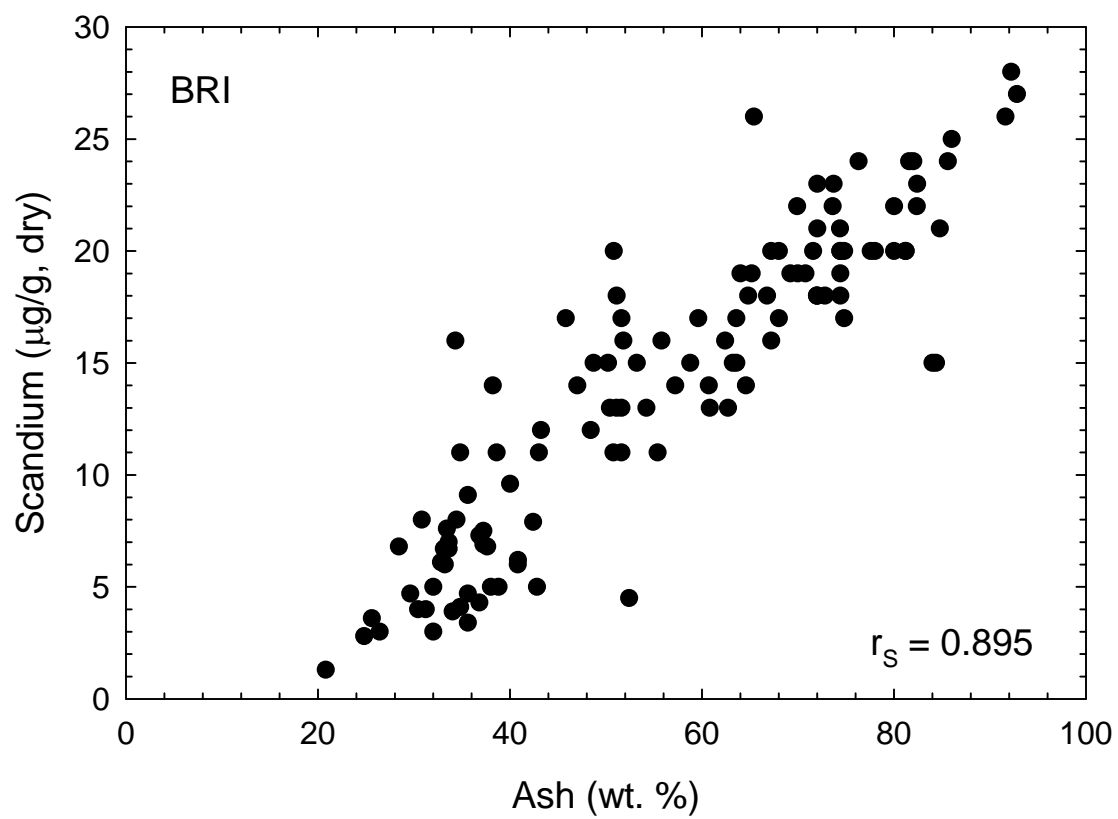


Fig. S-2A-3

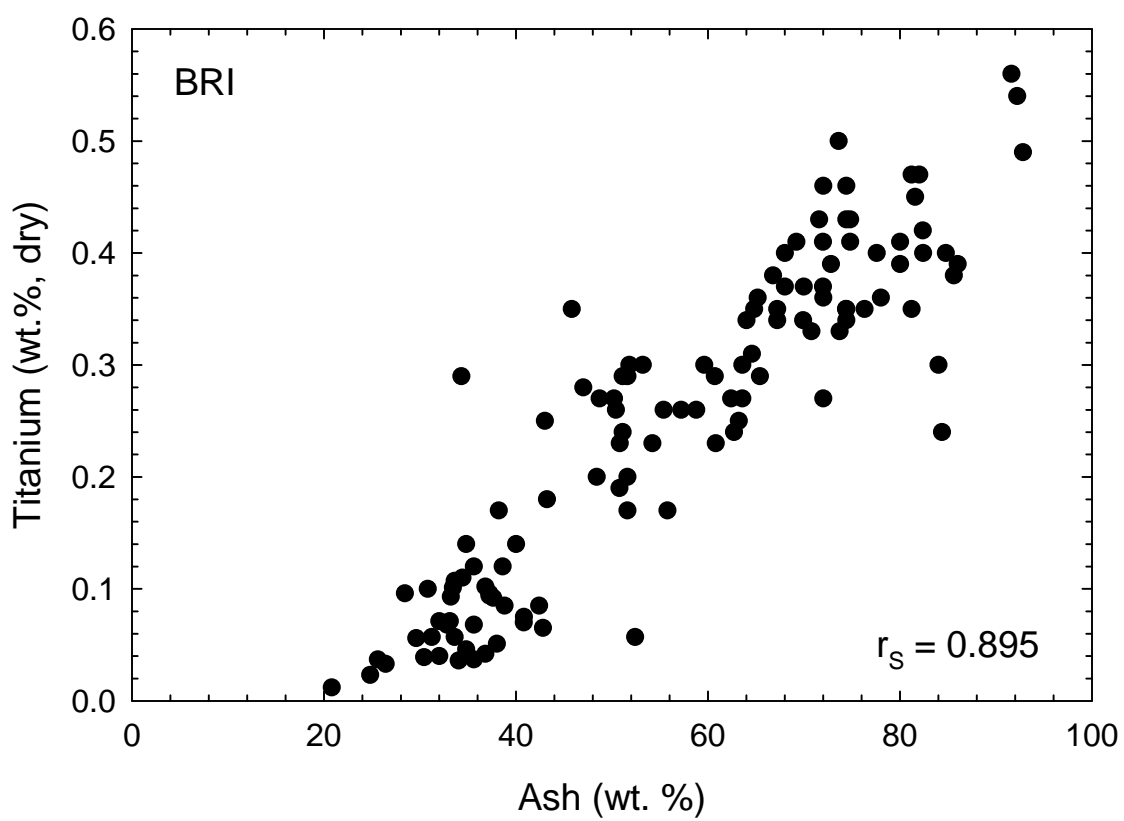


Fig. S-2A-4

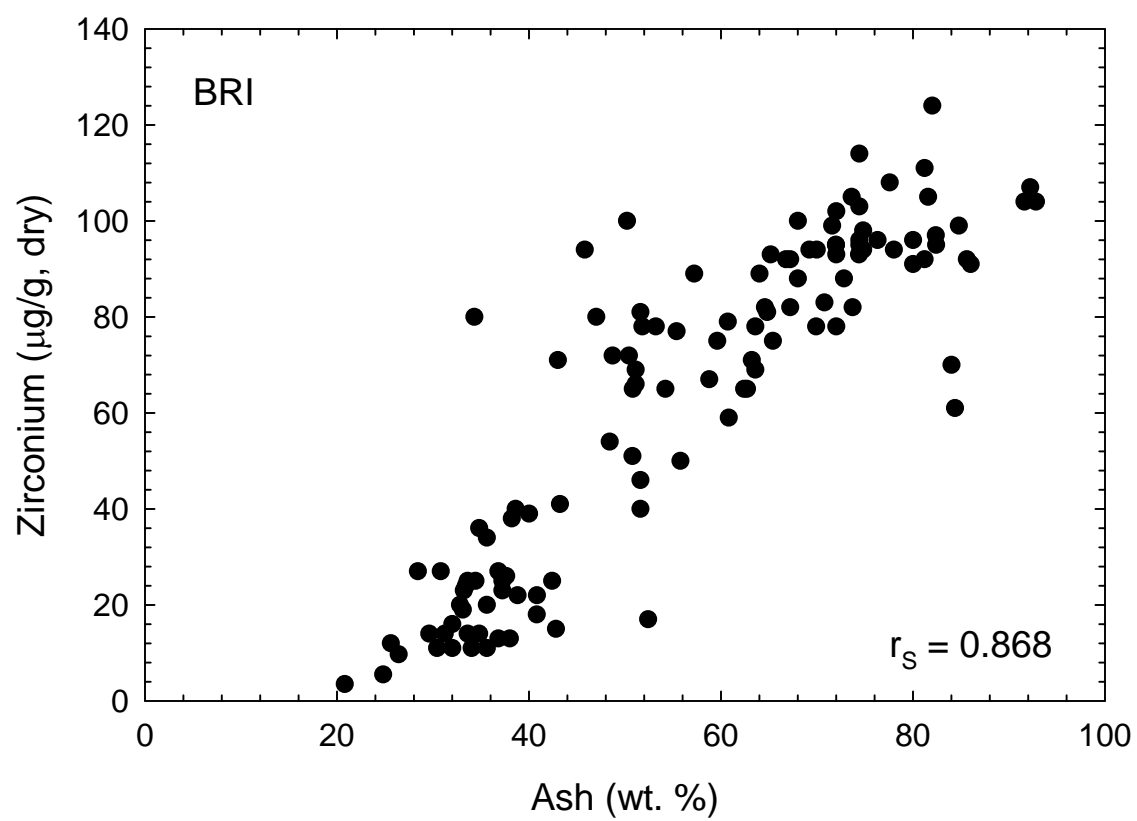


Fig. S-2A-5

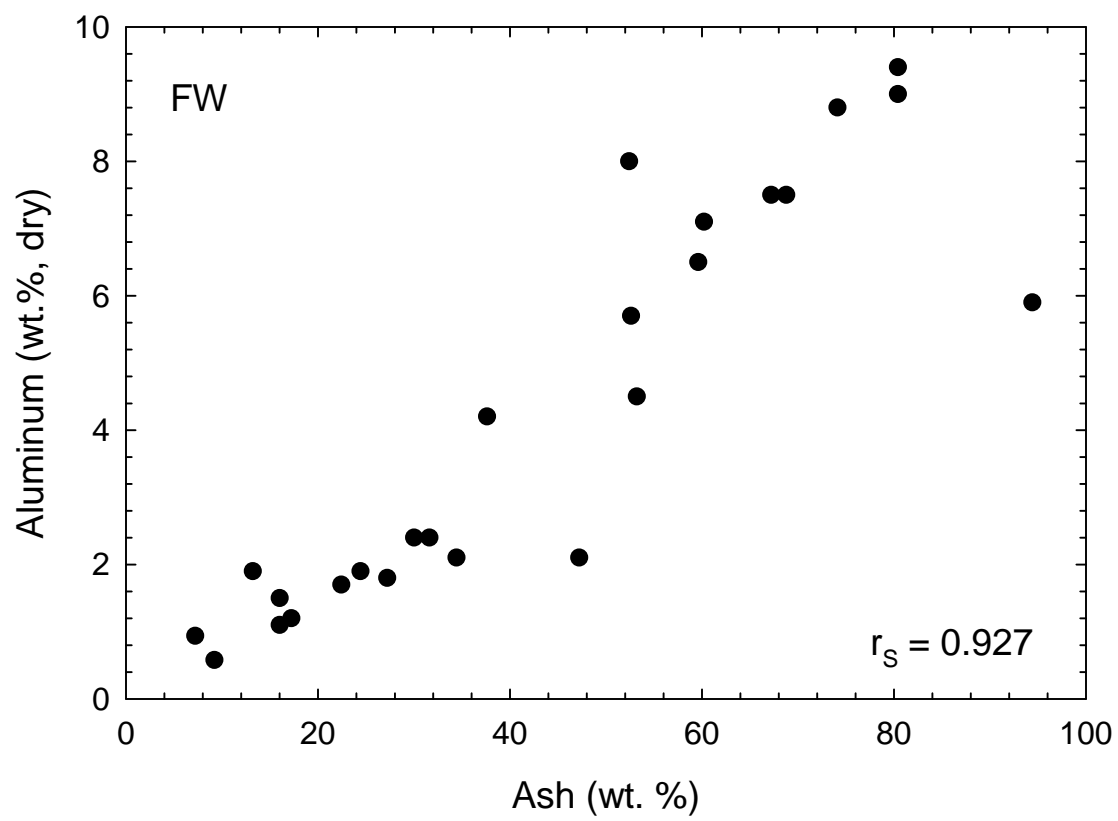


Fig. S-2B-1

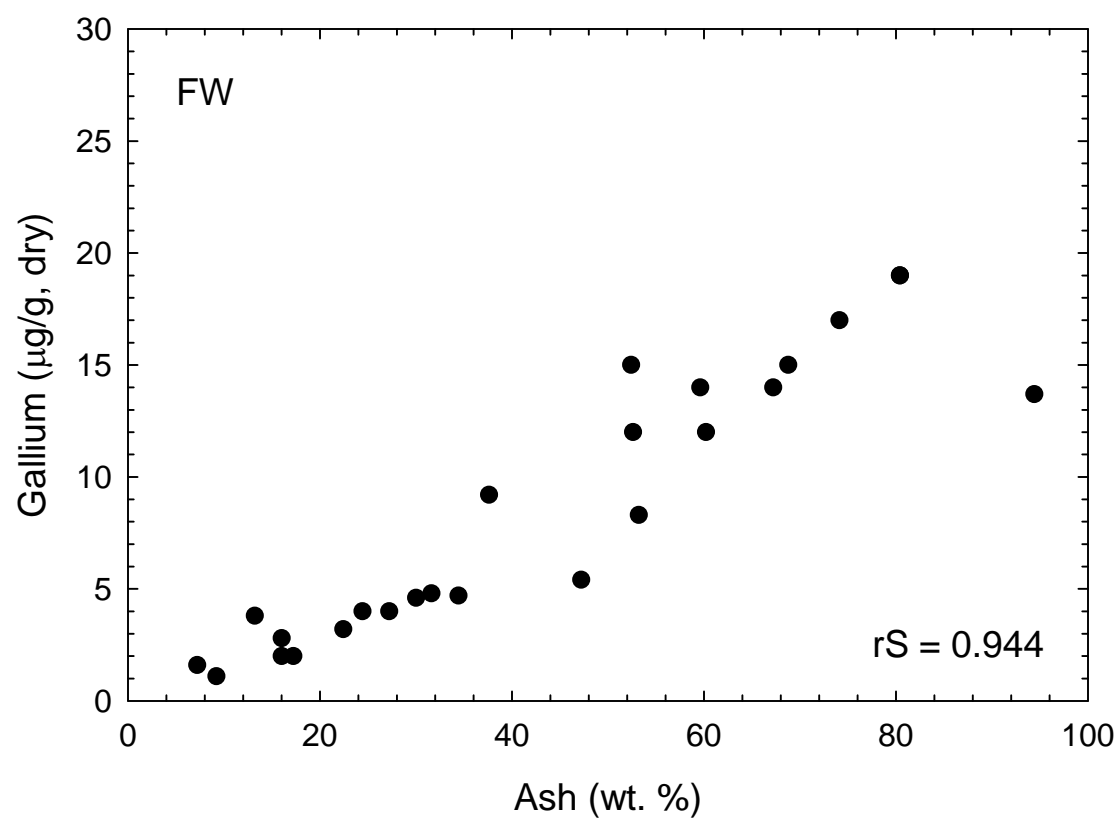


Fig. S-2B-2

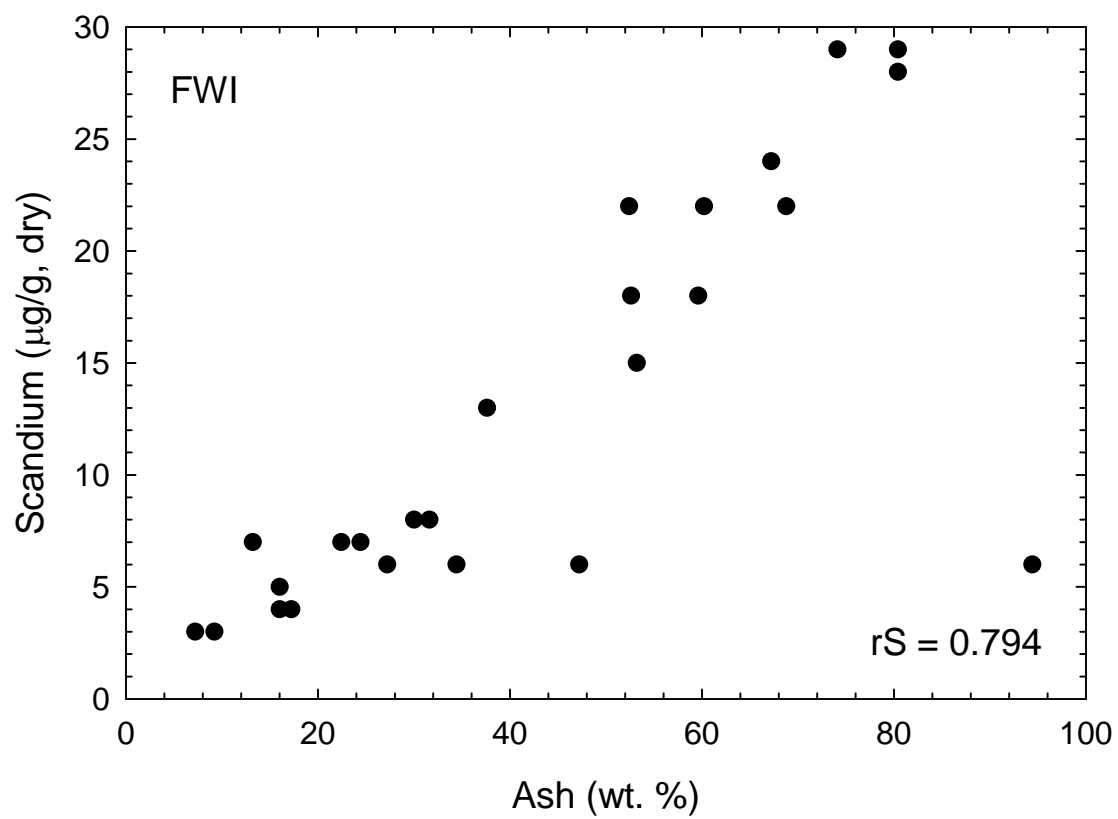


Fig. S-2B-3

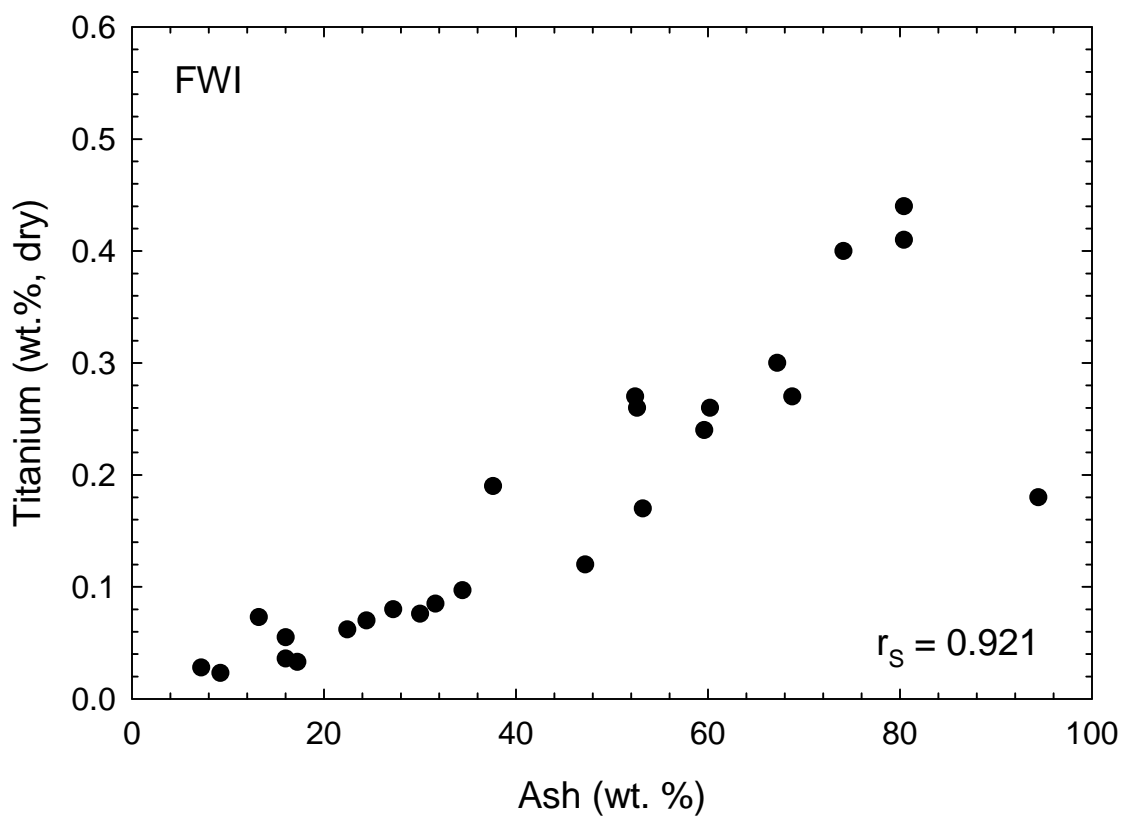


Fig. S-2B-4

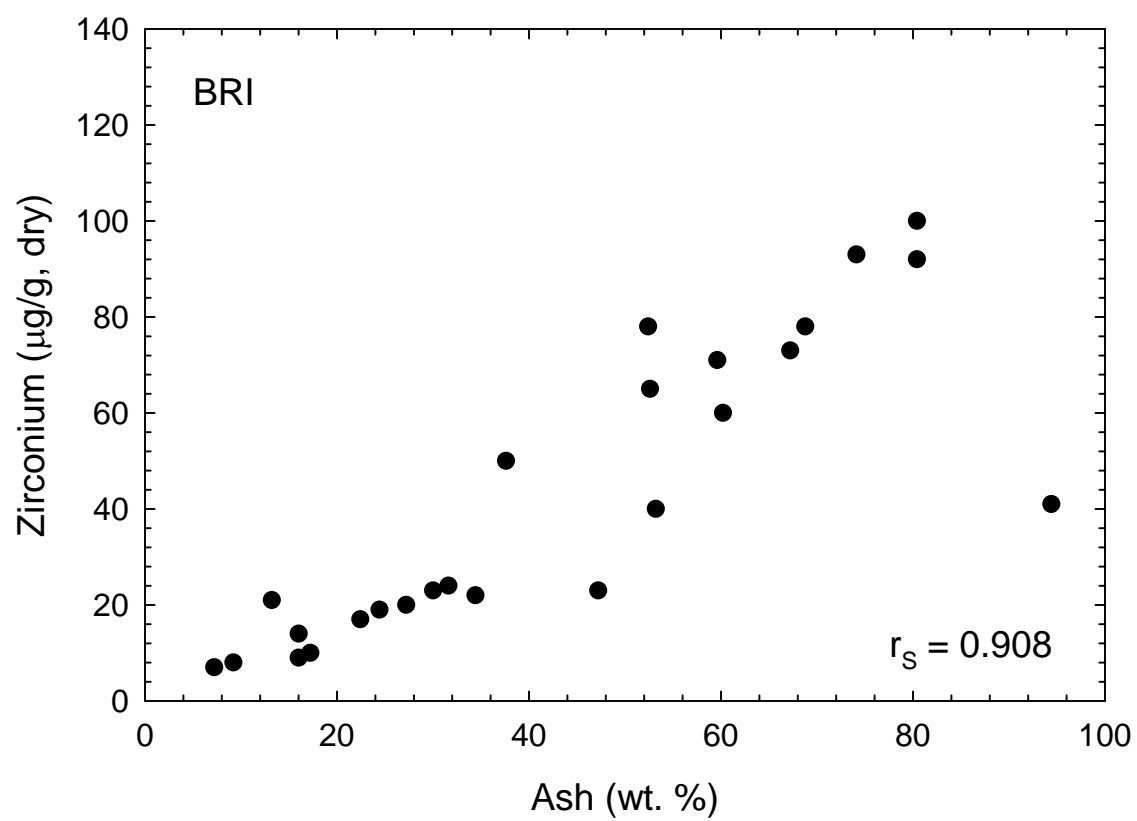


Fig. S-2B-5

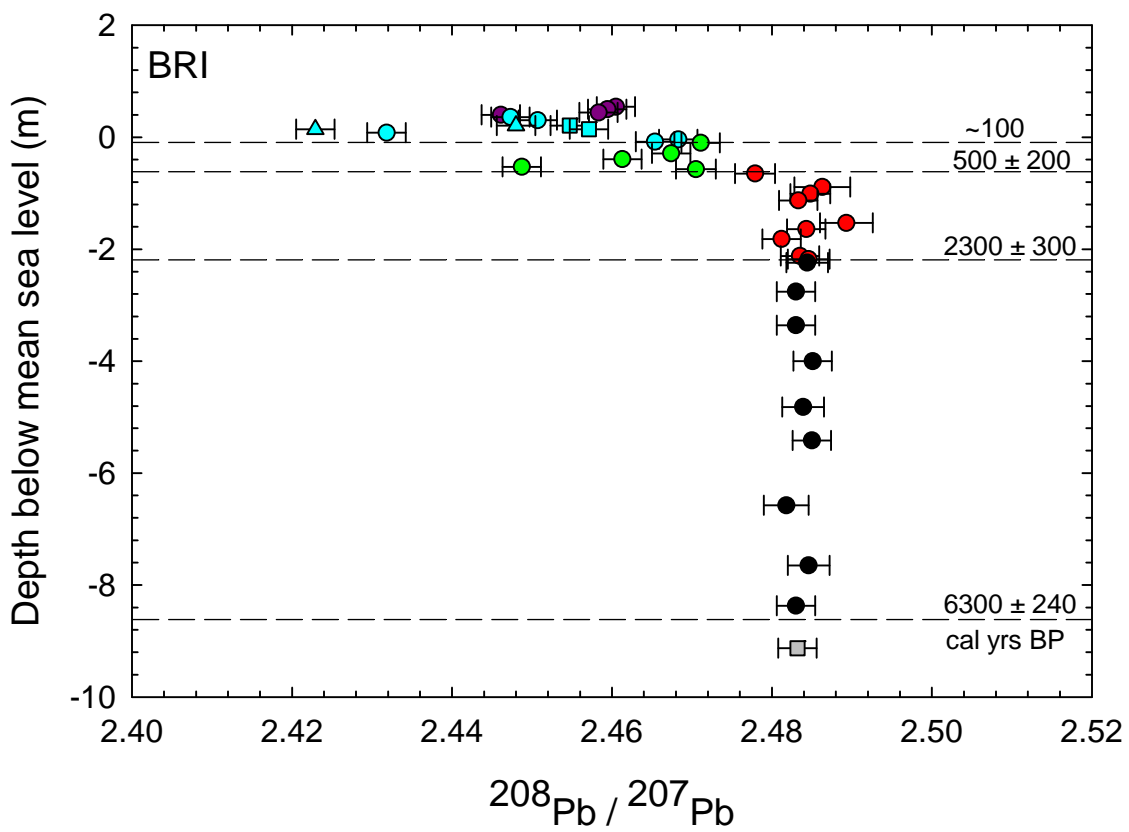


Fig. S-3A

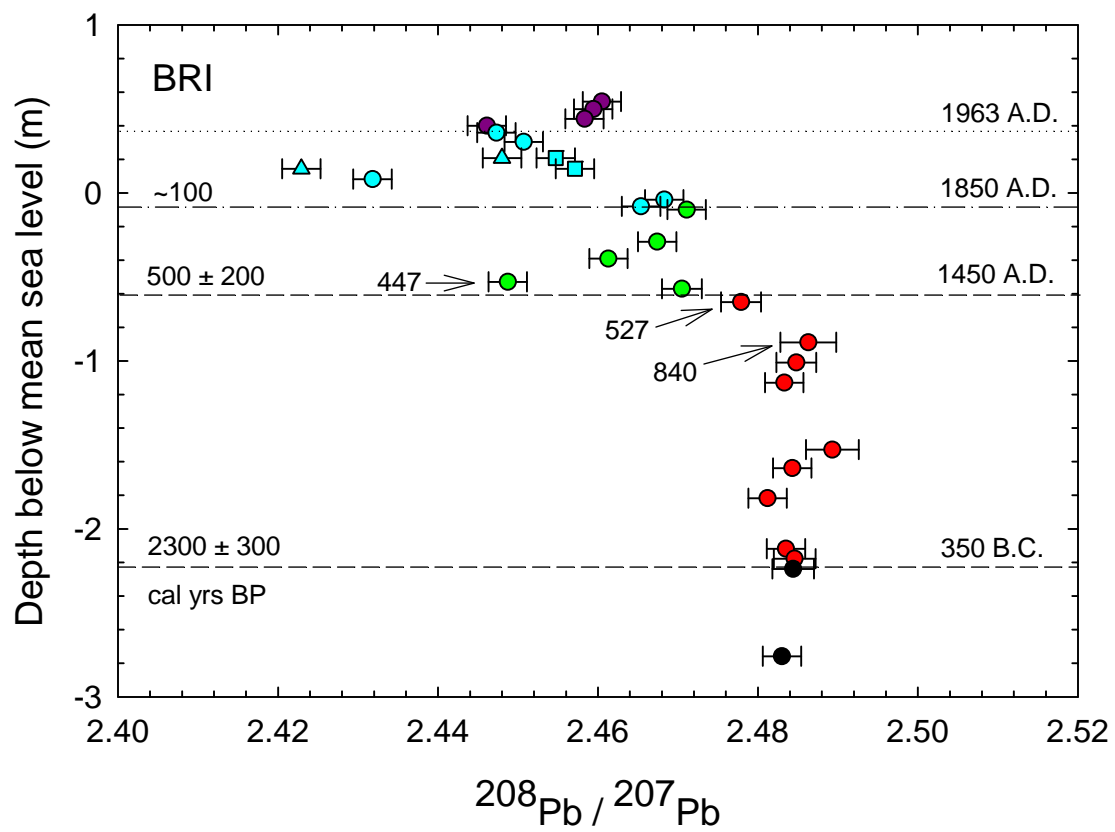


Fig. S-3B

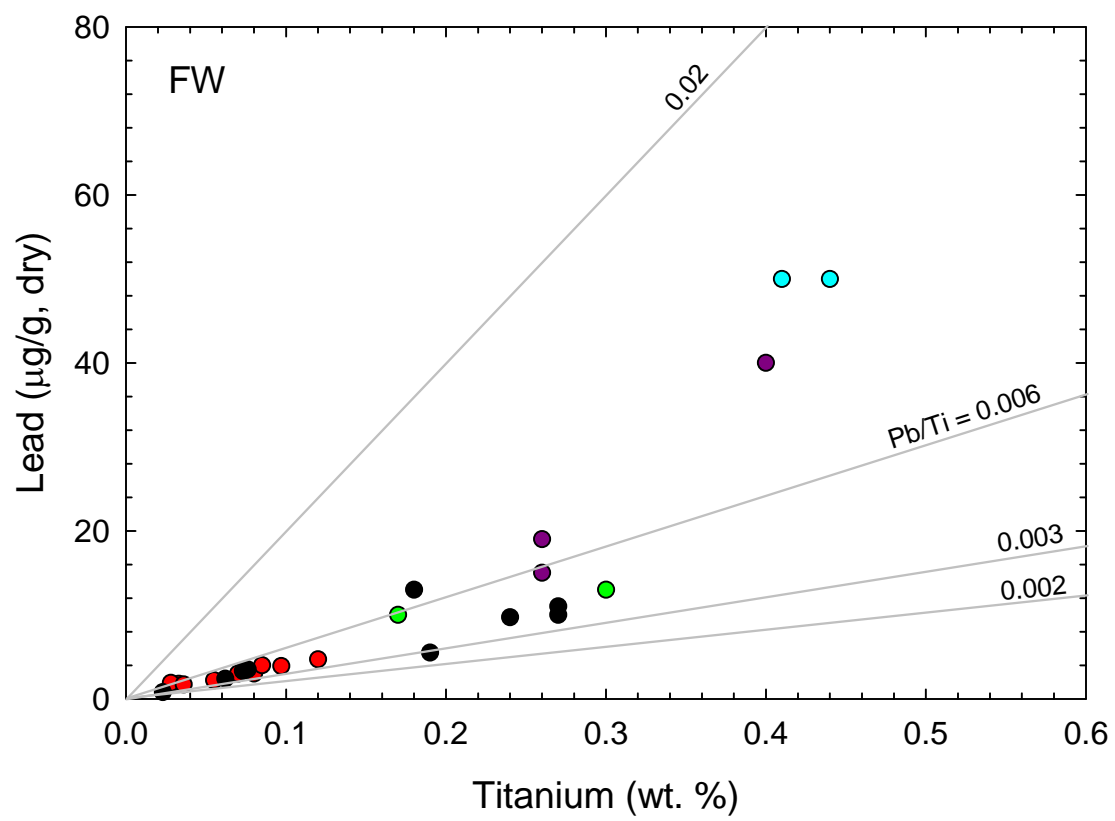


Fig. S-4A

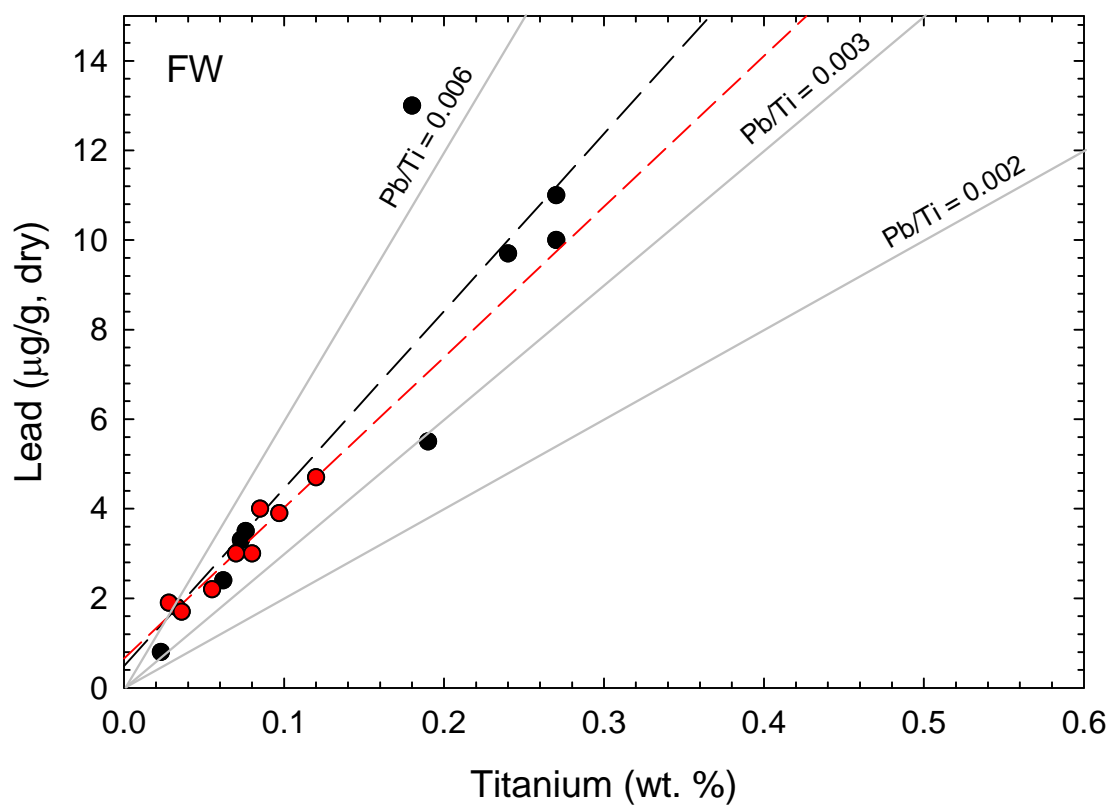


Fig. S-4B

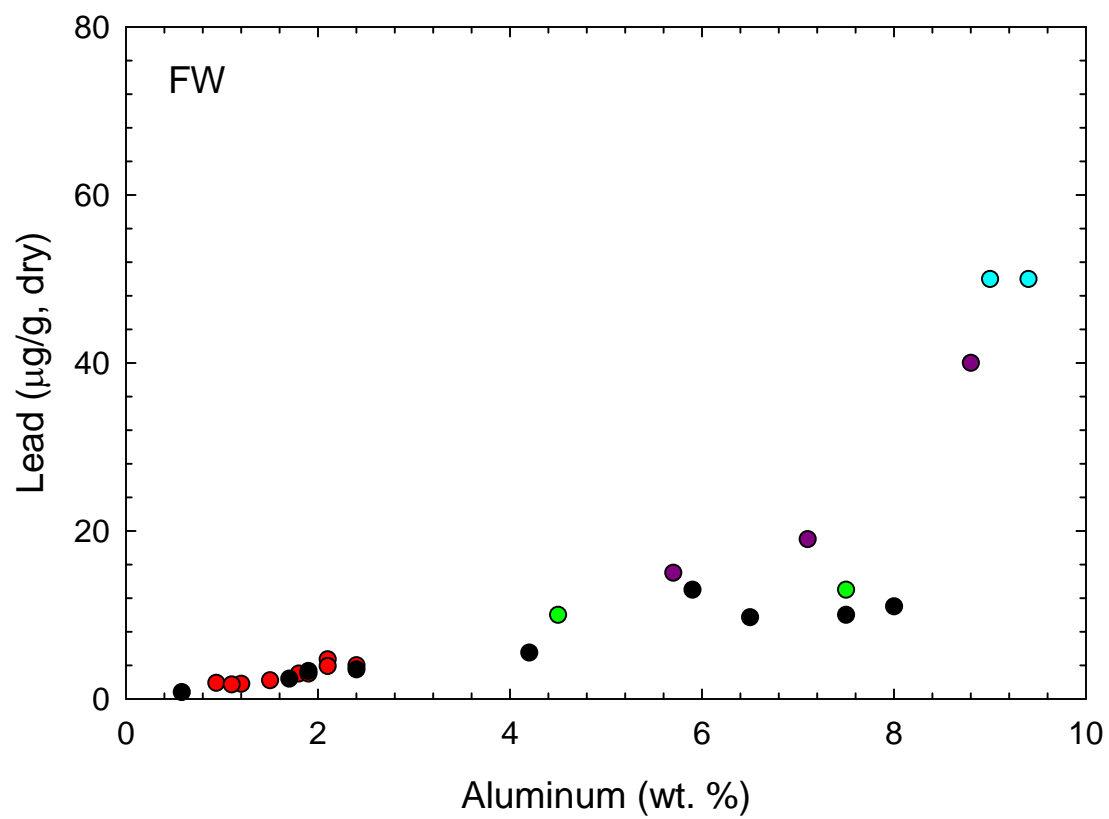


Fig. S-5A

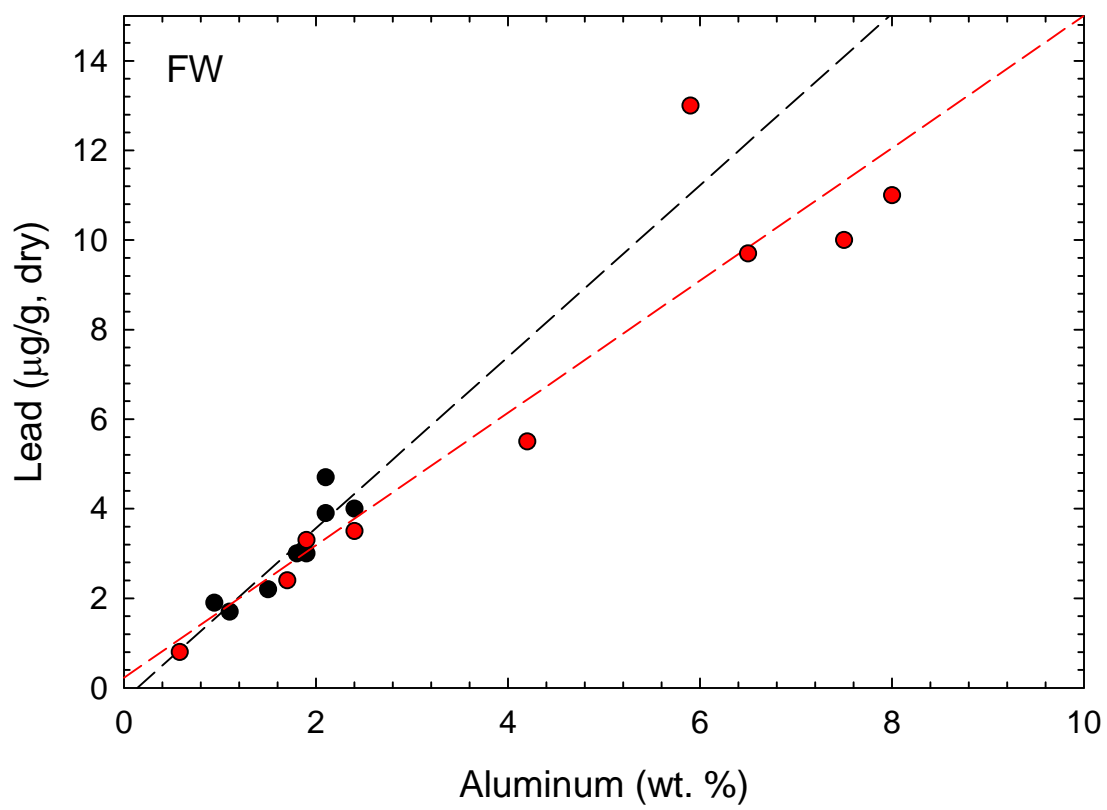


Fig. S-5B

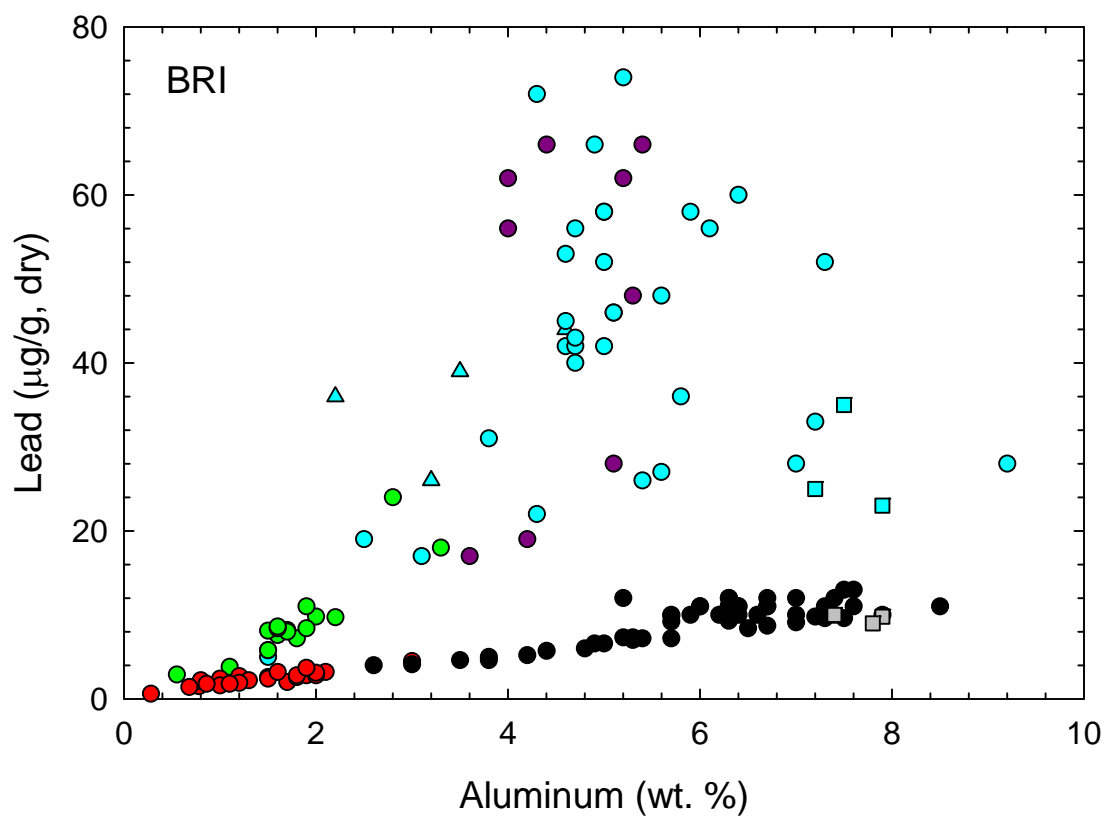


Fig. S-5C

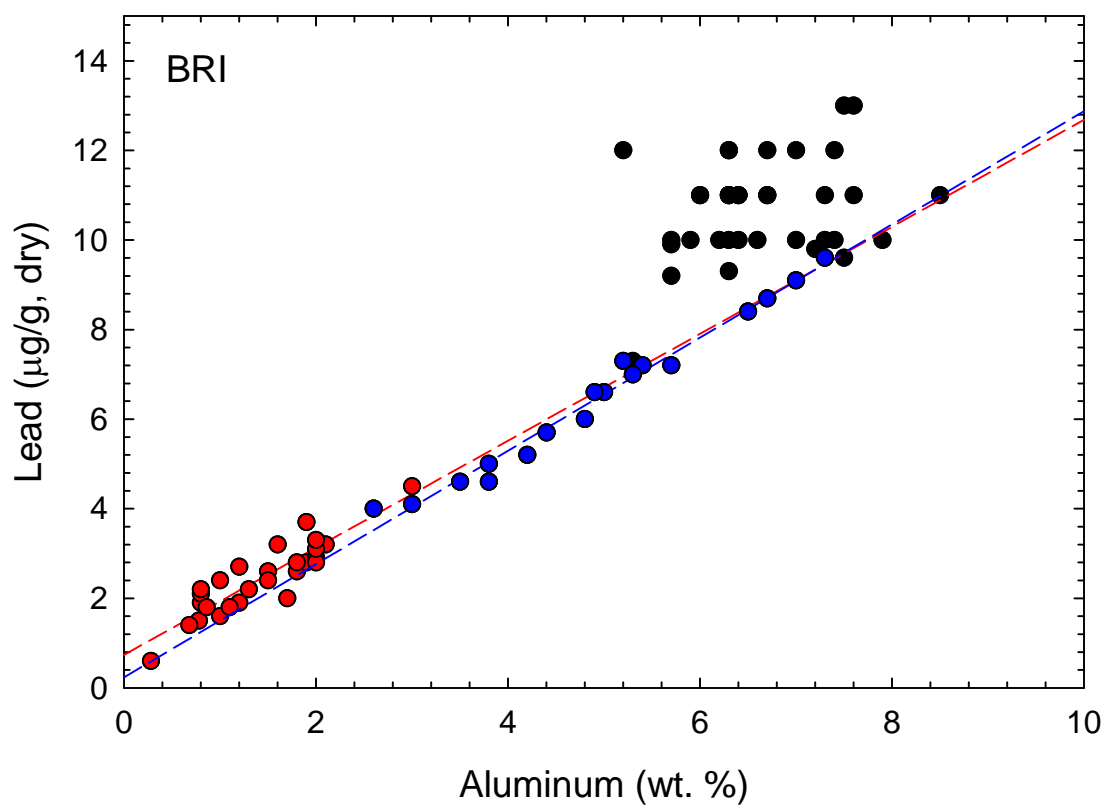


Fig. S-5D

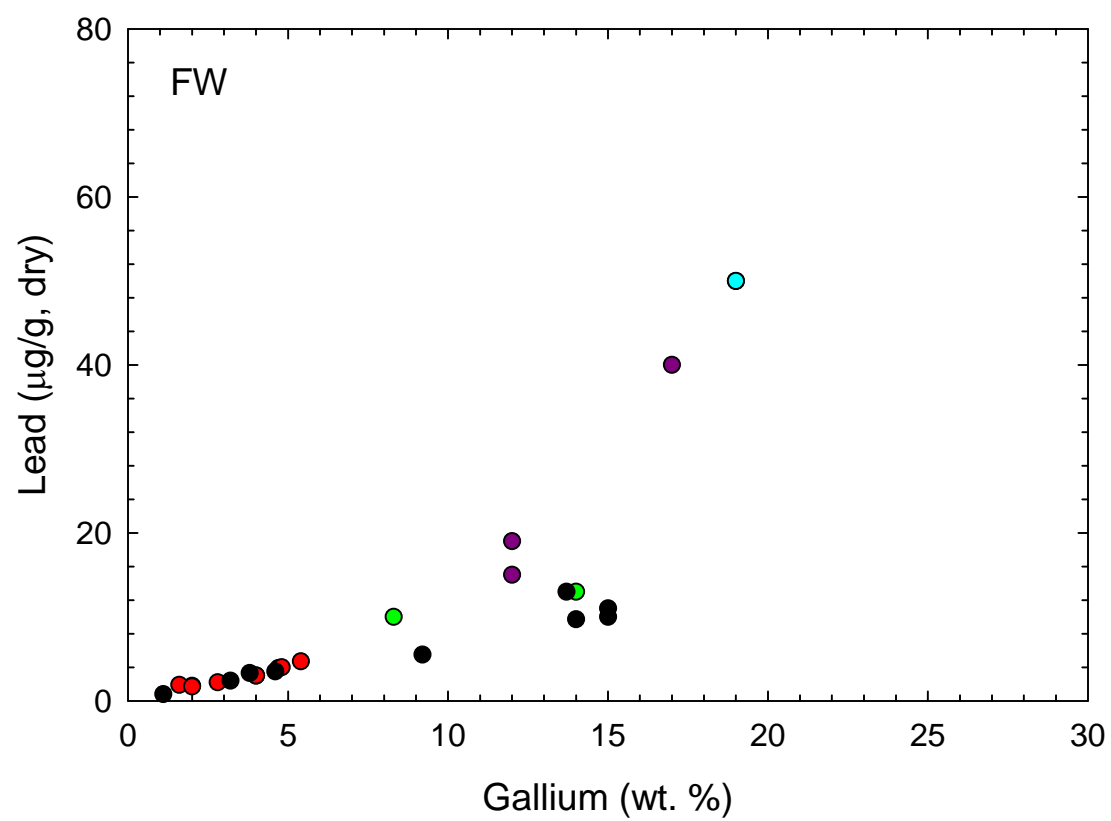


Fig. S-6A

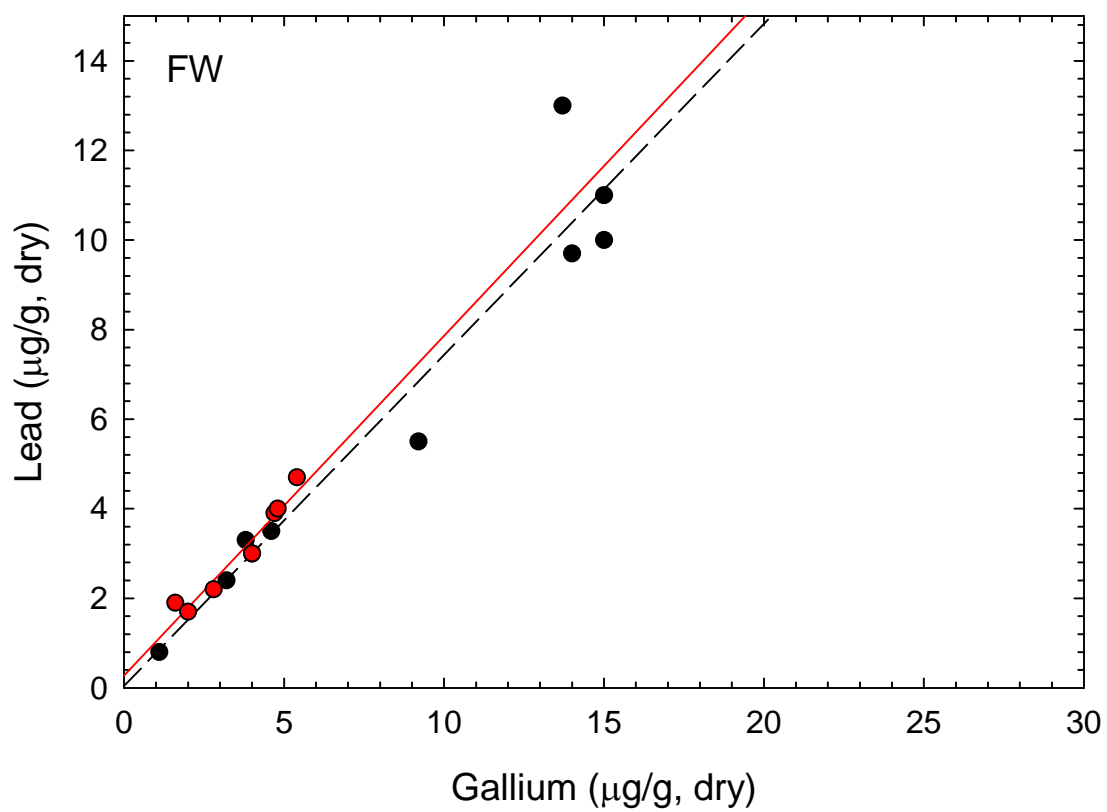


Fig. S-6B

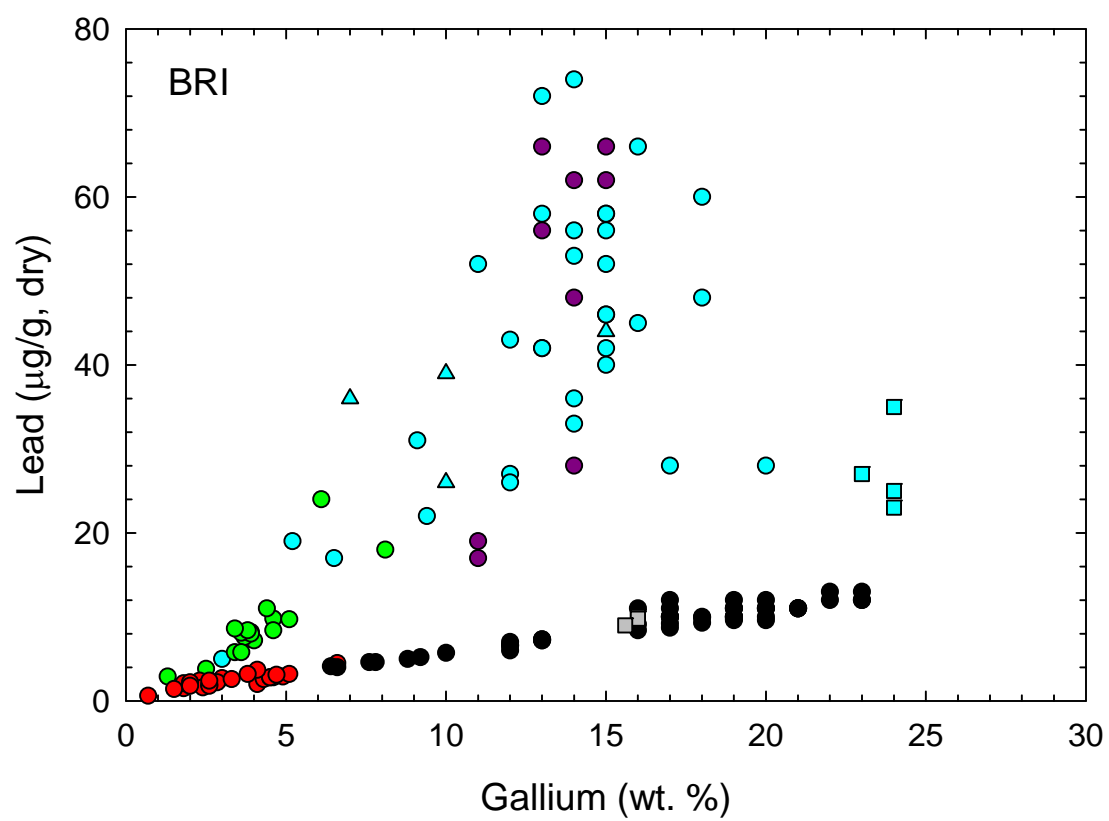


Fig. S-6C

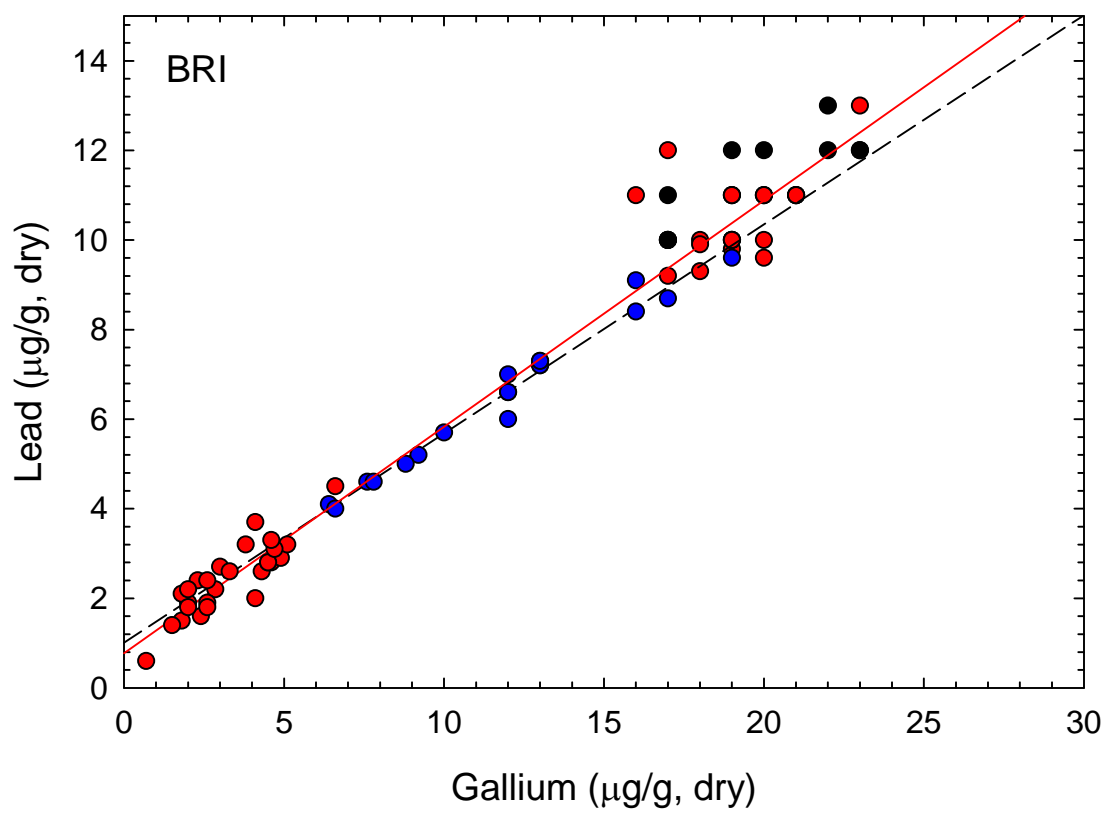


Fig. S-6D

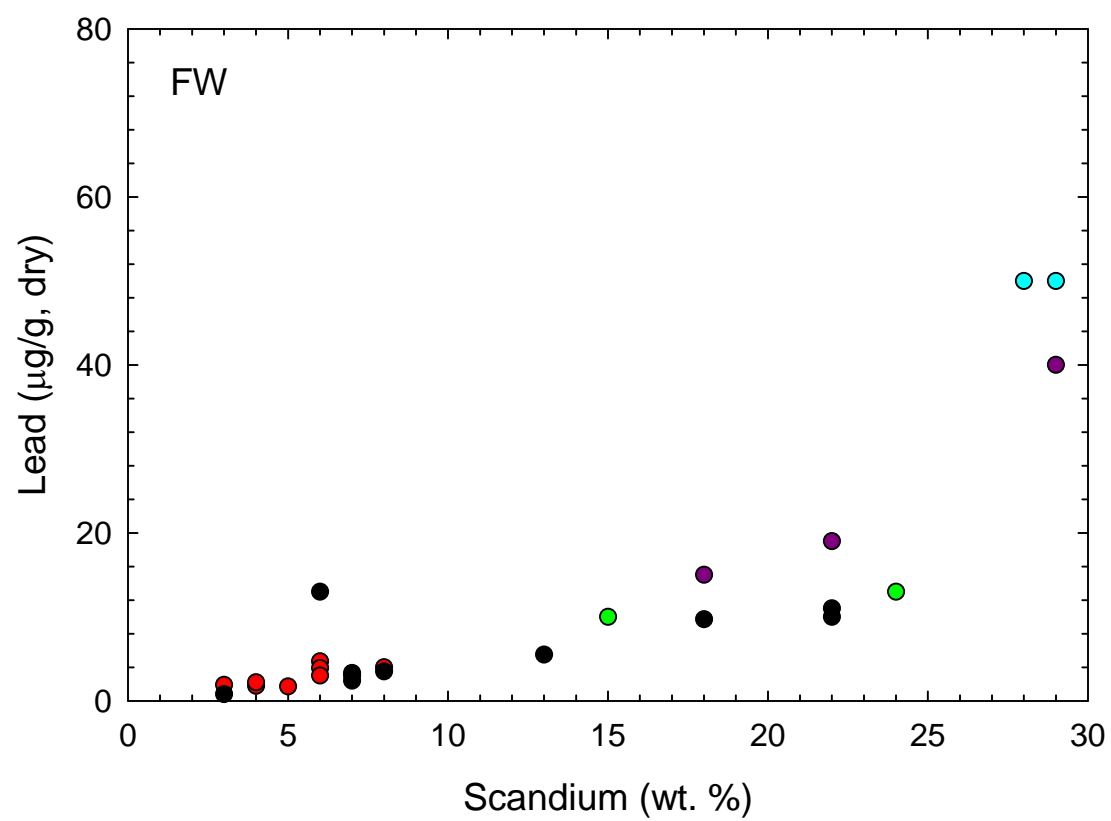


Fig. S-7A

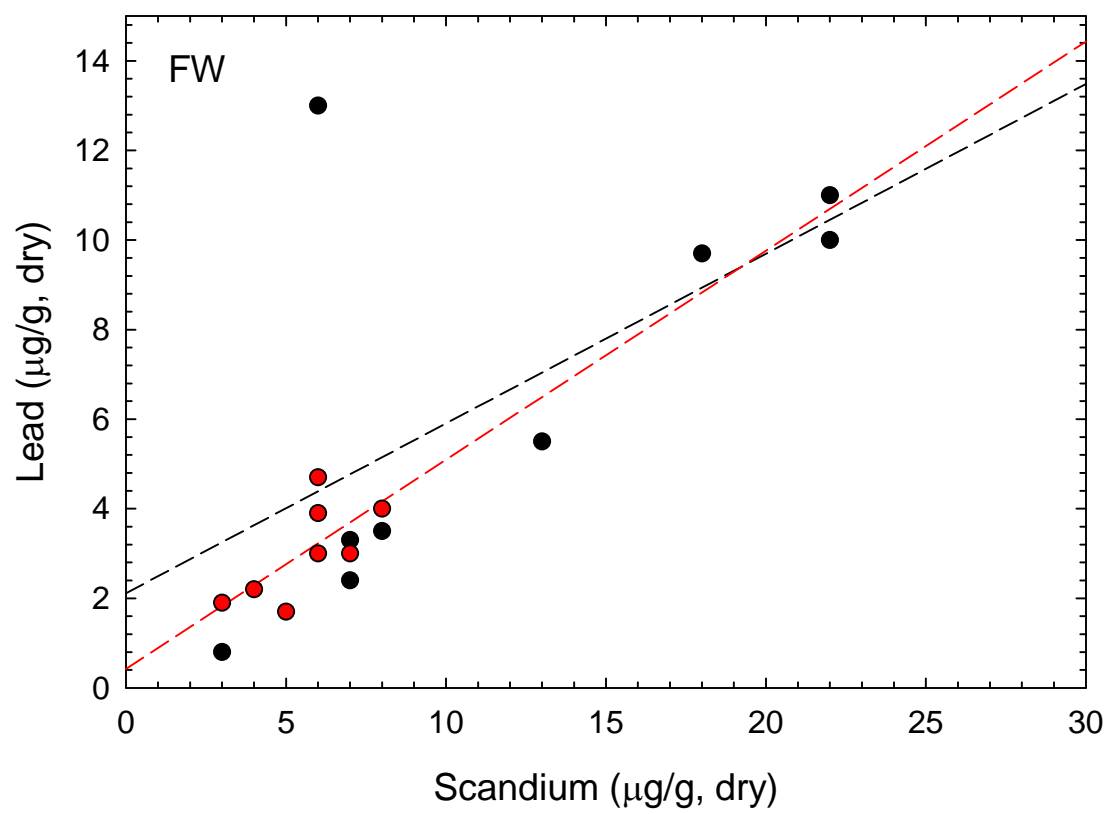


Fig. S-7B

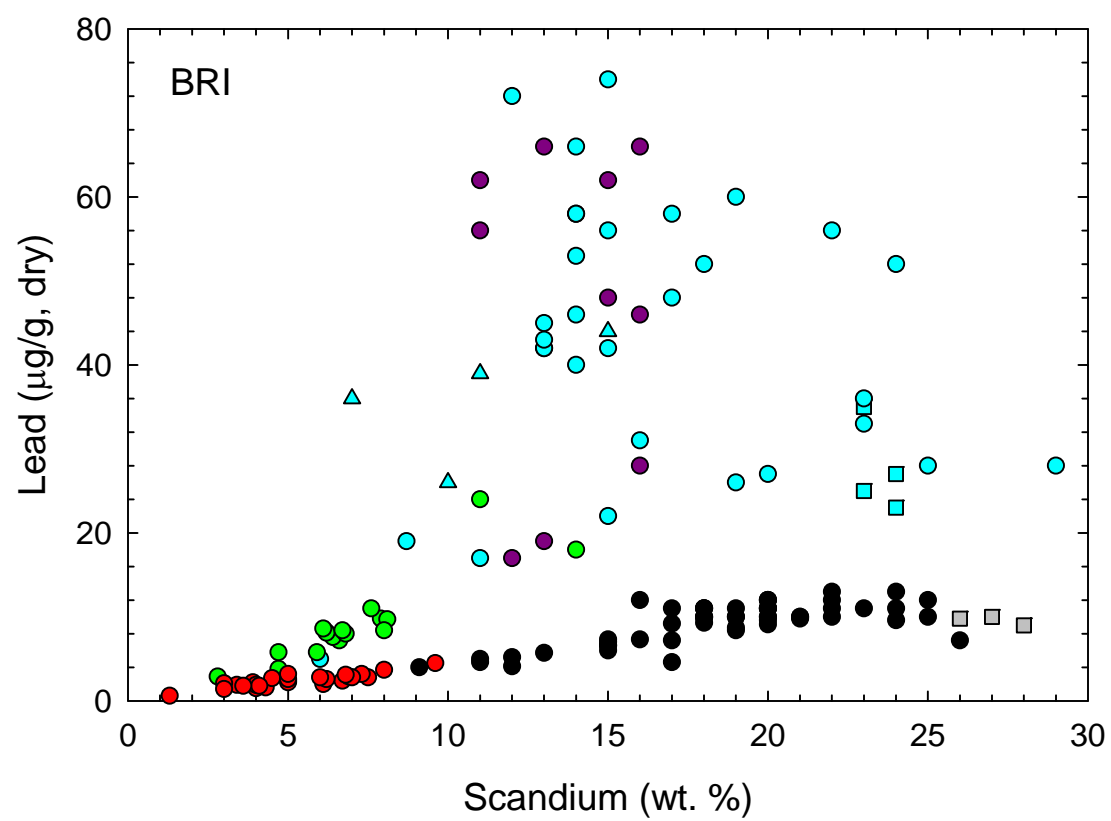


Fig. S-7C

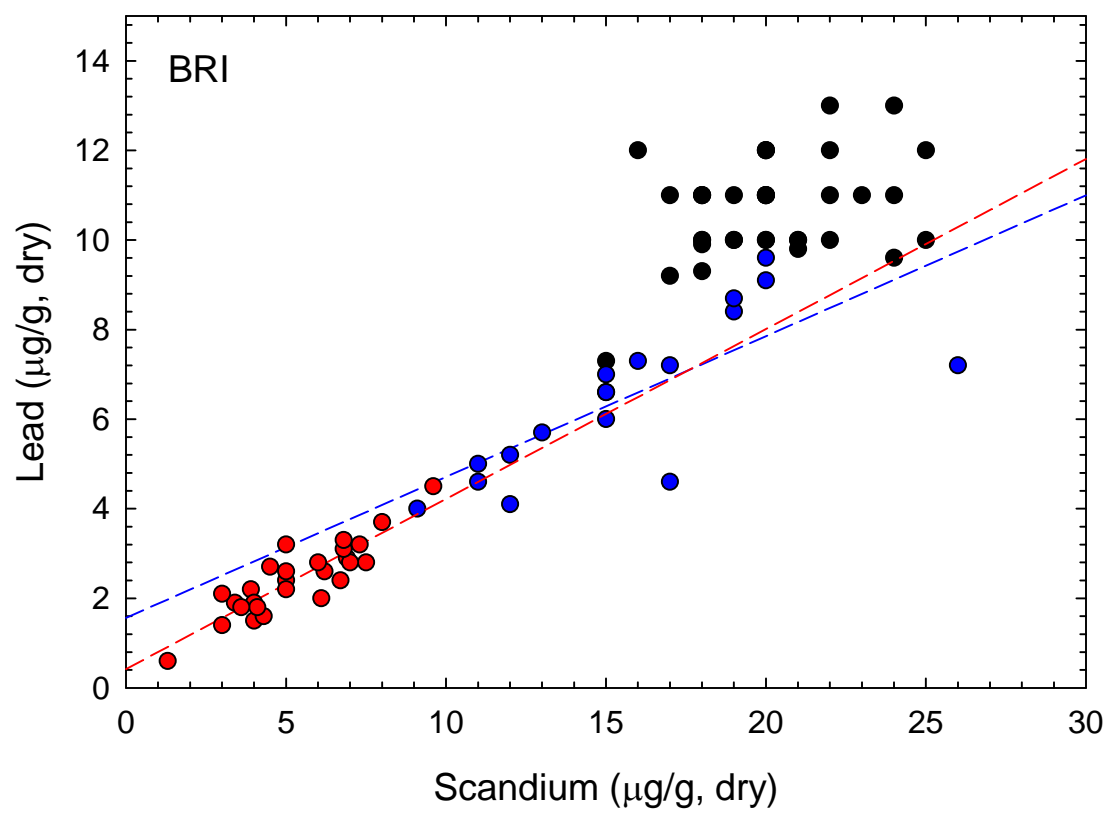


Fig. S-7D

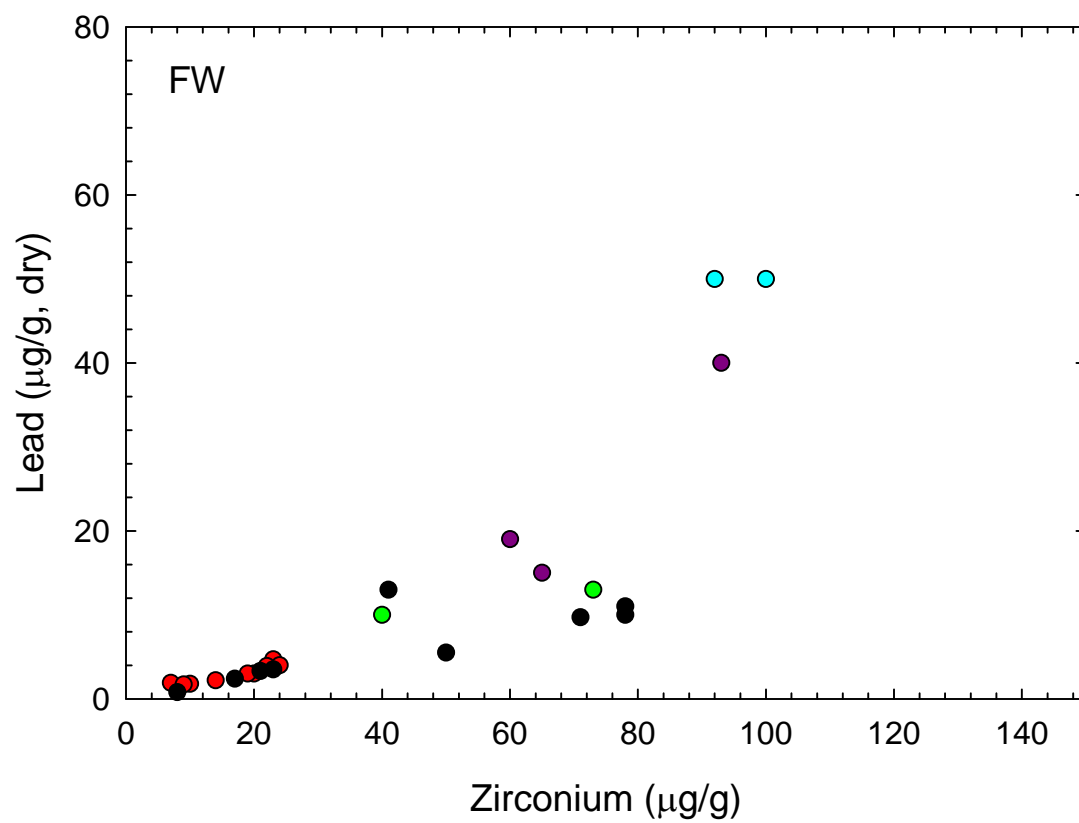


Fig. S-8A

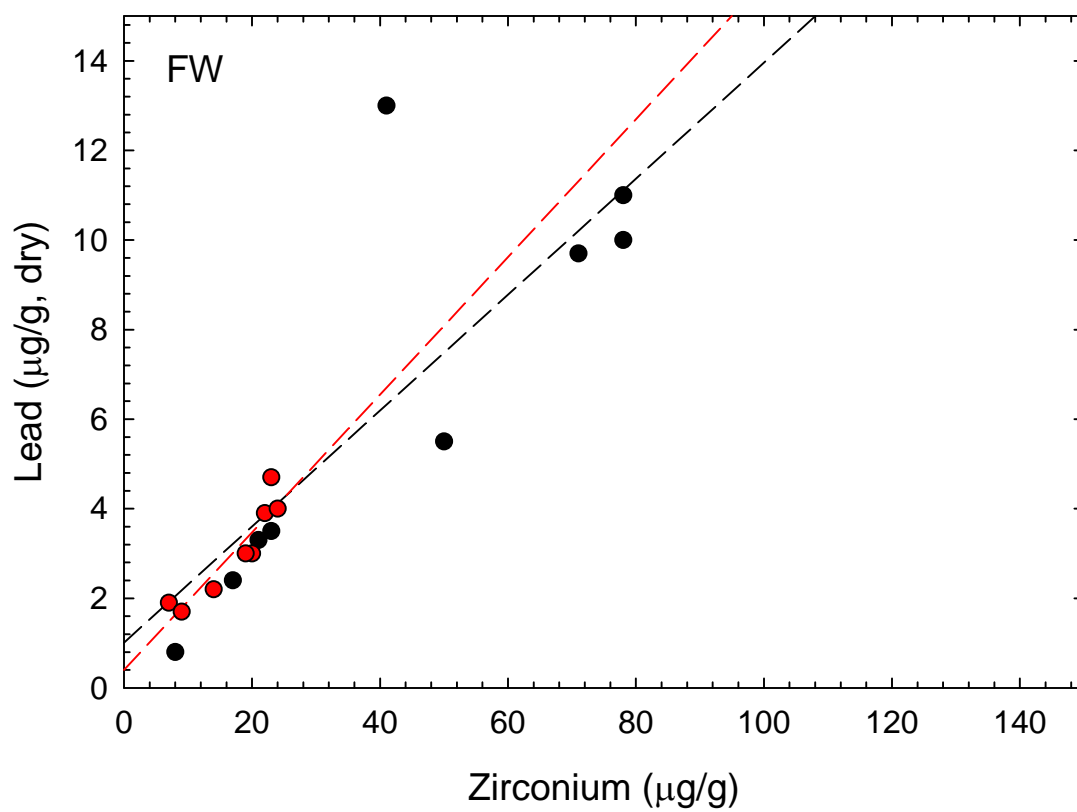


Fig. S-8B

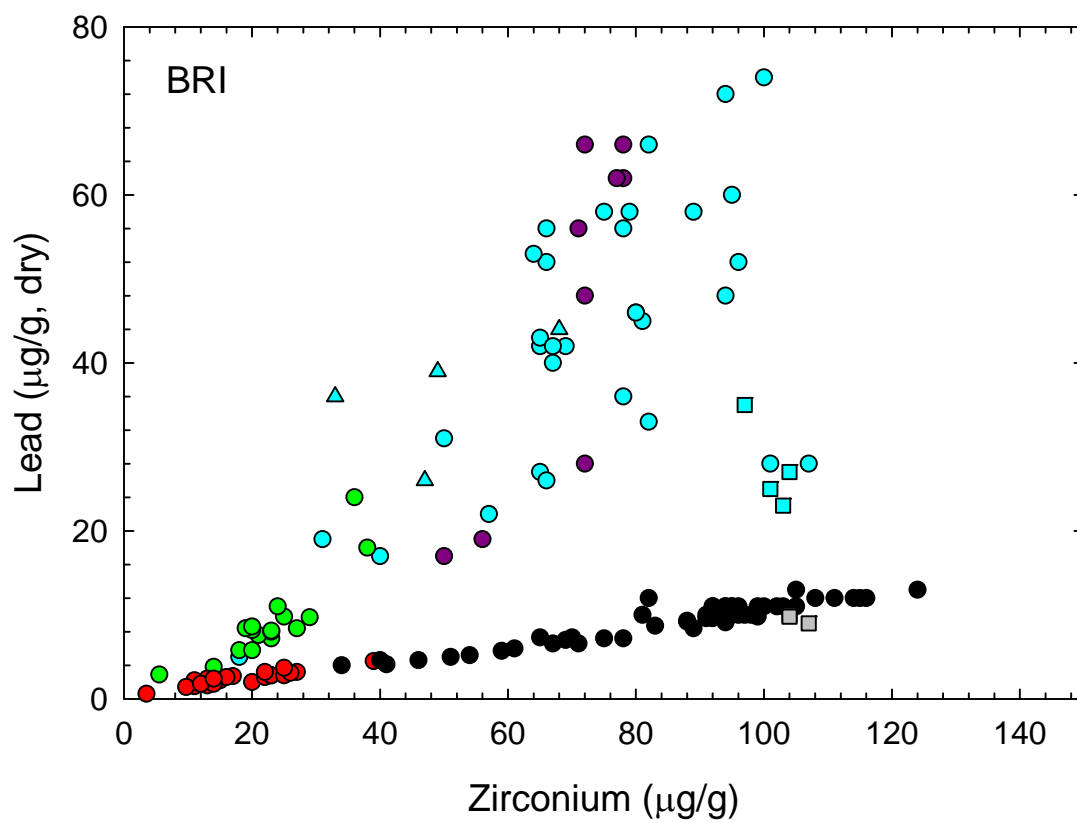


Fig. S-8C

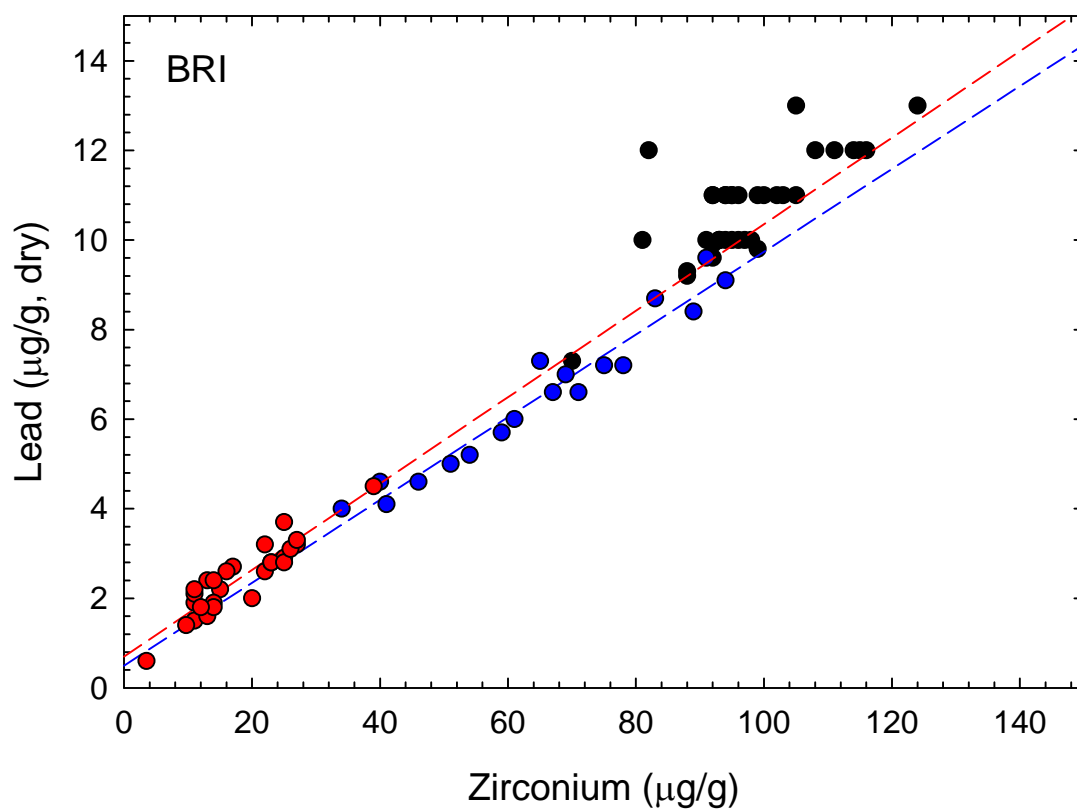
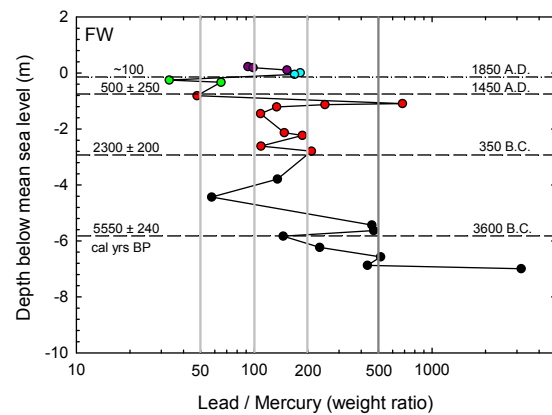


Fig. S-8D

A



B

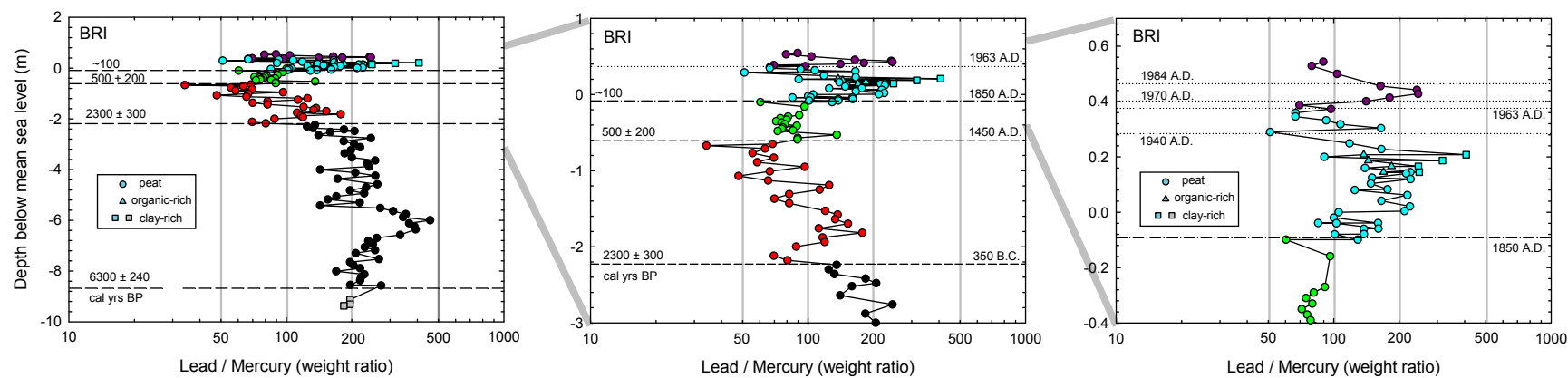


Fig. S-9

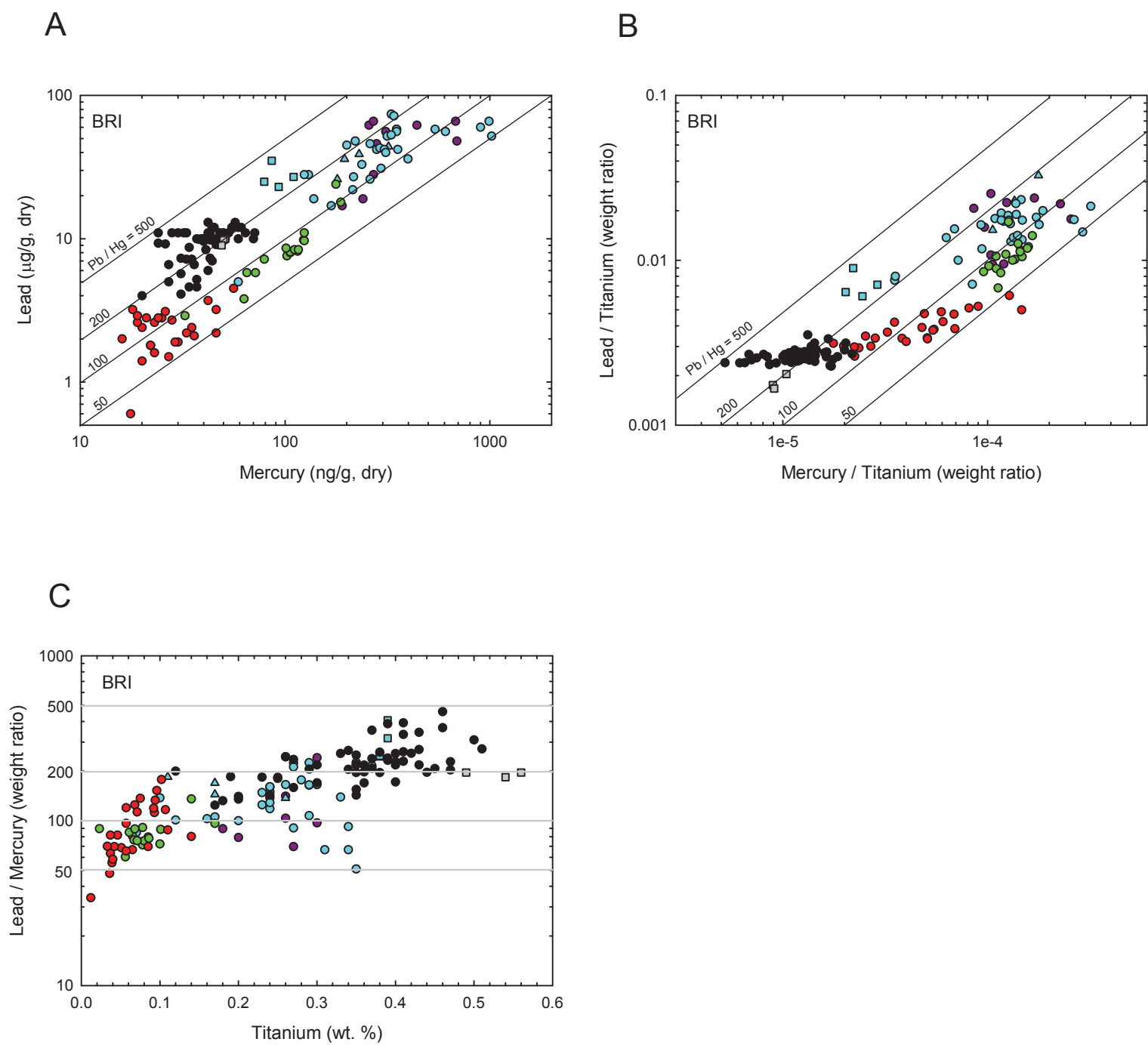


Fig. S-10